Norwegian University
of Life Sciences

Master's Thesis 2021 30 ECTS
Faculty of Science and Technology

Modeling Cortical Response to Visual Stimuli

Kajsa Sivertsen
Msc. Environmental Physics and Renewable Energy

Acknowledgements

First, I would like to thank my supervisors Gaute Einevoll and Espen Hagen for guiding me through the process of writing this thesis. I am thankful for the many hours spent on meetings and feedback throughout the semester. Even though physical meetings have been restricted these times, I am grateful that it hasn't stopped you from providing massive support and positive energy all the way.

I would also like to thank my fellow students. Being in the same situation, we have kept each other motivated and shared frustration in the emotional journey of the master's thesis. Thanks for reminding me to stand up from the chair once in a while and just enjoy hanging out.

I am looking forward to finally meet my family again, after a long time of uncertainties with this virus situation. I miss hugging my grandparents and playing with the kids. Let's catch up this summer!

At last, I will thank my fiancé Eivind Handegard for the love and support, all the patience and the inappropriate jokes. Your knowledge about academic writing and the process of writing a master's thesis has saved me from a lot of frustration. Thanks for being my biggest motivation of all.

Ås, June 1st, 2021

Kajsa Sivertsen

Summary

To understand the mechanisms of the brain is one of the biggest challenges in science. The biological processes of our brain are complex, and many functions are still unknown. To reach a deeper understanding of the brain, neuroscience provides models for different biological mechanisms.

A model of the early visual system is investigated in this thesis. The early visual system is one of the first steps of processing visual stimuli in the brain. The main cell layers involved are the retinal ganglion cell layer, the relay cells in the lateral geniculate nucleus (LGN), and the cortical cells in the visual cortex (V1).

Extended Difference-of-Gaussians (eDOG) is a linear model which enables simplified computation of firing rate based responses of the cell populations in the early visual system. eDOG involves the feedforward connections between the cell layers as well as the thalamocortical feedback loop between the cortical and relay cell layers.

The goal of this thesis is to use eDOG implemented in the software PyLGN to compute cortical responses. This software was developed and first applied to evaluate responses in relay cell populations. However, in this thesis, a cortical cell population was added with the direct feedforward signals from a relay cell population as the only input connection. The elongated spatial receptive field of cortical cells was chosen to be defined as an elliptic Gaussian function.

Three research questions were stated; Whether eDOG and the elliptic Gaussian can produce expected responses for the cortical population, whether cortical cells inherit response patterns from the relay cell layer, and if feedback loop effects appear in the cortical cell layer.

To answer the questions, tuning curves of the cortical response for different visual stimuli were computed. The results were compared to what has been observed for cortical cell responses from other studies, and what could be expected from the model. Diameter tuning curves of circular stimuli and suppression indexes were tools used to evaluate suppression in cortical cell populations. Furthermore, synaptic weights of the feedback loop were changed to test for feedback effects.

The results verify that eDOG, with the elliptic Gaussian kernel, is a good candidate to model cortical responses with a linear relation to the stimulus. Cortical cells are selective to orientation, and spatial preferences of stimulus change with parameters of the elliptic Gaussian. The cortical cells inherit suppression effects from the relay cells, dependent on properties of the stimulus and elliptic Gaussian parameters. The feedback loop effects appearing in relay cells appear in cortical cells as well. However, parameter adjustments can be done to produce response patterns not observed in this thesis.

This thesis shows that eDOG and the elliptic Gaussian function open new doors for simple modeling of cortical firing rate responses, including the thalamocortical feedback loop.

Sammendrag

Det å forstå mekanismene til hjernen er en av de største utfordringene i vitenskapen. De biologiske prosessene i hjernen vår er komplekse, og mange funksjoner er ennå ukjente. For å oppnå en dypere forståelse av hjernen bidrar nevrovitenskapen med modeller av ulike biologiske mekanismer.

En modell for det tidlige visuelle systemet er undersøkt i denne avhandlingen. Det tidlige visuelle systemet utgjør et av de første stegene i prosessering av visuelle stimuli i hjernen. Hovedlagene av celler som er involvert er ganglionceller i netthinnen, relayceller i laterale geniculate nucleus (LGN) og kortikalceller i visuell korteks (V1).

Extended Difference-of-Gaussians (eDOG) er en lineær modell som gjør det mulig å forenkle beregninger av fyringsratebaserte responser i cellepopulasjonene i det tidlige visuelle systemet. eDOG involverer feedforward koblinger mellom cellelag i tillegg til den thalamokortikale tilbakekoblingen mellom kortikalceller og relayceller.

Målet for denne avhandlingen er å bruke eDOG, som er implementert i programvaren PyLGN, til å kalkulere kortikalrespons. Programvaren ble utviklet og først brukt til å evaluere responser i populasjoner av relayceller. I denne avhandlingen ble en kortikal cellepopulasjon lagt til med de direkte signalene fra relaycellene som eneste koblingsinput. Det avlange romlige reseptoriske feltet til kortikalceller ble valgt til å være definert som en elliptisk Gauss-funksjon.

Tre spørsmål ble formulert; om eDOG og den elliptiske Gauss-funksjonen kan produsere forventede responser til kortikalpopulasjonen, om kortikale celler arver responsmønstre fra relaycellelaget, og om effekter av tilbakekoblingsmekanismen oppstår i kortikal cellerespons.

For å svare på disse spørsmålene ble det kalkulert tuningkurver av kortikalrespons til ulike visuelle stimuli. Resultatene ble sammenliknet med observasjoner av kortikalresponser fra andre studier og hva som kunne være forventet av modellen. Tuningkurver for diameter av sirkulære stimuli og indeks for reduksjon i respons er verktøy som ble brukt for å evaluere reduksjon i respons for kortikale cellepopulasjoner. Videre ble synaptiske vekter i tilbakekoblingsmekanismen endret for å teste effekter av tilbakekobling.

Resultatene kan bekrefte at eDOG, sammen med den elliptiske Gauss-funksjonen, er en god kandidat for å modellere kortikalresponser med lineære sammenhenger til stimulus. Kortikalceller er selektive til orientering, og romlige preferanser til stimulus endrer seg med parametrene til den elliptiske Gauss-funksjonen. Kortikalcellene arver effekter i dempning av respons fra relaycellene, avhengig av egenskaper til stimulus og parameterene til den elliptiske Gauss-funksjonen. Effektene av tilbakekoblingen som dukker opp i relayceller dukker også opp i kortikalcellene. Det kan være muligheter for at parameterjusteringer kan gjøres for å produsere responsmønstre som ikke ble observert i denne avhandlingen.

Denne avhandlingen viser at eDOG og den elliptiske Gauss-funksjonen åpner nye dører for enkel modellering av kortikal fyringsraterespons der den thalamokortikale tilbakekoblingsmekanismen er involvert.

Contents

1 Introduction

1.1 The human brain

The brain is one of the most complex systems known to us in the whole universe. The number of neuron connections is comparable to the number of stars on the Milky Way night sky (DeWeerdt, 2019). To understand the mechanisms of the brain, models are developed to describe, explore and predict signals propagating through the brain. Research related to the brain brings us closer to solving health issues, understanding behaviour, and gives inspirational ideas of artificial intelligence. In this thesis, the brain's role in vision is investigated by a simple model based on the neurons involved in the early processing of visual stimuli.

1.2 The early visual system

The early visual system involves the structures responsible for processing the nerve signals evoked by detection of light in the eye. These structures involve the cells in the eye's retina, the connection of retinal ganglion cells to the lateral geniculate nucleus (LGN), and at last, the primary visual cortex (V1) (Dagnelie, 2011). An illustration of the early visual system is shown in figure 1. The retinal cells have photoreceptors reacting to light and convert this into chemical and electrical signals (Gabbiani & Cox, 2017; Dagnelie, 2011). The retinal ganglion cells are the first cells in the pathway to fire action potentials, and these spikes propagate by the optic nerve to LGN (Gabbiani & Cox, 2017; M. Mobarhan, 2018). The retinal ganglion cells make synaptic contact with relay cells of the LGN. The layers of LGN can be divided into parvocells, magnocells and koniocells (Dagnelie, 2011). These cells provide direct feedforward projections to the layers of V1. Furthermore, the loop is closed by parvocellular and magnocellular feedback from layer 6 of the V1 (Dagnelie, 2011). These feedback nerve signals between LGN relay cells and cortical cells of V1 are referred to as the thalamocortical feedback. The functions of this pathway remain to be fully understood (Briggs & Usery, 2007; M. H. Mobarhan et al., 2018).

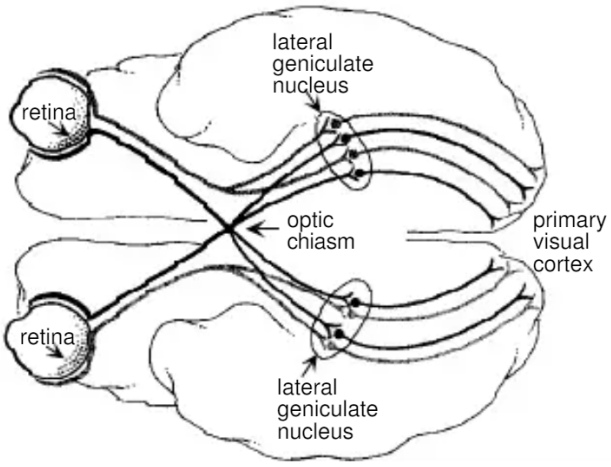

Figure 1: Dayan and Abbot (2001). The structures of the early visual system are shown. The retinal ganglion cell layer connects to the relay cell layer in the lateral geniculate nucleus through direct feedforward connections. The primary visual cortex receives the direct feedforward connections from the relay cells. However, the feedback connections are not shown in the figure. The optic chiasm is the structure where nerve fibers from both eyes cross and are combined in each of the hemispheres of the brain (Dagnelie, 2011). Figure from Dayan, P., & Abbot, L. F. (2001) *Computational Neuroscience, Computational and Mathematical Modeling of Neural Systems* (Vol. 2). Cambridge: Massachussetts Institute of Technology.

1.3 The feedback pathway

It has been highly supported that the thalamic responses are affected by the feedback connections with cortical cells in V1 (Alitto & Usrey, 2003; Briggs & Usery, 2011). The relay cells receive the most input from feedback connections, compared to feedforward connections from the retina (Sherman & Guillery, 2002). Furthermore, the feedforward connection between relay cells and V1 has proven to play a role in the selectivity of the visual stimuli in visual cortex (Carandini et al., 2002; Ozeki et al., 2009; Bruno & Sakmann, 2006; Ferster & Miller, 2000), in addition to the recurrent cortical connections (Stettler et al., 2002; Angelucci & Bressloff, 2006; Adesnik et al., 2012; Nassi et al., 2013; Ozeki et al., 2009).

I addition, the physical organization, related to retinotopic arrangement patterns (Kremkow & Alonso, 2018) of the feedback projections, make the feedback a good candidate for adjusting relay response (Born et al., 2021). The feedback consists of both inhibitory and excitatory signals (M. H. Mobarhan et al., 2018; Landisman & Connors, 2007; Cruikshank et al., 2010; Geisert et al., 1981). The excitatory are direct feedback connections from the cortical cells to the relay cells (Born et al., 2021). However, the inhibitory signals arise either from interneurons or from thalamic reticular nucleus (TRN) (Born et al., 2021). Cortical cells seem to excite cells in the TRN, which in turn inhibit the relay response (Cruikshank et al., 2010; Born et al., 2021). Feedback is likely dynamic and complex, as experiments have supported this (Born et al., 2021; Landisman & Connors, 2007; Cruikshank et al., 2010; Lam & Sherman, 2010; Sherman, 2016).

1.4 The suggested functions of the feedback loop

Even though studies have come up with various and sometimes contradictory results (Born et al., 2021; Denman & Contreras, 2015; Carandini et al., 2002; Ozeki et al., 2009), it has been proposed many suggestions for the function of the feedback loop. Several studies have supported that the feedback loop affects information processing of visual stimuli as the signals pass from the retina to the cortex (Marrocco, McClurikin, & Young, 1981; Ozeki et al., 2009). It seems to become established that the loop is important for how the early visual system processes visual stimuli (M. H. Mobarhan et al., 2018; Hasse & Briggs, 2017).

Suggested functions are, for example, response modulation of relay cell response (Marrocco et al., 1981; M. H. Mobarhan et al., 2018; Webb et al., 2002) and modulation of the center-surround antagonism (Jones et al., 2012; Andolina et al., 2013; Sillito & Jones, 2002; Alitto & Usrey, 2003; Molotchnikoff et al., 1984). This is related to effects on suppression patterns (M. H. Mobarhan et al., 2018; Rao & Ballard, 1999). In addition, changes in contrast gain (Przybyszewski, Gaska, Foote, & Pollen, 2000) and sharpening of the receptive fields of relay cells (Born et al., 2021; Murphy & Sillito, 1987; Sillito & Jones, 2002) are relevant suggestions of functions.

Functions related to the temporal domain are temporal adjustments of relay cell response (Hasse & Briggs, 2017; Sillito & Jones, 2002; Gulyás et al., 1990; Funke et al., 1996; Yousif & Denham, 2007), switches between tonic firing and burst firing (McCormick & Krosigk, 1992; Godwin et al., 1996; Sherman, 1996), and synchronization of firing patterns (Sillito et al., 1994; Hasse & Briggs, 2017; Sillito & Jones, 2002).

Consequently, feedback is a complex matter, and experiments have shown that it behaves dynamically (Born et al., 2021; Sherman, 2016). This can be one of the reasons why several studies have shown a wide range of different results.

1.5 The role of the cortical cells in the early visual pathway and feedback loop

The cortical cells themselves are directly involved in the loop and thereby have a crucial effect on how visual stimuli are processed in the early visual system (Carandini et al., 2002; Ozeki et al., 2009; Bruno & Sakmann, 2006; Ferster & Miller, 2000). It is established that most of them are highly selective for orientation and spatial frequency of stimuli (Hubel & Wiesel, 1962; Ayzenshtat, Jackson, & Yuste, 2016). The selectivity is mainly due to their elongated receptive fields and recurrent connections with other cells in V1 (Cudeiro & Sillito, 1996; Ozeki et al., 2009; Born et al., 2021). Consequently, the cortical cells with different preferences for orientation and spatial selectivity respond differently to lines and edges in stimuli (Hubel & Wiesel, 1962). However, studies suggest that orientation selectivity happens both in the cortical cells and projections from elongated receptive fields of retinal ganglion cells to the LGN (Zaltsman et al., 2015; Suematsu et al., 2013).

1.6 Modeling the early visual system including the feedback pathway

Studies have suggested to model this system in numerous ways. Even though the structure of the early visual system and the thalamocortical loop is mapped out (Kremkow & Alonso, 2018), the function of this feedback loop remains to be fully understood.

By activating and deactivating feedback, it is possible to see which effects are dependent on the thalamocortical feedback. Activation and deactivation of, or manipulating feedback have been done both experimentally (Born et al., 2021; Hasse & Briggs, 2017; McCormick & Krosigk, 1992; Andolina, Jones, & Sillito, 2007) and analytically (M. H. Mobarhan et al., 2018). Using the model called extended Difference-of-Gaussians (eDOG), the latter can be done efficiently and easily in the software PyLGN described in the paper by M. H. Mobarhan et al. (2018). PyLGN is available from `https://github.com/miladh/pylgn` M. Mobarhan et al. (2018).

eDOG is a model based on the Difference-of-Gaussians (DOG) model (Einevoll & Plesser, 2012). The model defines the output of a cell population in the early visual system, including the feedback-loop between V1 cortical cell populations and LGN relay cell populations. DOG builds receptive fields as Gaussian functions and can model center-surround antagonism in the relay cells by subtracting of two different Gaussian functions (Rodieck, 1965). However, the next step in modeling the whole pathway is the inclusion of the feedback. The spatial feedback connection kernel is simplified to a single circular Gaussian function between the cortical cells and the relay cells. Even though each separate cortical cell population has a specific preference of orientation, because of the elongated shape of their receptive field, the feedback from all these populations back to the LGN relay cells sum up to a circular shaped Gaussian function (Einevoll & Plesser, 2012). This simplification is a central aspect of eDOG.

1.7 Simulating the early visual system using PyLGN

The software PyLGN is a module developed to create a network of cell populations from the early visual system. Responses are computed by the combination of the synaptic input and the receptive field of the cell populations. Each population can be connected by user-defined synaptic weights, and both kernels and stimuli have user-defined parameter inputs.

PyLGN includes the retinal ganglion layer, the LGN relay layer and the V1 cortical layer. Each cell type response is linearly related to the output from the previous cell type in the pathway. The spatial receptive fields for the ganglion cell populations are based on DOG with center-surround antagonism, whereas the relay cell populations have Gaussian functions as their spatial receptive fields. The cortical cell populations added in the simulation of this thesis rather have elliptic Gaussian functions.

The reason behind the choice of an elliptic Gaussian for the cortical cell populations comes from the arguments of Hubel and Wiesel (1962). They described the shape of the receptive fields of cortical cells as elongated. This is a consequence of their inheritance from aligned cells upstream with center-surround antagonism. The elliptic Gaussian function accounts for this shape of the cortical spatial receptive field.

By using eDOG, PyLGN models the thalamocortical feedback efficiently. The implementation of eDOG in PyLGN allows for feedback to be changed by adjusting the weights of the synaptic strength between the connected neuron populations. This makes it easier to model responses during different conditions for a better fit to different situations.

The feedback loop to the relay cell populations is modeled as a superposition of all contributions from the cortical cells. Thus, to maintain linearity, the sum of all ellipses with their different orientation preferences must be radially symmetrical. If this is the case, the loop does not need to account for the elliptic shape of the receptive fields of the cortical cells. They add up in the loop to

be approximately a circular Gaussian function (Einevoll & Plesser, 2012), preserving the linearity of the model. There is, however, a nonlinearity included, which is the rectification of the real-spaced response of cortical cells. For a radially symmetric sum of contributions from cortical cell populations, the linearity of the model is still retained, despite this nonlinearity.

By this approximation, eDOG includes the loop and thereby accounts for feedback effects simultaneously as it retains linearity. In reality, the feedback includes other nonlinear effects as well as the rectification (Einevoll & Plesser, 2012), but these will not appear in simulations based on eDOG. Since eDOG is a linear model, it will only predict linear responses (Einevoll & Plesser, 2012).

1.8 The research questions of the thesis

M. H. Mobarhan et al. (2018) showed that PyLGN models both spatial and temporal dependent effects of the relay cells (M. H. Mobarhan et al., 2018). The questions of this thesis are related to this in the new context related to the responses of cortical cell populations.

The research questions of this thesis can be summed up in three questions:
1. To what extent does the elliptic Gaussian function together with eDOG give responses consistent with what is expected for cortical cells?
2. Will the cortical cell populations in the eDOG model inherit effects from the direct connections with the relay cells?
3. Will the thalamocortical feedback also give a significant change in the cortical cell response?

As the information is affected in the relay cell, due to the direct connections to the cells in V1, it is expected that the cortical cells inherit these effects. If the cortical cells affect relay cell response through the thalamocortical feedback loop, they are expected to inherit the loop effects as well (Dayan & Abbot, 2001; Einevoll & Plesser, 2005). The model considered in this thesis assumes that the cortical cells in V1 have elongated spatial receptive fields. This contributes to cortical preferences of input signals, like orientation selectivity and frequency preferences (Hubel & Wiesel, 1962).

The strategy of answering the research questions is use of the software PyLGN to compute responses to visual stimuli. By building a network of the cell populations of the early visual system and connect them with defined kernels, responses for each cell type can be computed. The elliptic Gaussian function needs to be defined as a kernel and connected to a cortical cell population in the simulation.

The effects of the elliptic kernel can be tested by changing the parameters included in the kernel, such as shape and orientation. In addition, comparing the relay response and the cortical response can reveal the heritage of effects. The user-defined weights in PyLGN also make it easy to turn on and off the feedback connections and test feedback effects.

Suppose the model gives results that are expected by theory. In that case, it will be a door-opener for efficient prediction of cortical responses in the early visual system, including the feedback loop in the future.

2 Theory

2.1 Firing rate models

Firing rate models simplify network signaling dynamics modeling by depending on rates rather than exact spiking times (Sterratt et al., 2011). The firing rate is defined as the integral of the trial-averaged neural response function over a time-interval, divided by the length of the time interval (Dayan & Abbot, 2001). The neural response function is the number of spikes occurring during the time interval considered (Dayan & Abbot, 2001). The models are stripped down of detailed information, making them suited for fast simulations (Sterratt et al., 2011). eDOG is a firing rate based model (Einevoll & Plesser, 2012) which allows for simple and fast simulations of neuron activity (M. H. Mobarhan et al., 2018).

2.2 Computation of responses due to stimulus - the importance of the Fourier domain

The computation of the response $R(\mathbf{r}, t)$ is generally based on a convolution between the impulse-response function and a stimulus. The integral

$$R(\mathbf{r}, t) = \int_{\tau} d\tau \iint_{\mathbf{r}'} d^2\mathbf{r}' W(\mathbf{r} - \mathbf{r}', \tau) S(\mathbf{r}', t - \tau) \tag{1}$$

describes this convolution in real space (M. H. Mobarhan et al., 2018; Einevoll & Plesser, 2012; Heeger, 1991; Einevoll & Plesser, 2002). The response $R(\mathbf{r}, t)$ is evaluated at position $\mathbf{r}$ of the responding cell at time t. The impulse-response function $W(\mathbf{r} - \mathbf{r}')$ is evaluated at the position $\mathbf{r}'$ relative to the position of the responding cell $\mathbf{r}$ and is dependent on the time interval τ after the stimulus (M. H. Mobarhan et al., 2018; Myklebust, 2020). The impulse-response function is convolved with the stimulus occurring at position $\mathbf{r}'$ at the time $t - \tau$ (M. H. Mobarhan et al., 2018; Heeger, 1991; Einevoll & Plesser, 2002). One can think of the impulse-response function as the filter of the neuron, passing through selected information from the stimulus. In fact, the impulse-response function consists of two different functions. One considers spatial filtering, and the other temporal filtering. In this thesis, these factors of the impulse-response functions are considered separable, although non-separable functions exist.

A simpler representation of the integral in equation 1 can be written as

$$R(\mathbf{k}, \omega) = W * S \tag{2}$$

(M. H. Mobarhan et al., 2018). The star indicates that the operation is a convolution between W and S.

The convolution of two functions can, by the convolution theorem, be computed as the product of their Fourier transforms (Mallot, 2013). Thus, the equation can be expressed in the Fourier domain as

$$\tilde{R}(\mathbf{k}, \omega) = \tilde{W}(\mathbf{k}, \omega)\tilde{S}(\mathbf{k}, \omega). \tag{3}$$

This means that the response is now evaluated for the angular spatial frequency $\mathbf{k}$ and the temporal angular frequency ω simply by multiplying the Fourier transformed impulse-response function with the Fourier transformed stimulus. This is the way the software PyLGN computes the

responses of the different cell types involved. Consequently, the operation is a computational efficient way of computing the response. PyLGN is thus an applicable program for use in more complicated and bigger models.

The Fourier transform represents a function as a sum of sinusoidals with different frequencies (Shapley & Lennie, 1985). This can be expressed as an integral over all the sinusoidals contributing to the function. In fact, the Fourier transform used in this case is complex. The definition of the complex Fourier transform of a function $y(\mathbf{r}, t)$ is

$$\tilde{y}(\mathbf{k}, \omega) = \int_t \iint_{\mathbf{r}} e^{-i(\mathbf{kr}-\omega t)} y(\mathbf{r}, t)\, dx\, dy\, dt \tag{4}$$

(Einevoll & Plesser, 2005).

The complex term allows for the amplitude and phase to combine, and simplifies the computations of convolutions (Mallot, 2013).

The procedure of computing the response of a stimulus passing through a filter like mentioned, is called the Fourier synthesis (Shapley & Lennie, 1985). The benefit of the Fourier synthesis is that it can predict the response of any input to a linear system without changing the spatial frequencies (Shapley & Lennie, 1985; Mallot, 2013).

All continuous functions can be expressed as a sum of sinusoidals with different frequencies (Mallot, 2013; Shapley & Lennie, 1985). Since a function expressed as such a sum is linear, the output from the function passing through a linear filter yields the unchanged shape and spatial frequency of the input (Shapley & Lennie, 1985). Linear filtering of a sum of sinusoidals only has modulatory effect on the amplitude and displacement of phase (Shapley & Lennie, 1985).

The Fourier transform of the stimulus can pass through the linear filter, and each sinusoidal component with its corresponding frequency is modulated differently for amplitude and phase shifted (Shapley & Lennie, 1985). Some frequency components pass, while others are removed or damped in the process (Mallot, 2013). The filtered components are added to produce the response (Shapley & Lennie, 1985), thus the response is also a function represented by a sum of sinusoidals. The whole operation is simply a multiplication between the Fourier transformed stimulus and the frequency response (Shapley & Lennie, 1985), corresponding to the convolution between the impulse-response function and stimulus in equation 3.

In order to present the responses in real space and compute center responses, it is possible to apply the inverse Fourier transform (Shapley & Lennie, 1985) $\mathcal{F}^{-1}$:

$$R(\mathbf{r}, t) = \mathcal{F}^{-1}\{\tilde{W}(\mathbf{k}, \omega)\tilde{S}(\mathbf{k}, \omega)\} \tag{5}$$

(Weisstein, n.d.; M. H. Mobarhan et al., 2018).

The inverse Fourier transform of a function $y(\mathbf{r}, t)$ is defined as

$$y(\mathbf{r}, t) = \frac{1}{(2\pi)^3} \int_\omega \iint_{\mathbf{k}} e^{i(\mathbf{kr}-\omega t)} \tilde{y}(\mathbf{k}, \omega)\, dk_\mathrm{x}\, dk_\mathrm{y}\, d\omega \tag{6}$$

(Einevoll & Plesser, 2005).

The response is then again a function of the position $\mathbf{r}$ and time t in real space.

Furthermore, the cell type response depends on the output from previous cell types, the receptive fields and the synaptic weight between the connections. The impulse-response function corresponds to the receptive fields of each cell type. PyLGN incorporates the impulse-response functions in the form of spatiotemporal coupling kernels K to model the receptive fields.

The spatiotemporal coupling kernels themselves are separable in space and time, which means that they can be expressed as a multiplication between the spatial and temporal component of the kernel. In addition, the synaptic strength of the connection is included in the kernel in the form of a scalar. The equation

$$K(\mathbf{r}, t) = wf(\mathbf{r})h(t) \tag{7}$$

describes the kernel as a function of the synaptic weight w, the spatial component $f(\mathbf{r})$, and the temporal component $h(t)$ in real space (M. H. Mobarhan et al., 2018).

There exist nonseparable spatiotemporal kernels as well, but these are yet not implemented in PyLGN.

2.3 Spatial component of the receptive field

One of the simplest choices for transferring spatial frequencies from one cell to the next is by the Dirac delta function. The function is defined in real space as in equation 8.

$$f(\mathbf{r}) = \delta(yy_{\text{shift}} - xx_{\text{shift}}) \tag{8}$$

x and y are the spatial positions of the visual field in real space, whereas x_{shift} and y_{shift} are the shifted directions in the xy-plane.

The delta function in the Fourier domain is

$$\tilde{f}(\mathbf{k}) = e^{-i(k_{\text{x}}x_{\text{shift}} + k_{\text{y}}y_{\text{shift}})} \tag{9}$$

with k_{x} and k_{y} being the components of the spatial frequency of the visual plane, and x_{shift} and y_{shift} being the shifts in x- and y-direction.

DOG functions are commonly used as functions for the spatial component of the separable kernel in retinal and LGN cells (Dayan & Abbot, 2001). However, these are built up by Gaussian functions, as described below. The Gaussian function is defined as

$$f(\mathbf{r}; a) = \frac{1}{\pi a^2} e^{(-\mathbf{r}^2/a^2)}, \tag{10}$$

where a is the width parameter of the Gaussian curve (M. H. Mobarhan et al., 2018), and $\mathbf{r}$ is the position vector in the visual field.

In Fourier domain the Gaussian function is

$$\tilde{f}(\mathbf{k}; A, a, dx, dy) = Ae^{-a^2(k_{\text{x}}^2 + k_{\text{y}}^2)/4} e^{-i(k_{\text{x}} * dx + k_{\text{y}} * dy)} \tag{11}$$

where k_x and k_y are the components of the spatial frequency $\mathbf{k}$, and dx and dy are the displacement vector components of the receptive field from the center of the visual field. A is the amplitude, and a is again the width parameter of the Gaussian function.

In panel (a) in figure 2, the amplitude of the Gaussian is denoted by A. The amplitude is the height of the peak of the curve. It tells the strength and sign of the response when the receptive field is illuminated. A positive sign means that the response will be exited by illumination. This is referred to as an ON-response or an ON-type region of the receptive field (Dayan & Abbot, 2001; Rodieck, 1965). If the sign should be negative, this means that the response is excited when the receptive field is covered by darkness, and suppressed if illuminated (Rodieck, 1965; Einevoll & Plesser, 2002).

Furthermore, the DOG function is defined as

$$f(\mathbf{r}; A, a, B, b) = \frac{A}{\pi a^2} e^{-a^2/r^2} - \frac{B}{\pi b^2} e^{-b^2/r^2} \tag{12}$$

with A being the center amplitude, B the surround amplitude, and a and b the width parameters of the center and surround receptive field, respectively (M. H. Mobarhan et al., 2018). Compared with the definition of the Gaussian kernel, the pattern of DOG is revealed as the subtraction of the Gaussian function of the surround from the Gaussian function of the center. This structure was first proposed by Rodieck (1965). An illustration of the DOG kernel and the two Gaussians which contribute to the function are is shown in panel (b) in figure 2.

The center represents the ON-type region of the receptive fields, whereas the surround represents the OFF-type (Rodieck, 1965). ON-regions of receptive fields are positions in the visual field that will trigger a positive response if the position is illuminated, suppressed if covered by darkness. The OFF-field behaves in the opposite way. This means that the maximum response is achieved if the center is covered by an iso-luminant spot of the same diameter (Myklebust, 2020; Einevoll & Plesser, 2005; Rodieck, 1965). If the diameter of the spot should expand outside the ON-center, it will exhibit surround suppression since the OFF-surround then will be covered in light (Myklebust, 2020; Einevoll & Plesser, 2005; Rodieck, 1965).

If the width parameter of the ON center should be wider than the surround, the antagonism switches to an OFF-center receptive field. In this case, maximum response is achieved when the center is covered in darkness, and the surround is illuminated.

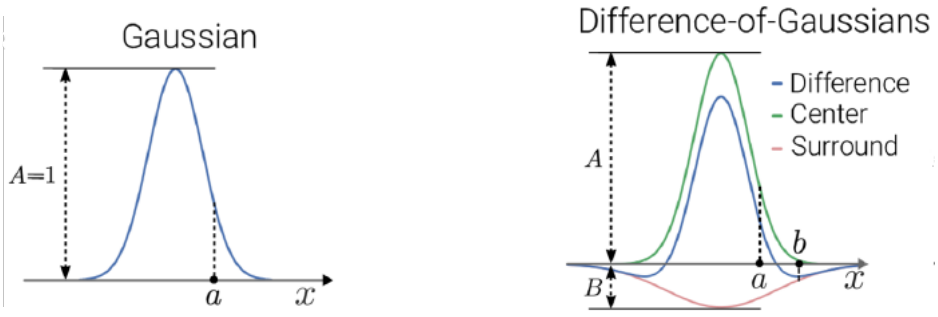

(a) (b)

Figure 2: M. H. Mobarhan et al. (2018). (a) The Gaussian function is described by the parameters A, its amplitude, and a, its width parameter along the x-axis of the visual field. (b) The parameters A and B describe the amplitude of the center and surround Gaussian, respectively. a and b are the corresponding width parameters along the x-axis. An ON-centered DOG has b larger than a. Figures from Mobarhan et al. (2018), Firing-rate based network modeling of the dLGN circuit: Effects of cortical feedback on spatiotemporal response properties of relay cells, *PLOS Computational Biology*. doi: https://doi.org/10.1371/journal.pcbi.1006156.

The Fourier transform of the DOG kernel is

$$\tilde{f}(\mathbf{k}) = Ae^{-k^2a^2/4} - Be^{-k^2b^2/4} \tag{13}$$

for the spatial frequency $\mathbf{k}$. A, B, a and b have the same interpretation as explained for equation 12 (Einevoll & Plesser, 2005; Enroth-Cugell & Robson, 1966).

A model for the spatial receptive field of cells in V1 was proposed by Hubel and Wiesel (1962). Their model for simple cells in V1 suggests that alternating rows of ON- and OFF-fields from the LGN provide input to a single V1 cell. This is simply a sum of receptive fields from LGN, which form a directed and elongated shape of the V1 receptive field (Dayan & Abbot, 2001; Einevoll & Plesser, 2012; Hubel & Wiesel, 1962). Illumination along the direction of the elongated field would give a maximum response since most of the ON-contributions from LGN would be covered in light (Hubel & Wiesel, 1962). Consequently, V1 cells achieve selectivity for orientation of grated stimuli.

There are several suggestions for how the receptive field of the V1 cells could be modeled, based on the proposal by Hubel and Wiesel (1962). In this thesis, the elongated shape of the receptive field is defined as an elliptic Gaussian function, according to the derivations done by Einevoll and Plesser (2012).

The ellipse is defined in real space as

$$f_{\mathrm{rc_nr}}(\mathbf{r}) = \frac{C_{\mathrm{rc_nr}}}{\pi\sigma_\mathrm{l}\sigma_\mathrm{n}} e^{-(x\cos\theta_\mathrm{n}+y\sin\theta_\mathrm{n})^2/\sigma_\mathrm{l}^2-(y\cos\theta_\mathrm{n}-x\sin\theta_\mathrm{n})^2/\sigma_\mathrm{n}^2} \tag{14}$$

where $C_{\mathrm{rc_nr}}$ is the loop coupling strength, σ_n and σ_l are the lengths of the narrow axis and long axis,

respectively, θ_n is the orientation of the ellipse relative to the x-axis, and x and y give the center position (Einevoll & Plesser, 2012). In the Fourier domain, this equation is

$$f_{rc_nr}(\mathbf{k}) = C_{rc_nr} e^{-(k_x \cos\theta_n + k_y \sin\theta_n)^2 \sigma_l^2/4 - (k_y \cos\theta_n - k_x \sin\theta_n)^2 \sigma_n^2/4} \tag{15}$$

where the spatial receptive field is a function of spatial frequency $\mathbf{k}$, and k_x and k_y represent the x- and y-components of $\mathbf{k}$ (Einevoll & Plesser, 2012).

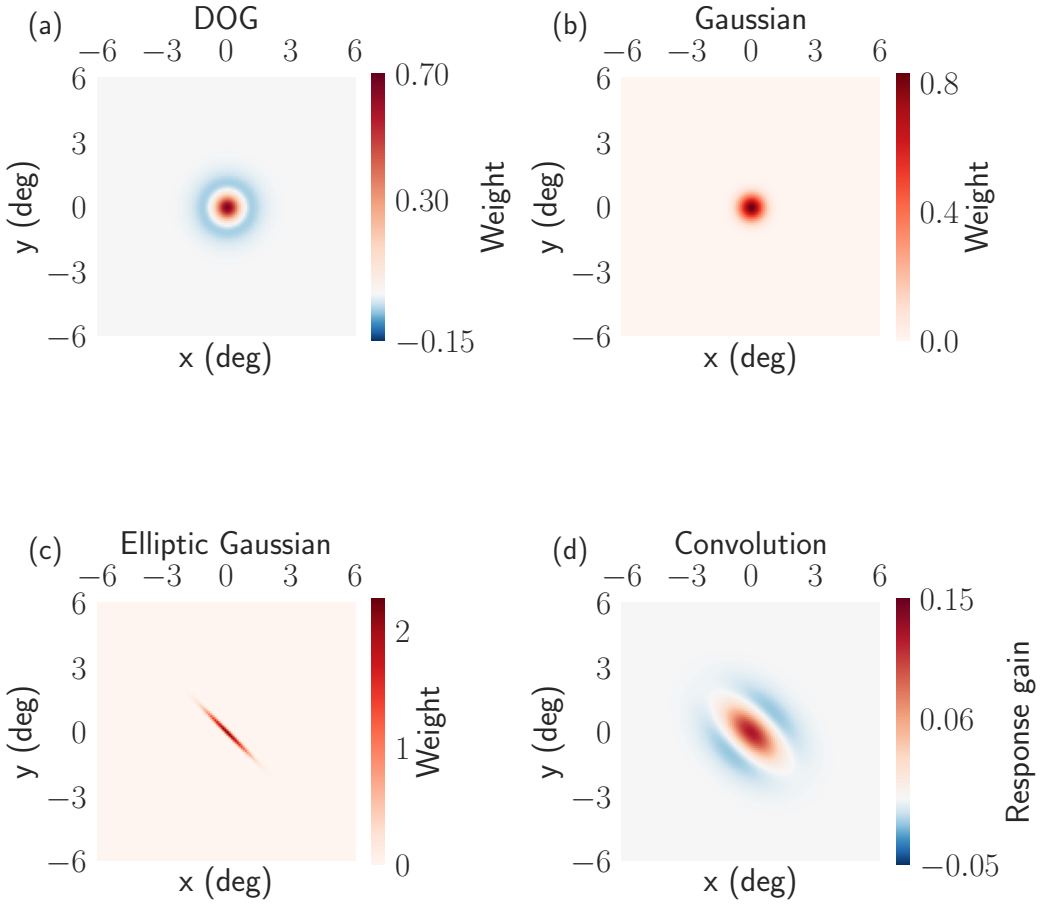

Figure 3: Image representation of the different spatial kernels included and their convolution as expected for cortical cells. Positive values indicate that the response gain would be positive when covered in light. Negative values yield negative gain in response. (a) The DOG function with parameters $A = 1$, $a = 0.62$ deg, $B = 0.85$ and $b = 1.26$ deg. (b) The Gaussian function with the parameters $A = 1$ and $a = 0.62$ deg. (c) The elliptic Gaussian function with the parameters $A = 1$, $\sigma_n = 0.1$ deg, $\sigma_l = 1.4$ deg, and $\theta = \pi/4$ rad. (d) The convolution of the three kernels.

Figure 3 shows image representations of how the kernels look in the spatial xy-plane. The col-

ormap is adjusted for the four images in the figure separately to give a clear indication of the weight from each kernel. The convolution is the combination of the DOG, Gaussian, and elliptic Gaussian, yielding the gain expected for the response of the cortical cells. However, the loop and combination of excitatory and inhibitory kernels are not included, which means that this is just a simplified image of how the convolutions form the response gain in cortical cell populations.

The operation is done in the Fourier domain, but by inverse transforming back to real space, it is possible to see how the kernels form the response in real space. The ON- and OFF-fields are "smoothed" out in an elongated shape by the convolution. The orientation of this "smoothing" is dependent on the orientation of the longest axis of the elliptic Gaussian function.

When cortical cell responses are computed, a rectification is included. This means that the negative responses for cortical cells will be set to zero. Illumination of the flanks would cause a dampening of the response in cortical cells. However, this will never go below zero because of the rectification.

2.4 Temporal component of the receptive field

The Dirac delta function

$$h(t; \Delta_{\text{delta}}) = \delta(t - \Delta_{\text{delta}}) \tag{16}$$

is the simplest choice of temporal connection kernel, and represents the temporal dynamics without any dispersion (Einevoll & Plesser, 2002; Norheim et al., 2012). Δ_{delta} corresponds to the delay of the signal (Einevoll & Plesser, 2002). This kernel passes on the signal without any modifications, other than a possible delay by the Δ_{delta} parameter. The delta function is normalized and weighs all frequency contributions equally.

Its Fourier transform is

$$\tilde{h}(\omega) = e^{i\Delta_{\text{delta}}\omega}, \tag{17}$$

as implemented in PyLGN.

However, the exponential decay kernel, defined as

$$h(t; \Delta_{\text{exp}}, \tau) = \frac{1}{\tau} e^{-(t-\Delta_{\text{exp}})/\tau} \Theta(t - \Delta_{\text{exp}}), \tag{18}$$

describes the signal as damped over time (Norheim et al., 2012; Einevoll & Plesser, 2002). This can be considered a more realistic way to model signal propagation over time than delta functions (Einevoll & Plesser, 2002). An illustration of the exponential kernel as a function of t is shown in panel (a) in figure 4.

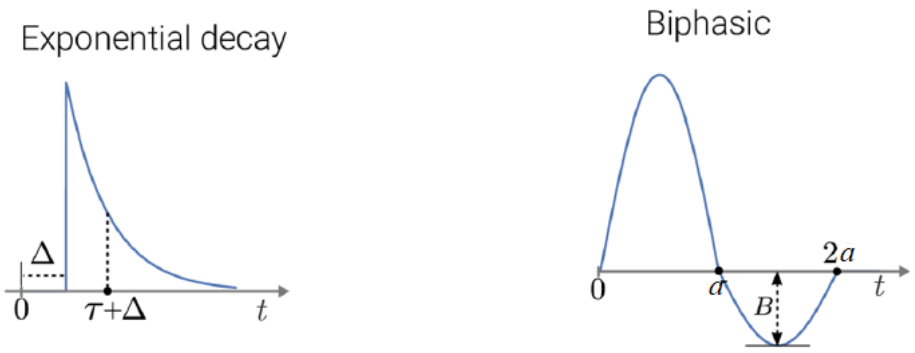

(a) (b)

Figure 4: M. H. Mobarhan et al. (2018). (a) The parameters Δ_{exp} and τ form the exponential decay temporal kernel. Δ_{exp} determines the delay of the response along the time axis. τ controls the steepness of the curve by setting the point on the time axis where the curve has dropped by a factor of 1/e of the maximum value. (b) Figure from M. H. Mobarhan et al. (2018), modified to include parameter a. The biphasic temporal kernel is determined by the parameters B and a. B decides the amplitude of the second phase, and a is the time duration of both phases. Figures from Mobarhan et al. (2018), Firing-rate based network modeling of the dLGN circuit: Effects of cortical feedback on spatiotemporal response properties of relay cells, *PLOS Computational Biology*. doi: https://doi.org/10.1371/journal.pcbi.1006156.

Δ_{exp} represents a combination of the axonal and synaptic delay (Einevoll & Plesser, 2002), and is measured in ms. Θ is the Heaviside step function (M. H. Mobarhan et al., 2018; Einevoll & Plesser, 2002). Θ is zero if $t - \Delta_{exp}$ is negative, which means that the time of the response has not happened yet at time t. Thus, the Heaviside step function assures that the time propagated since stimulus has reached the delay before the response is generated. τ decides how the duration changes during simulation (M. Mobarhan, 2018). The value of τ forms the damping steepness of the signal over time, by deciding at what time the curve has been reduced by a factor of 1/e.

The Fourier transform of the exponential decay kernel is

$$\tilde{h}(\omega) = \frac{e^{i\Delta_{exp}\omega}}{1 - i\tau\omega} \tag{19}$$

(Einevoll & Plesser, 2002). The function is now dependent on the temporal angular frequency ω.

According to studies done to investigate the temporal dynamics of LGN, the observed response has a biphasic nature (Yousif & Denham, 2007; Cai et al., 1997; Reid et al., 1997). When the temporal kernel is biphasic, this means that the polarities of the center and surround of the receptive fields reverse over time (Yousif & Denham, 2007; Cai et al., 1997).

The definition of the biphasic kernel is

$$h(t; a, B) = \begin{cases} sin(\pi t/a), & \text{for } 0 \leq t \leq a \\ Bsin(\pi t/a), & \text{for } a < t \leq 2a \\ 0 & \text{otherwise} \end{cases} \tag{20}$$

B is the weight of the second phase, and a is the duration of each phase (Norheim et al., 2012; M. H. Mobarhan et al., 2018).

In the Fourier domain, the biphasic kernel is defined as

$$h(\omega; a, B) = \frac{\pi a}{\pi^2 - a^2\omega^2} e^{i\Delta_{\text{biph}}\omega}(1 + (1 - B)e^{ia\omega} - Be^{ia2\omega}) \tag{21}$$

.

The phases are visualized in panel (b) in figure 4. The first phase covers the time from 0 to a in the figure. In cells with DOG receptive fields, this part of the duration is when the cell center acts as an ON-center. Bright stimuli covering the center will cause a positive response. When the duration passes the time a, the cell shifts from being an ON-center to an OFF-center (Yousif & Denham, 2007). Bright stimuli covering the center will, in this case, cause a negative response. The weight B decides how strong the negative response will be in this phase.

2.5 Model of the early visual system and feedback - eDOG

eDOG is based on the response computations with the impulse-response functions along with the DOG model. A central part of the model is the inclusion of the feedback loop, with the assumption that it gives a phase-reversed push-pull effect on LGN cells (Einevoll & Plesser, 2012; Wang et al., 2006). This means that both ON-cells and OFF-cells from V1 contribute to the inhibitory and excitatory feedback respectively, to an LGN relay cell (Einevoll & Plesser, 2012).

The feedback on one relay cell comes from both ON- and OFF-cells from V1, but these cortical cells are dependent separately of ON- and OFF-centered relay cells respectively. This means that the full eDOG model of the early visual system has an ON-pathway and OFF-pathway. The only connection between those two is the feedback from the cortical cells in the OFF-pathway to the ON-centered relay cells and opposite.

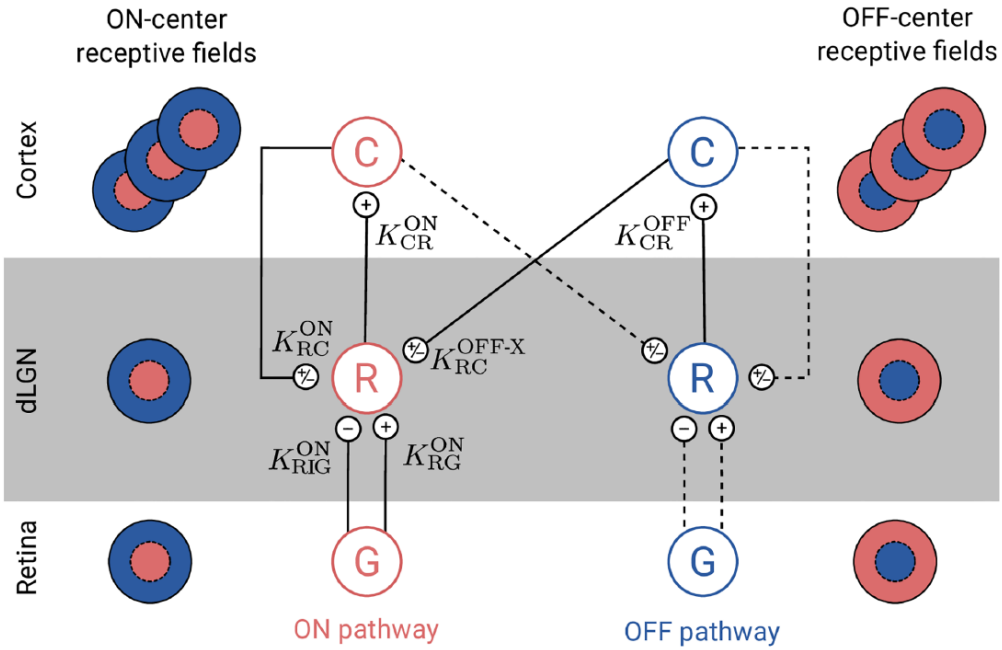

Figure 5: M. H. Mobarhan et al. (2018). The ON and OFF pathway and the cross-connection between them are shown in the figure. The nodes each represent the cell type, *G* for retinal ganglion cells, *R* for relay cells, and *C* for cortical cells. The spatial receptive field structures are represented on each side of the figure. All kernel connections are shown, where $+$ means that the connection is excitatory and $-$ means that it is inhibitory. The solid lines indicate which connections are included in the simulations in this thesis. Figure from Mobarhan et al. (2018), Firing-rate based network modeling of the dLGN circuit: Effects of cortical feedback on spatiotemporal response properties of relay cells, *PLOS Computational Biology*. doi: https://doi.org/10.1371/journal.pcbi.1006156.

By considering only the ON-pathway, it is possible to derive the ON-centered relay-cell response. This includes both excitatory and inhibitory feedforward signals from retinal ganglion cells and the feedback from both ON- and OFF-cells. The OFF-centered relay cell response can be derived similarly, considering the OFF-pathway instead (M. H. Mobarhan et al., 2018).

Equation 2 can be adjusted to represent the relay cell response. This is done by letting the stimulus be the output from both ganglion and the feedback, and the impulse-response function be the kernel connecting the cells. The feedforward signals from retinal ganglion cells can, for example, be expressed as

$$R_{\mathrm{R}}^{\mathrm{ON}} = K_{\mathrm{RG}}^{\mathrm{ON}} * R_{\mathrm{G}}^{\mathrm{ON}} + K_{\mathrm{RIG}}^{\mathrm{ON}} * R_{\mathrm{G}}^{\mathrm{ON}}, \tag{22}$$

where $R_{\mathrm{G}}^{\mathrm{ON}}$ is the ganglion output due to stimulus, $K_{\mathrm{RG}}^{\mathrm{ON}}$ and $K_{\mathrm{RIG}}^{\mathrm{ON}}$ are the kernels connecting the excitatory and inhibitory output of the ganglion cells to the relay cells, respectively (M. H. Mobarhan et al., 2018).

Furthermore, the feedback to the relay cell consists of the sum of N populations of orientation-selective V1 cells, including both ON- and OFF-cells. The N cell populations are each denoted as C_n with $n = 1, 2, 3, ..., N$. The respective kernels connecting the ON/OFF populations to the relay cells are denoted as $K_{RC_n}^{ON/OFF}$ (M. H. Mobarhan et al., 2018).

The phase-reverse of the feedback means that the feedback from ON-cells in the direct feedback connection and OFF-cells in the feedback cross-connection have opposite signs (M. H. Mobarhan et al., 2018). This means that the kernels corresponding to the OFF-cell feedback cross-connection $K_{RC_n}^{OFF-x}$ (OFF $-$ x denotes that the OFF-feedback to the relay cells in the ON-pathway is a cross-connection between the two pathways), can be rewritten as $-K_{RC_n}^{ON}$ (M. H. Mobarhan et al., 2018).

The response of the V1 cells serves as input for the relay cells through the feedback. In order to derive the response of relay cells, including the feedback, the expression for V1 cortical response due to feedforward signals from relay cells is needed. In fact, there is a non-linearity included in the response of cortical cells (M. H. Mobarhan et al., 2018). It can be expressed as

$$R_{C_n}^{ON/OFF} = H[K_{C_nR}^{ON/OFF} * R_R^{ON/OFF}] \tag{23}$$

where the H stands for the half-wave rectification of the response. This is the non-linearity that assures that the response of cortical cells is never negative (M. H. Mobarhan et al., 2018).

Assuming that the response of OFF-cells has opposite sign than ON-cells, the response of the OFF-cells in V1 can be rewritten as

$$R_{C_n}^{OFF} = H[-K_{C_nR}^{ON} * R_R^{ON}] \tag{24}$$

(M. H. Mobarhan et al., 2018).

The total relay response can be summed up in the expression

$$R_R^{ON} = K_{RG}^{ON} * R_G^{ON} + K_{RIG}^{ON} * R_G^{ON} + \sum_n K_{RC_n}^{ON} * R_{C_n}^{ON} + \sum_n K_{RC_n}^{OFF-x} * R_{C_n}^{OFF} \tag{25}$$

(Einevoll & Plesser, 2012; M. H. Mobarhan et al., 2018).

As a consequence of the assumptions mentioned, the equation can be simplified and expressed in the Fourier domain as

$$\tilde{W}_R^{ON} = \frac{\tilde{K}_{RG}^{ON} + \tilde{K}_{RIG}^{ON}}{1 - \sum_n \tilde{K}_{RC_n}^{ON} \tilde{K}_{C_nR}^{ON}} \tilde{W}_G^{ON} \tag{26}$$

using the fact that $\tilde{R}(\mathbf{k}, \omega) = \tilde{W}(\mathbf{k}, \omega)\tilde{S}(\mathbf{k}, \omega)$ from equation 3.

This response is what serves as the only input to the cortical V1 cells in the model. Thus, a change in the relay cell response is expected to affect the cortical cell response.

The sum of the cortical elliptic receptive fields in the loop can be simplified into a circular Gaussian function. This is possible because, as ellipses of different orientations are summed, the shape approximates a circle, as shown in figure 6.

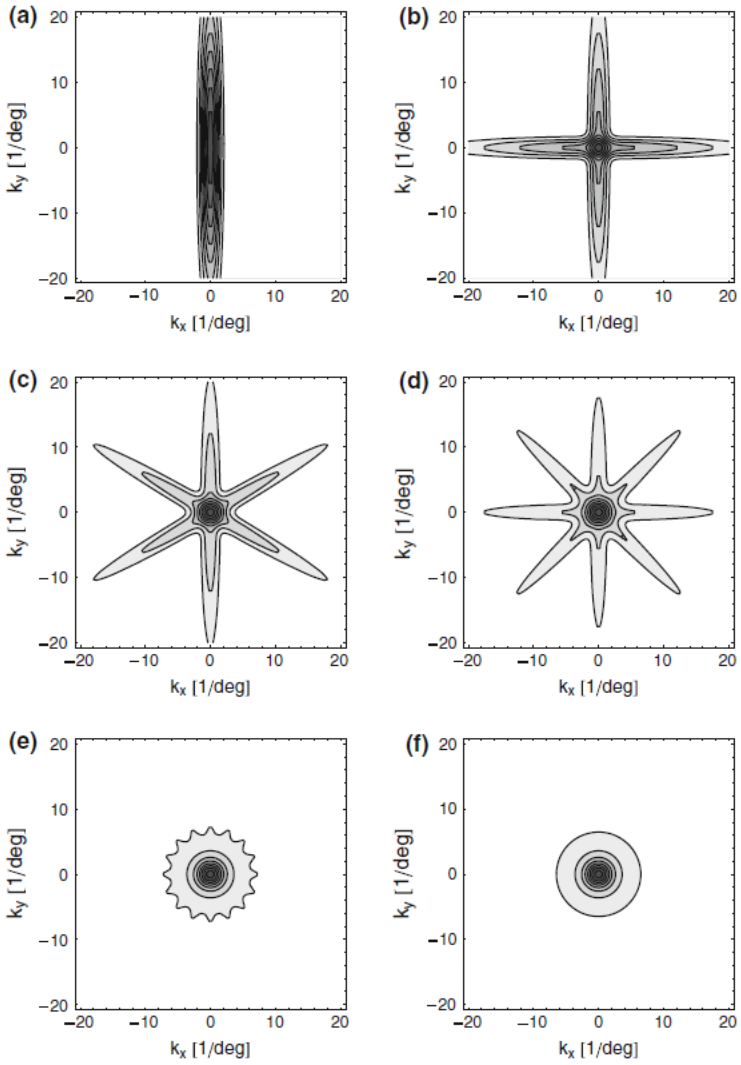

Figure 6: Einevoll and Plesser (2012). The summation in the Fourier domain of elliptic Gaussian functions of different orientations approximate a circular shape. From panel (a) to panel (e) an increasing number of radially oriented ellipses are summed. In panel (e), there are eight number of ellipses, and these are already well on the way to approximate a circular shape. Panel (f) shows a sum of infinite many ellipses. The width parameters of the elliptic Gaussian, from equation 15, used to produce the figure are $\sigma_n = 0.1$ deg, and $\sigma_l = 1.4$ deg. Figure from Einevoll, G. T., & Plesser, H. E. (2012). Extended difference-of-Gaussians model incorporating cortical feedback for relay cells in the lateral geniculate nucleus of cat. *Cognitive Neurodynamics, 6*, 307-324. doi: https://doi.org/10.1007/s11571-011-9183-8.

eDOG enables the response of the LGN cells to modeled linearly even though the cortical cell responses contain nonlinearities. The impulse-response function of relay cells with the feedback included in eDOG maintains the linearity by filtering input without changing the frequencies. Thus, it ensures that the response can be computed from any input. Responses to sinusoidal gratings have been observed to be sinusoidal as well, and a linear model will be able to predict such responses (Carandini et al., 2002; Movshon et al., 1978b).

2.6 Stimuli

Visual stimuli commonly used are simple shapes of light and dark varying in space and time, such as the counterphase sinusoidal grating (Dayan & Abbot, 2001). The cells of the visual cortex respond the most vigorously to flashing and moving bars and gratings (Dayan & Abbot, 2001). Sinusoidal gratings are a type of stimuli that suit well for the modeling of visual stimuli, because of the linearity of the kernels (Sherman, 1996). Linear summation is common among simple cells and not complex cells (Movshon, Thompson, & Tolhurst, 1978a; DeAngelis, Ohzawa, & Freeman, 1993; Dayan & Abbot, 2001). The terms simple and complex cells were first described by Hubel and Wiesel (1962), to distinguish between cell properties in modeling. The main difference is that simple cells can be divided into separate ON- and OFF-regions, a linear model can describe their properties. Complex cells can not be divided into these regions and are not compatible with linear models (Dayan & Abbot, 2001). However, the model considered in this thesis is only based on simple cells.

Full-field grating

A full-field grating is a counterphase sinusoidal grating defined as

$$s_{\mathrm{fg}}(x, y, t) = C_{\mathrm{fg}} cos(k_{\mathrm{fg}} \cos(\theta_{\mathrm{fg}})x + k_{\mathrm{fg}} \sin(\theta_{\mathrm{fg}})y - \omega_{\mathrm{fg}} t) \tag{27}$$

(Dayan & Abbot, 2001; M. H. Mobarhan et al., 2018).

The spatial properties of the grating are defined by the wavenumber k_{fg}, contrast C_{fg}, and orientation θ_{fg}. Equation 27 can be reformulated to include the spatial phase ϕ as well. The temporal part of the stimulus is defined by the temporal angular frequency ω_{fg}.

The wavenumber is related to the wavelength λ of the sinusoidal by means of $\lambda = 2\pi/k$. Usually, the wavenumber is measured in cycles per degree since the spatial coordinates often are measured in degrees (Dayan & Abbot, 2001). The phase is measured in radians and is the parameter that shifts the phase of the grating along the direction perpendicular to the grating orientation (Dayan & Abbot, 2001). C_{fg} is a dimensionless number describing the contrast amplitude (Dayan & Abbot, 2001). The orientation θ_{fg} is measured in degrees and describes the tilt of the grating relative to the x-axis (Dayan & Abbot, 2001).

The temporal angular frequency is related to the frequency f of the grating by the relation $\omega = 2\pi f$ (Einevoll & Plesser, 2005), and is measured in rad/ms.

Visualization of the full-field grating can be done in two dimensions as a square filling the visual field with light and dark stripes, as illustrated in panel (a) in figure 7. The full-field grating in the illustration has the parameters $C_{fg} = 1$, $k_{\mathrm{fg}} = 2.45$ /deg, $\omega_{\mathrm{fg}} = 0$ rad/ms and $\theta_{\mathrm{fg}} = 90$ deg.

Its Fourier transform is

$$\begin{aligned}\tilde{s}_{\mathrm{fg}}(\mathbf{k},\omega) =& 4\pi^3 C_{\mathrm{fg}}[\delta(k_{\mathrm{x}}, k_{\mathrm{fg}}\cos\theta_{\mathrm{fg}})\delta(k_{\mathrm{y}}, k_{\mathrm{fg}}\sin\theta_{\mathrm{fg}})\delta(\omega,\omega_{\mathrm{fg}}) \\ &+ \delta(k_{\mathrm{x}}, -k_{\mathrm{fg}}\cos\theta_{\mathrm{fg}})\delta(k_{\mathrm{y}}, -k_{\mathrm{fg}}\sin\theta_{\mathrm{fg}})\delta(\omega,-\omega_{\mathrm{fg}})]\end{aligned} \tag{28}$$

in PyLGN (M. H. Mobarhan et al., 2018). k_{fg} is the wavenumber of the stimulus, and k_{x} and k_{y} are the spatial frequencies of the visual field grid. ω is the temporal angular frequency in the temporal dimension of the same grid. θ_{fg} is the orientation of the stimulus grating, and ω_{fg} is the temporal angular frequency of the stimulus. The Kronecker delta δ is a function that evaluates whether the difference between its inputs is small enough to be considered equal. If so, the function is 1.0, otherwise, it is 0.

For each spatial frequency k_{x} and k_{y}, the stimulus value is computed. Suppose the combination of the wavenumber and orientation is equal to the point considered in the spatial frequency grid. In that case, the Kronecker delta function is 1.0 and allows for a nonzero stimulus value to be computed. The same procedure happens with the temporal frequencies.

Patch grating

The full-field grating described above is actually a special case of the patch grating stimulus. The patch grating is described in the equation

$$s_{\mathrm{pg}}(\mathbf{r},t) = C_{\mathrm{pg}}[1-\Theta(\mathbf{r}-d_{\mathrm{pg}}/2)]cos(\mathbf{k}_{\mathrm{pg}}\mathbf{r}-\omega_{\mathrm{pg}}t). \tag{29}$$

with C_{pg} as the contrast of the patch grating, d_{pg} the patch grating diameter, k_{pg} the patch grating wave vector and ω_{pg} the temporal angular frequency (Einevoll & Plesser, 2005; M. H. Mobarhan et al., 2018). $\mathbf{r}$ is the position and is defined as $\mathbf{r} = \sqrt{x^2+y^2}$. Θ denotes the Heaviside step function. The Heaviside step-function creates the patch by evaluating the position $\mathbf{r}$ relative to the diameter d_{pg}. If the position $\mathbf{r}$ is inside the diameter, the stimulus is a sinusoidal grating. Otherwise, the stimulus is zero.

The patch grating is visualized in panel (b) in figure 7. The pattern shows a circular patch with a sinusoidal grating with the parameters $C_{\mathrm{pg}} = 1$, $d_{\mathrm{pg}} = 5.0$ deg, $k_{\mathrm{pg}} = 2.45$ /deg, $\omega_{\mathrm{pg}} = 0$ rad/ms and θ_{pg}.

By letting the diameter d_{pg} go to infinity, this limit can be considered as a full-field grating (Einevoll & Plesser, 2005; M. H. Mobarhan et al., 2018).

The Fourier transform of a patch grating is

$$\tilde{s}_{\mathrm{pg}}(\mathbf{k},\omega) = 2\pi^2 d_{\mathrm{pg}} C_{\mathrm{pg}} \frac{J_1(|\mathbf{k}-\mathbf{k}_{\mathrm{pg}}|d_{\mathrm{pg}}/2)}{|\mathbf{k}-\mathbf{k}_{\mathrm{pg}}|}\delta(\omega-\omega_{\mathrm{pg}}) \tag{30}$$

(Einevoll & Plesser, 2005).

In this case, J_1 represents the first-order Bessel function, and the delta-function δ is included. The difference between ω and ω_{pg} must be zero for the delta function to be 1.0. Otherwise, it is zero. The orientation of the grating is decided by the combination of the orientation and wavenumber,

by the same principles as for the full-field grating. For the full-field grating, the spatial frequencies k_{fg} for the stimulus itself are defined as a function of the wavenumber and orientation. This was which was written out in the Fourier transform of the full-field grating in equation 28. The equation of the patch grating (equation 30) is written in a more compact form with $\mathbf{k}$ as the spatial frequencies of the visual field grid, and $\mathbf{k}_{pg}$ as the wave vector. The wave vector represents the combination of the wavenumber and the orientation θ_{pg}.

Flashing spot

A flashing spot is a circular spot of the same stimulus intensity which is turned on and off during the simulation.

A flashing spot is given in real space in PyLGN as

$$s_{fs}(\mathbf{r}, t) = C_{fs}(1 - \Theta(\mathbf{r} - d_{fs}/2))(\Theta(t - \Delta_{fs}) - \Theta(t - \Delta_{fs} - dt)) \tag{31}$$

where C_{fs} is the flashing spot contrast, Θ is the Heaviside step function, Δ_{fs} is the delay, dt is duration, and d_{fs} is flashing spot diameter (M. H. Mobarhan et al., 2018). The definition can also be found in the paper by Einevoll and Plesser (2005), but this definition does not include the delay.

The Fourier transform of the flashing spot is included in PyLGN as

$$\tilde{s}_{fs}(\mathbf{k}, \omega) = C_{fs} d_{fs}^2 \frac{\pi}{4} dt \frac{\sin(\omega dt/2)}{\omega dt/2} e^{i\omega(\Delta_{fs} + dt/2)} \frac{J_1(\mathbf{k} d_{fs}/2)}{\mathbf{k} d_{fs}/2} \tag{32}$$

with $\mathbf{k} = \sqrt{k_x^2 + k_y^2}$, and J_1 being the first-order Bessel function (M. H. Mobarhan et al., 2018).

The plot of panel (c) in figure 7 is an example of how a flashing spot may look. During the simulation, the spot appears and vanishes as defined by the delay $\Delta_{fs} = 0$ ms and duration $dt = 20$ ms. The diameter d_{fs} of the spot is 5.0 deg and $C_{fs} = 1$.

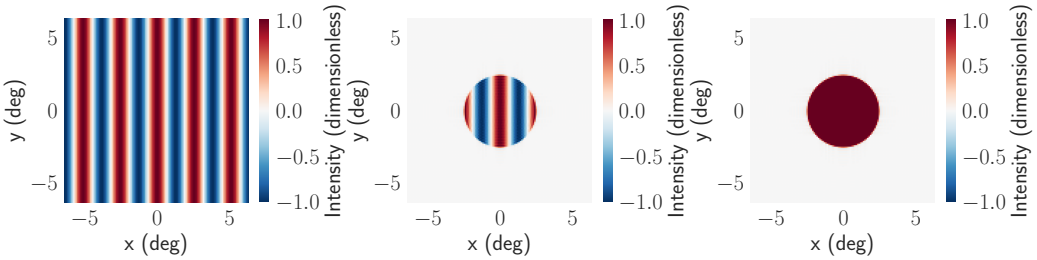

(a) (b) (c)

Figure 7: The main stimuli types in the spatial xy-plane in real space. The intensity values are dimensionless, and range from -1 for dark areas to 1 for light areas. (a) A full-field grating with $C_{fg} = 1$, $k_{fg} = 2.45$ /deg $\omega_{fg} = 0$ rad/ms and orientation $\theta_{fg} = 90$ deg. (b) A patch grating with $C_{pg} = 1$, $k_{pg} = 2.45$ /deg, $\omega_{pg} = 0$ rad/ms, $d_{pg} = 5.0$ deg and orientation $\theta_{pg} = 90$ deg. (c) A flashing spot of diameter $d_{fs} = 5.0$ deg, with contrast C_{fs}, duration $dt = 20$ ms and delay $\Delta_{fs} = 0$ ms.

Natural stimuli

Natural stimuli allow for an input image to be treated as a stimulus in PyLGN. However, this is only implemented for real space and not in the Fourier domain. This means that the responses to this stimulus are computed by numerical integration. PyLGN adjusts the image input such that it can be defined as a three-dimensional matrix of stimulus intensity values over space and time in real space.

2.7 Experimental findings and expected results for simulations

In the eDOG model, all input to the V1 cortical cells comes from direct feedforward signals from LGN (Einevoll & Plesser, 2012).

However, there are uncertainties as to what extent the loop effects dominate the V1 responses. Recurrent feedback between layers in the visual cortex can affect the cortical cell response to visual stimuli (Stettler et al., 2002; Angelucci & Bressloff, 2006; Adesnik et al., 2012; Nassi et al., 2013; Ozeki et al., 2009). However, Carandini et al. (2002) provide results suggesting that it is not the cortical network which accounts for the most important response properties of cortical cells but rather synaptic connections with the LGN.

On the contrary, Chung and Ferster (1998) conclude that the orientation selectivity of cortical cells is strong for the thalamic input, and that it is not determined by intracortical inputs. It may be a combination of both recurrent connections and feedforward signals that contribute to the selectivity in V1 (Ozeki et al., 2009).

The feedback loop effects on relay response in LGN are only dependent on magnitude and not orientation of stimuli (Einevoll & Plesser, 2012). This is caused by the summation of all contributions from the cortical cell populations in the eDOG model (Einevoll & Plesser, 2012). Orientation selectivity will thus only be a consequence of the elliptic Gaussian kernel in the simulation.

The cortical cells themselves are selective to orientation, spatial frequency, and direction of the stimulus (Ayzenshtat et al., 2016; Hubel & Wiesel, 1962; DeAngelis et al., 1993). The orientation of a receptive field can be determined from the response to the most effective stimulus (Hubel & Wiesel, 1962). In addition to the elongated shape of the receptive field, excitatory connections to other V1 cells with similar preferences contribute to orientation selectivity in V1 cells (Cudeiro & Sillito, 1996). These connections are not included in the simulation.

Ayzenshtat et al. (2016) found that the orientation selectivity also depended on the spatial frequency of the stimulus. This included not only the strength of the response, but also the preferred orientation. A common observation in LGN response is the shift between band-pass and low-pass from the cortical feedback. Cudeiro and Sillito (1996) suggested that the cortical cells have spatial frequency biases affecting preferred spatial frequencies in the LGN. Mixed inhibitory and excitatory connections from V1 were observed by M. H. Mobarhan et al. (2018) to cause a shift in the maximum response towards higher spatial frequencies in LGN.

Low-pass filtering means that the higher frequencies do not pass through the filter (Shapley & Lennie, 1985). However, a high-pass filter lets through the higher frequencies and removes the lower frequencies from the signal, whereas a band-pass filter is a combination of the two.

The shift between low-pass and band-pass is also observed for patch gratings of different diameters. eDOG shows this shift for relay cells as the stimulus changes from a small patch to a bigger one (M. H. Mobarhan et al., 2018). Patches with small diameter sizes express low-pass filtering of the signal, whereas the bigger diameters have band-pass filters (M. H. Mobarhan et al., 2018). This is in accordance with what has been observed for DOG in the paper by Einevoll and Plesser (2005). They observed low-pass characteristics for the same situation, with a response maximum for the lowest spatial frequencies (Einevoll & Plesser, 2005). Cudeiro and Sillito (1996) compared the spatial frequency preferences between patch gratings and full-field gratings. Low-pass characteristics which appeared in patch gratings were replaced by band-pass as the stimulus was changed into a full-field grating (Cudeiro & Sillito, 1996). Full-field gratings can be derived from patch gratings by letting the diameter go to infinity (Einevoll & Plesser, 2005). Thus, it is expected that the response patterns of increasingly bigger diameters approach the response of a full-field grating.

An interesting point in the cortical response is the effect of suppression. Suppression is inhibition of response due to stimulus, and is typically observed when an ON- or OFF-region gets covered by non-optimal light conditions. Surround suppression is a common phenomenon in cells with DOG receptive fields. One way to provoke strong surround suppression, in for example an ON-center cell, is by gradually increasing the diameter of an iso-luminant spot. When the diameter of the spot expands outside the ON-center, such that the OFF-surround gets covered in light, the response of the cell is suppressed (Einevoll & Plesser, 2005; M. H. Mobarhan et al., 2018; Hubel & Wiesel, 1962).

Surround suppression is also observed for drifting patch gratings, but this is highly dependent on the spatial frequency of the grating pattern in the patch (Einevoll & Plesser, 2005; Myklebust, 2020). In contrast to iso-luminant spots, patch gratings may even show surround enhancement (Einevoll & Plesser, 2005).

Based on what happens of suppression in DOG cells, is it possible that the cortical cells would inherit the suppression effects from the feedforward connection of the relay cells? This was tested for another model referred to as the Allen model in the master thesis by Myklebust (2020). Originally, this is a model on mouse V1 and LGN developed by the Allen Institute of Brain science and is described in the paper (Billeh et al., 2020).

The Allen model did not show strong suppression in the V1, which deviated from what was found in experiments (Myklebust, 2020). The Allen model is center-only based, and the argument is that modification is needed for this model to catch suppression effects. The first modification was to modify the Allen model into a center-surround structure, like DOG. This modification was able to take into account suppression and band-pass tuning in both LGN and V1. However, this was only applicable to iso-luminant spots (Myklebust, 2020). The second modification needed to take into account non-linear suppression. Normalization of the firing rates showed inheritance of suppression in V1 from LGN, but there are probably several mechanisms behind these effects (Myklebust, 2020).

Recurrent connections in V1 may affect the suppression effects as well as orientation selectivity. Suppression in one neuron in V1 may be caused by the connections from other V1 neurons selective for other orientations (Carandini et al., 2002). These effects are not included in the linear eDOG model. Thus, such effects are not expected to be observed in the simulations.

Surround suppression was observed by Einevoll and Plesser (2005) in the relay response for both

flashing spots and patch gratings. The DOG model was used in this paper, and it can be a good candidate for showing the inheritance of suppression in V1. By the direct connection between relay cells and cortical cells in eDOG, it is expected that suppression is observed in V1.

Feedback weights included in the eDOG model were changed in the paper by M. H. Mobarhan et al. (2018) to see if they could produce significant changes in the response of relay cells. Feedback effects have been observed to have an effect on LGN relay cell response in many experimental studies, as discussed in sections 1.3 and 1.4. The results of feedback weights in the paper by M. H. Mobarhan et al. (2018) showed that the feedback modulates the center-surround antagonism of the relay cells (M. H. Mobarhan et al., 2018). Mixed feedback consisting of both excitatory and inhibitory feedback connections can increase the excitation of the center and the inhibition in the surround in an ON-centered relay cell.

Nassi et al. (2013) confirmed that the inactivation of cortical feedback significantly reduced surround suppression in V1. Furthermore, V1 cell responses increased for large stimuli by inactivation (Nassi et al., 2013). Thus, it seems feedback mechanisms from the loop affects responses not only in LGN, but also significantly in V1.

Suppression was observed to be stronger for patch gratings experiencing increasingly stronger mixed feedback weights than for static spots (M. H. Mobarhan et al., 2018). A difference in surround suppression has also been observed between patch gratings and flashing spots (Einevoll & Plesser, 2005). In the paper by Sillito and Jones (2002) removal of the cortical feedback led to a significant reduction in surround suppression for patch gratings for the largest diameters.

Feedback is known to change the optimal diameter of patches as well, but experiments have shown various results. Andolina et al. (2013) observed that with feedback present, shifts of the preferred diameter went to smaller sizes. However, this contradicts with results from Webb et al. (2002) and Przybyszewski et al. (2000).

In natural images, the tendency is that feedback sharpens the receptive fields of relay cells (M. H. Mobarhan et al., 2018). With mixed feedback, the selectivity for spatial frequencies is shifted towards higher frequencies (M. H. Mobarhan et al., 2018). The areas in a natural image with high frequencies are the areas with big differences in luminance. This means that in a natural image, the edges of the image will be the most prominent information being passed on to the cortical cells (M. H. Mobarhan et al., 2018). Neurons in V1 are most responsive to edges (Ayzenshtat et al., 2016). Thus, it is expected that the edges of a natural image will cause the highest responses in V1.

Moving stimuli are the most effective stimuli (Hubel & Wiesel, 1962). Thus, the maximum response of a stimulus is expected to be higher if the stimulus is moving rather than static. An explanation is that the synergism of a stimulus leaving an OFF-area and at the same time entering an ON-area (Hubel & Wiesel, 1959) enhances the maximum response. When considering moving gratings, direction selectivity has been observed in cortical cells (Usrey et al., 2009; Wilent & Contreras, 2005). Direction selectivity is enabled for cells with non-separable receptive fields (Dayan & Abbot, 2001). This means that the direction the grating of the stimulus moves causes different responses in cells with different preferences of direction. However, non-separable kernels are not included in the simulation.

Carandini et al. (2002) suggest that depression of the synaptic connections between the LGN relay cells and cortical cells contributes to gain control of cortical responses. The synaptic signal can be depressed based on the activity level (Citri & Malenka, 2008). This is an example of an effect that

may appear over a time interval. It represents, however, synaptic plasticity, which is not included in the simulation.

With moving stimuli, temporal kernels, and simulations driven over a specific time interval, temporal effects take part in the response patterns. The temporal kernels of the cell types in the early visual system decide how the cells respond to the different stimuli over time.

According to studies, the LGN temporal receptive field has a biphasic nature (Yousif & Denham, 2007; Cai et al., 1997; Reid et al., 1997). The amplitude of the biphasic kernel cause gain effects in the cell response. Furthermore, the amplitude changes during the time course, and thus, polarity shifts sign between the two phases. As the time course passes, gain effects from the biphasic kernel are expected to determine the magnitude of the responses.

The exponential decay kernels can filter out the highest frequencies, only letting the lowest frequencies pass on. The filtering rather outputs the low frequent patterns of a signal, and removes high frequent fluctuations. The exponential decay kernels thus work as low-pass filters.

The temporal behaviour of cells in the early visual system is, in reality, more varying and complex than what will be considered in this thesis. Usually, different temporal profiles have been used on the center and surround (Dayan & Abbot, 2001), and the biphasic kernels of LGN cells often differ in shape and phase duration (Allen & Freeman, 2006; Alitto & Usrey, 2015). Non-separable spatiotemporal receptive fields and nonlinear effects exist (Dayan & Abbot, 2001), and some of the effects and functions still remain to be studied. It is, for example, proposed that the temporal behaviour of ganglion retinal cells and LGN are dependent on contrast and surround suppression However, these effects are nonlinear (Alitto & Usrey, 2015).

eDOG is a linear model. Moreover, the kernels are separable in space and time. Thus, the effects of the temporal kernels in the simulations are expected to affect temporal frequencies and response magnitude, independently of the spatial receptive fields. Nevertheless, there is a claim that the feedback is expected to sharpen the temporal precision of LGN responses (Hasse & Briggs, 2017), which is supposed to transmit further in the feedforward connection to the cortical cell layer (Hasse & Briggs, 2017).

3 Materials and methods

3.1 Short on how PyLGN models the whole system

PyLGN makes it possible to create a network based on the three different cell types in the early visual system; retinal ganglion cells, LGN relay cells, and cortical cells in the visual cortex V1. The neuronal layers are connected inside the network through user-defined kernels, each with user-defined synaptic weights.

The kernels decide how the response for one cell type affects the input of the next cell type in the connection. Their purpose is to model the receptive fields of each cell type, and form responses due to input signals. Different types of stimuli can be added to the network and incorporate into the computation of the response. This happens mainly in the Fourier domain. The Fourier transformed stimulus matrix is element-wise multiplied with the Fourier transformed impulse-response function evaluated in the defined grid for the relevant layer. The filtered signal is passed

on to the next neuronal layer, and new responses are computed by the same principle in the Fourier domain.

3.2 Network structure

In PyLGN the domains are initiated by creating an `integrator` object, an instantiation of the class `Integrator`. This object stores the arrays defining the spatial and temporal resolutions both in the real value domain and in the frequency domain. These arrays are used as the domain grid points are computed. The domain grid points contribute as inputs in both stimuli and kernels, such that the simulation always exists in the defined domain.

The `integrator` object is an instant in class `Network`. The network stores the domain, the neurons and the stimulus, and have functions to connect the neurons and compute the impulse response functions and responses to stimuli.

Using the class methods of the `Network` class, it was created a ganglion cell population, relay cell population, cortical cell population (which was included in the feedback). In addition, another cortical cell population was created. This population was the one used to compute the responses of the cortical cells.

The function `Network.connect` was used to create the connections between the neurons by their spatiotemporal kernels and specify the synaptic strength by the "weight" parameter.

The spatial kernels used in the simulation were DOG for the ganglion cell population, and Gaussian for the relay population and the feedback connections. These spatial connections involved a combination of both excitatory and inhibitory kernels. Furthermore, the direct feedforward spatial connection from the relay to the cortical population was through the elliptic Gaussian kernel. The cortical cell population involved in the feedback loop had Dirac delta kernels, in accordance with the network from M. H. Mobarhan et al. (2018).

However, the temporal kernels were chosen to be the biphasic kernel for the ganglion population and exponential decay for the relay population and the feedback connection. Delta kernels were chosen for both cortical populations directly connected with the relay cells.

3.3 The elliptic Gaussian function added in PyLGN

Compared to what has already been implemented in PyLGN, the new element is the inclusion of the elliptic Gaussian kernel. The definition of the kernel in the Fourier domain is found in equation 15. The syntax for the kernel is found in Appendix A. In this syntax, the parameter A represents C_{rc_nr}, and an and al represent σ_n and σ_l, respectively.

The kernel incorporates in the spatial connection between a LGN relay cell population and a cortical population. The cortical cell population with this connection kernel is a separate population from the one included in the feedback loop.

3.4 Stimuli

The stimulus classes used for the simulation were the Fourier domain defined full-field gratings, patch gratings and flashing spots. Their definitions are shown in equation 28, 30, and 32, respec-

tively. Static spots were, however, defined by setting the wavenumber of a patch grating to zero. Moreover, a natural image was used for the simulation. The natural images are the only stimuli that cannot be defined analytically in the Fourier domain and must be numerically defined instead. In this thesis, the purpose was to create analytical solutions. However, one natural image was created to demonstrate the orientation selectivity of cortical cells and the response to edges in the visual field.

The intensity values of the stimuli as input are dimensionless and normalized into the interval -1 to 1. A value of 1 means that the stimulus has a luminance of the highest intensity, whereas a value of -1 means that there is no luminance at all. In the case of natural images, PyLGN is equipped with the function `create_natural_image` in the module `stimulus`. This function converts a raw image input into a stimulus array applicable to the model.

The solutions to cell responses for different stimuli are computed in the Fourier domain. Both the impulse-response function and the stimulus need to be defined in Fourier space to predict responses. In PyLGN, the stimuli inputs need to fulfill the periodicity of the limit conditions of the domain defined when the integrator is set. PyLGN is equipped with validity checks that ensure that the stimulus is valid for the frequency domain. To define stimuli correctly, the wavenumber and orientation combined must fit into the spatial grid points defined by the `integrator` object in the Fourier domain. This applies to the temporal frequency on the temporal grid points as well.

Choosing values for orientation, wavenumber, and temporal angular frequency thus meet some restrictions. A possible way to choose the parameters is by using the values directly from the spatial and temporal Fourier domain vectors from the `integrator` object stored in the `Network` class. It should be noted that this requires that the combination of the spatial parameters is valid, and that the temporal parameters are within the range of the parameters of the temporal kernels.

In this thesis, the wavenumber and temporal angular frequency parameters were chosen directly from the Fourier domain vectors of the spatial- and temporal angular frequencies, respectively. However, instead of rotating the grating of the stimulus by the orientation parameter, the elliptic Gaussian kernel of the cortical cell population was rotated by the parameter θ. This avoids the validity problem of defining the stimulus for different orientations with the same wavenumber, thereby enabling the simulation to tune for a wanted range of orientation values.

3.5 Response computations

The computation of the tuning curves is inspired by the setup in "Examples" included in the PyLGN repository (available from `https://github.com/miladh/pylgn`, (M. Mobarhan et al., 2018)). This involves looping over the varying stimulus parameter and set the new stimulus for the `Network` class each time. The Fourier transformed impulse-response function is computed for each cell layer and multiplied with the Fourier transformed input matrix. The product is the response in the Fourier domain, stored as a three-dimensional matrix.

Computing the responses for each new stimulus input in the loop allows for further investigation of relations between response and stimulus change. Each defined cell type has their own class (`Ganglion`, `Relay`, and `Cortical`) and the `Neuron` keeps track of all specifications stored for each cell population. This class has the function `center_response`, which returns the spatial center response value of the real space response stored for the cell population.

Center responses reduce the matrices by one dimension, leaving the response over all time steps for only one spatial point. The maximum response returns the value which was the highest for the response during the time of the simulation. Thus, the response value is reduced into a single value. If the maximum value is computed anew for each variation of the stimulus, the relation between stimulus and response can easily be visualized in tuning curve plots. Tuning curves allow visualizing the neuron selectivity to visual stimuli (Ayzenshtat et al., 2016).

The three-dimensional responses stored in the Fourier domain can be inverse-transformed by the function of the `integrator` class called `compute_inverse_fft`. This function utilizes the functions `numpy.fft.irfftn` and `numpy.fft.fftshift` from the `numpy` module, along with a factor to account for grid resolution. Responses in real space can be plotted as image plots with the `matplotlib` module for a better visual understanding of the filter effects.

3.6 Computation of suppression index and orientation index

In the master's thesis by Myklebust (2020), a definition of the suppression index was defined:

$$SI = \frac{R_{\text{peak}} - R_{\text{large}}}{R_{\text{peak}}}, \tag{33}$$

where R_{peak} is the peak value of the response, and R_{large} is the response value for the biggest values of spot diameter. Thus, this definition of the suppression index is commonly used for diameter tuning of spots. Equation 33 is based on what was proposed in the papers Vaiceliunaite et al. (2013) and Self et al. (2014). A similar definition is used in the paper by M. H. Mobarhan et al. (2018).

However, there are some issues related to this definition of the suppression index. For patch gratings, on the other hand, it has been observed that the highest maximum response is achieved for the biggest diameters, dependent on wavenumber (Einevoll & Plesser, 2005). In these cases, a more informative definition would be that the first local peak replaces R_{peak}. This is expected to be the point where the stimulus patch exactly covers the center of the DOG-kernel. Furthermore, R_{large} can be replaced by the response at the first local minimum after the local peak. If surround suppression is present, the response will be reduced when the diameter of the stimulus expands into the surround of the receptive field. In that case, this would yield the local minimum. The local peak and the local minimum would give a suppression index independent of the largest diameter. If the first local peak would be reached for the largest diameter, there are no local minima, and suppression index is zero.

With this in mind, a new definition is proposed in this thesis as

$$SI_2 = \frac{R_{\text{first local peak}} - R_{\text{local minimum}}}{R_{\text{first local peak}}}. \tag{34}$$

The index ranges between 0 and 1. There is surround suppression present if the index is larger than zero.

On the other hand, the orientation index can be used as a measure of orientation selectivity. In the paper by Mazurek, Kager, and Van Hooser (2014) the orientation index used was defined as

$$OI = \frac{R_{\text{pref\_ori}} - R_{\text{orth}}}{R_{\text{pref\_ori}}}. \tag{35}$$

$R_{\text{pref\_ori}}$ is the response value for the preferred orientation of the stimulus, which is the orientation that yields the highest response. R_{orth} is the response when the stimulus grating is orthogonal to the ellipse. A similar definition has been used in the paper by Usrey et al. (2009). In their analysis, the index was used as a measure of the strength of orientation selectivity.

3.7 Parameters used in the simulation

The kernel parameters were chosen such that they should be able to reproduce results from (M. H. Mobarhan et al., 2018) and (Einevoll & Plesser, 2012).

The temporal frequency domain is chosen to be at a resolution of 1 ms (`dt` parameter in the `Integrator` object equal to 1 ms in the script) with at least 1024 grid points (`nt` parameter of `Integrator` object equal to 10 in the script). The duration of the simulation is thus 1024 ms long. This resolution allows to choose temporal frequencies for stimuli which are perceived by the temporal kernels. The parameters `dr` and `nr` correspond to the resolution and number of points in the spatial grid, respectively. In the simulations, `dr` was set to 0.1 deg, and `nr` to 7. This results in a spatial grid in real space of 128×128 grid points, where the visual field extends from -6.4 deg to 6.4 deg.

For both M. H. Mobarhan et al. (2018) and Einevoll and Plesser (2012) the parameters chosen made the best fit with observed characteristics. All the kernel parameters, except the ellipse and exponential decay, are comparable with the parameters from the paper by M. H. Mobarhan et al. (2018). The ellipse was defined similarly as in the paper by (Einevoll & Plesser, 2012), whereas the exponential decay kernel was chosen as simple as possible with no delay. For feedback, the network with the mixed feedback from M. H. Mobarhan et al. (2018) was used with the corresponding parameters of the kernels included. The reason is that M. H. Mobarhan et al. (2018) concluded that the mixed feedback gave the best fit for experimentally observed results.

All the parameters used for the kernels and stimuli are listed in table 1 and 2, respectively. Tuning happens with that the specified parameter for tuning is varied, while the others are held fixed. When there is consistency in which parameters are varied, and which are fixed, it is easier to determine which parameters are responsible for the observed effects.

Table 1: The kernels used in the network are listed. The kernels are related to the eDOG model from equation 25. $K^{ex}_{RC_n}$ and $K^{in}_{RC_n}$ are the excitatory and inhibitory kernels of the feedback connection. In addition, $K^{resp}_{C_nR}$ stands for the kernel connecting the relay and cortical cell population which is not included in the feedback. The weights are scalars representing the synaptic strength from equation 7. The spatial and temporal components of each kernel are represented, with their respective parameters according to the definitions from sections 2.3 and 2.4. "Biph" and "Exp" stand for biphasic and exponential decay kernels, respectively.

Kernel	**Weight**	**Spatial**	**Temporal**
W_G		DOG ($A = 1$, $a = 0.62$ deg, $B = 0.85$, $b = 1.26$ deg)	Biph ($a = 43$ ms, $B = 0.38$, $\Delta_{biph} = 0$ ms)
K_{RG}	1	Gaussian ($A = 1$, $a = 0.1$ deg)	Exp ($\tau = 5$ ms, $\Delta_{exp} = 0$ ms)
K_{RIG}	0.5	Gaussian ($A = -1$, $a = 0.3$ deg)	Exp ($\tau =$5 ms, $\Delta_{exp} = 0$ ms)
$K^{ex}_{RC_n}$	1	Gaussian ($A = 0.3$, $a = 0.1$ deg)	Exp ($\tau = 5$ ms, $\Delta_{exp} = 0$ ms)
$K^{in}_{RC_n}$	1	Gaussian ($A = -0.6$, $a = 0.9$ deg)	Exp ($\tau = 5$ ms, $\Delta_{exp} = 0$ ms)
K_{C_nR}	1	Delta (shift_x $= 0$ deg, shift_y $= 0$ deg)	Delta ($\Delta_{delta} = 0$ ms)
$K^{resp}_{C_nR}$	1	Ellipse ($C_{rc_nr} = 1$, $\sigma_l =$1.4 deg, $\sigma_n = 0.1$ deg, $\theta = \pi/2$ rad)	Delta ($\Delta_{delta} = 0$ ms)

Table 2: The stimuli used in simulations are listed. Each stimulus has its parameters from its definition in section 2.6. The static spot was created by using the definition of the patch grating, only with the wavenumber equal to zero. In addition, it is important to keep in mind that when the ellipse orientation $\theta = \pi/2$ rad, its long axis is aligned with the stimulus grating, if the grating orientation $\theta_{stimulus} = 90$ deg.

Stimulus	**Input parameters**
Drifting patch grating	$k_{pg} = 1.96$ /deg, $\omega_{pg} = 0.055$ rad/ms, $d_{pg} = 2.0$ deg, $\theta_{pg} = 90$ deg, $C_{pg} = 1$
Static patch grating	$k_{pg} = 1.96$ /deg, $\omega_{pg} = 0$ rad/ms, $d_{pg} = 2.0$ deg, $\theta_{pg} = 90$ deg, $C_{pg} = 1$
Drifting full-field grating	$k_{fg} = 1.96$ /deg, $\omega_{fg} = 0.055$ rad/ms, $\theta_{fg} = 90$ deg, $C_{fg} = 1$
Static full-field grating	$k_{fg} = 1.96$ /deg, $\omega_{fg} = 0$ rad/ms, $\theta_{fg} = 90$ deg, $C_{fg} = 1$
Flashing spot	$dt = 50$ ms, $\Delta = 0$ ms, $d_{fs} = 2.0$ deg
Static spot	$k_{pg} = 0$ /deg, $\omega_{pg} = 0$ rad/ms, $d_{pg} = 2.0$ deg, $\theta_{pg} = 90$ deg

In the paper by M. H. Mobarhan et al. (2018), the ellipse was not included in the simulation. The reason is that the purpose was to evaluate whether the feedback affected the relay cell response. The parameters of the ellipse in this thesis are taken from a different paper, the paper by Einevoll and Plesser (2012). Thus, it is not confirmed that the parameters of the ellipse and the rest of the kernels are consistent with each other.

3.8 Technical specifications

Python version 3.6.12

PyLGN version 0.92, available from
`https://github.com/miladh/pylgn/tree/0.92/pylgn`,
(M. Mobarhan et al., 2018).

Numpy version 1.19.4

Matplotlib version 3.3.3

Quantities version 0.12.4

4 Results

4.1 Presentation strategy for responses

The effects on the cortical cell response can be tested in numerous ways. Therefore, testing of responses must be restricted to a few essential points related to the research questions of this thesis. This includes testing for the spatial properties of the elliptic Gaussian on cortical response, consequences of stimuli and kernel parameter choices on response patterns, and the matter of feedback. Earlier, PyLGN was used to compute the responses of relay cells. In this thesis, the cortical responses are computed as well, and relay response has been included in some plots. The purpose is to show the effect of the ellipse in contrast to the circular receptive fields of relay cells.

The option of having an elliptic Gaussian function building the spatial receptive field of cortical cells fits well with the eDOG model. Ellipses of different orientations sum up to a circular Gaussian in the feedback mechanism, as explained in section 2.5. The elliptic Gaussian function is included in the simulation with user-defined parameter inputs for amplitude, position, and shape. The elongation can be adjusted by changing the size of the long and narrow axis. The elliptic Gaussian function can easily become a circular Gaussian by setting the length of the narrow axis equal to the long axis. Thus, the shape has a potential in changing the orientation selectivity of cortical cells.

Kernel choice is important, not only for spatial shapes of receptive fields, but also for temporal dynamics throughout the time duration of the simulation. It impacts the computation of maximum response during a simulation. Thus, maximum response can change by the choice of temporal kernels. Moreover, the preference of the temporal frequency is determined by the temporal kernels.

Patch diameter, wavenumber and temporal frequency of stimuli have been used in computing tuning curves. In addition, rotation of the elliptic kernel includes the orientation property. Rotating the ellipse itself avoids the validity problem of defining stimuli in the resolution of the grid. The relative difference between the orientation of the stimulus grating and the long axis of the ellipse is the same, independently of which one is rotated.

The properties of stimuli have been tested for the different stimulus types that can be created in PyLGN; full-field grating, patch grating and flashing spot. The stimuli can move or be static depending on temporal parameters. In some cases, the stimulus type can affect the response to a tuning characteristic.

Furthermore, preferences can shift depending on the value of another characteristic. Exploring the dynamics of preference when another characteristic is changed can expose shifts in preferred stimuli parameters.

At last, the feedback mechanism of eDOG can affect cortical response. In the paper by M. H. Mobarhan et al. (2018), feedback effects were tested for relay cell response, and the conclusion was that feedback with mixed excitatory and inhibitory signals gave the most promising results. Feedback seem to have a significant impact on relay cell response to visual stimuli. In this thesis, feedback weights were adjusted to explore whether cortical cells inherit the feedback effects from relay cells.

4.2 Validation of the elliptic Gaussian

The spatial receptive fields throughout the network contribute to decide how the different cell types respond spatially to stimuli. The spatial response of the cortical cell population will be formed by the convolution between the elliptic Gaussian function and the output of the relay cell population. Figure 3 from section 2.3 illustrates simplified how the spatial receptive fields build the cortical response pattern.

The new element to the simulations with PyLGN is the elliptic Gaussian kernel as it was defined in equation 15. It was added by the syntax from Appendix A. To assure that the elliptic kernel is correctly defined, validation should be performed. The idea is that it should be possible to reproduce the ellipse from the responses computed if the computation went correctly.

In order to implement the validation, the response to white noise was computed for both a relay cell population and cortical cell population. The results are in figure 8. Panel (a) is the noise stimulus with intensities ranging from -1 for no luminance to 1 for full luminance. The color map of both the stimulus and the responses in the figure was chosen to range from blue to red to distinguish between positive and negative values. The relay response is shown in panel (b), whereas the cortical response is shown in panel (d). The elliptic kernel in panel (c) is included to clarify the preferred orientation.

By dividing the cortical spatial response on the relay spatial response, the ellipse should appear as a result. The elliptic Gaussian, as it was defined in the syntax in Appendix A, is shown panel (a) in figure 9. The result of the division is shown in panel (b). The residuals were computed as the difference between the two, and are shown as an image plot in panel (c).

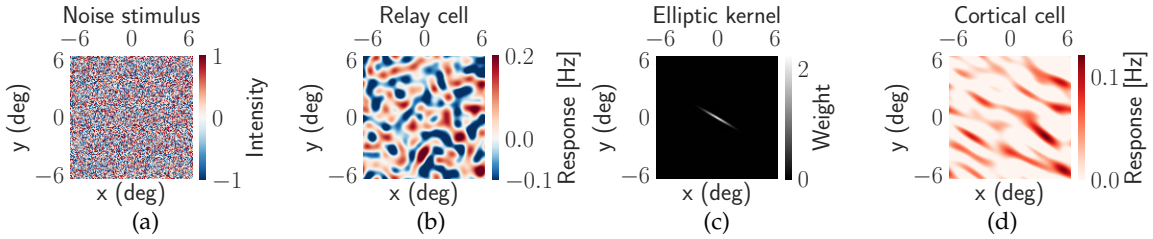

Figure 8: Relay and cortical responses were computed for a white noise stimulus. (a) The noise shown as an image plot in real space with intensity values ranging from -1 to 1. A value of -1 means no luminance, whereas a value of 1 means full luminance. (b) The relay response was computed for the noise stimulus in panel (a). The image plot shows the two-dimensional response in real space. (c) The elliptic Gaussian kernel is included to verify that the pattern of cortical response in panel (d) is consistent with the elliptic orientation. (d) The cortical response computed, shown as an image plot in real space. The kernels in the network were defined as in table 1, except from the elliptic Gaussian, with an orientation of $\theta = \pi/6$ rad.

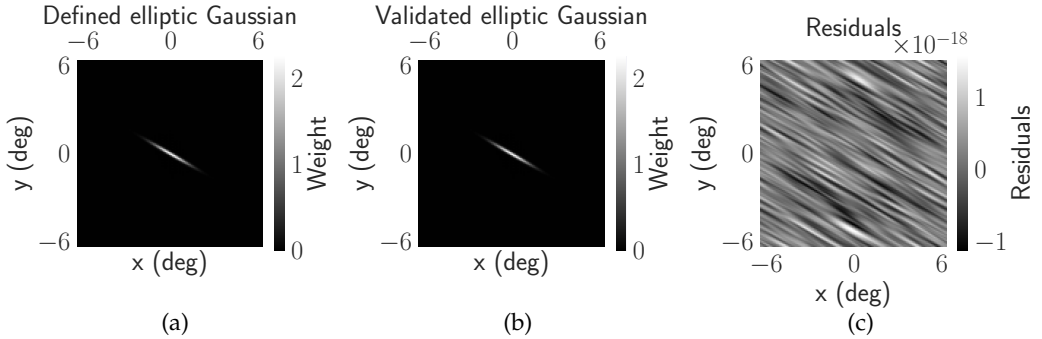

Figure 9: (a) The defined elliptic Gaussian is based on the syntax from Appendix A, with parameters as listed in table 1, except θ, which is $\pi/6$ rad. (b) The validated elliptic Gaussian is a result of dividing the cortical response by the relay response. (c) The residuals were computed by subtracting the validated from the defined elliptic Gaussian.

When comparing the images of figure 9, the ellipses appear alike. The values do also seem to be similar. If the ellipses are identical, the residuals between the two plots should be zero. These are computed by subtracting the validated ellipse from the defined elliptic Gaussian. The differences are shown as an image plot in real space of the residuals in panel (c) in the figure. The pattern reveals that the difference is not zero. However, the values are in an order of 10^{-18}, which is very small. Numerical inaccuracies are common in computations of floating point operations and may cause minor deviations like this number.

4.3 Cortical response to natural stimuli

The selective nature of the different cells in the early visual system contributes as a building block to the brain's interpretation of a complete image. Orientation selectivity of the cortical cells serves as one of these selective abilities. The orientation of the "smoothed out" cortical response to white noise in figure 8 reveals that the response pattern follows the orientation of the ellipse. This is expected to appear, not only for white noise, but for natural images as well.

Figure 10 shows the natural image used in the simulation. The image is cropped from an image of a drawing of a horse. The image is inverted, such that the pencil lines themselves have the highest positive intensity values. The ON-centered relay cells respond positively on bright areas covering the center. (Rodieck, 1965). To demonstrate the orientation selectivity of the cortical cells, the effect is most visible if the lines are the bright parts in the image.

The values of the natural image shown in figure 10 are grayscale pixel values ranging from zero to 255. However, the function `create_natural_image` in PyLGN takes the image as raw input and converts it to fit into the interval -1 to 1. -1 corresponds to the darkest areas, and 1 corresponds to the brightest areas.

Each row of figure 11 represents the cortical responses to the natural image in figure 10. The elliptic Gaussian kernels are shown to clarify which orientation is preferred for each cell population.

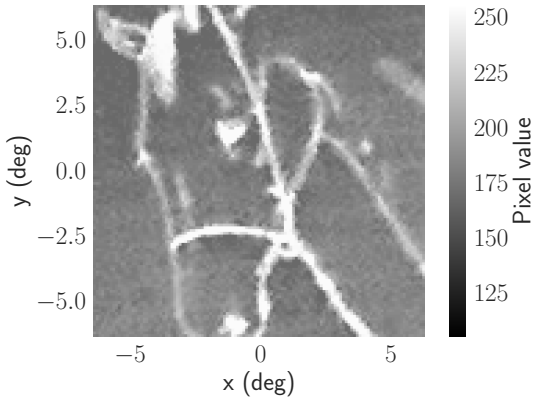

Figure 10: The natural image as the raw input to the natural stimulus module `create_natural_image` in PyLGN. The image is shown in real space as a grayscale inverted image with pixel values ranging from 0 to 255.

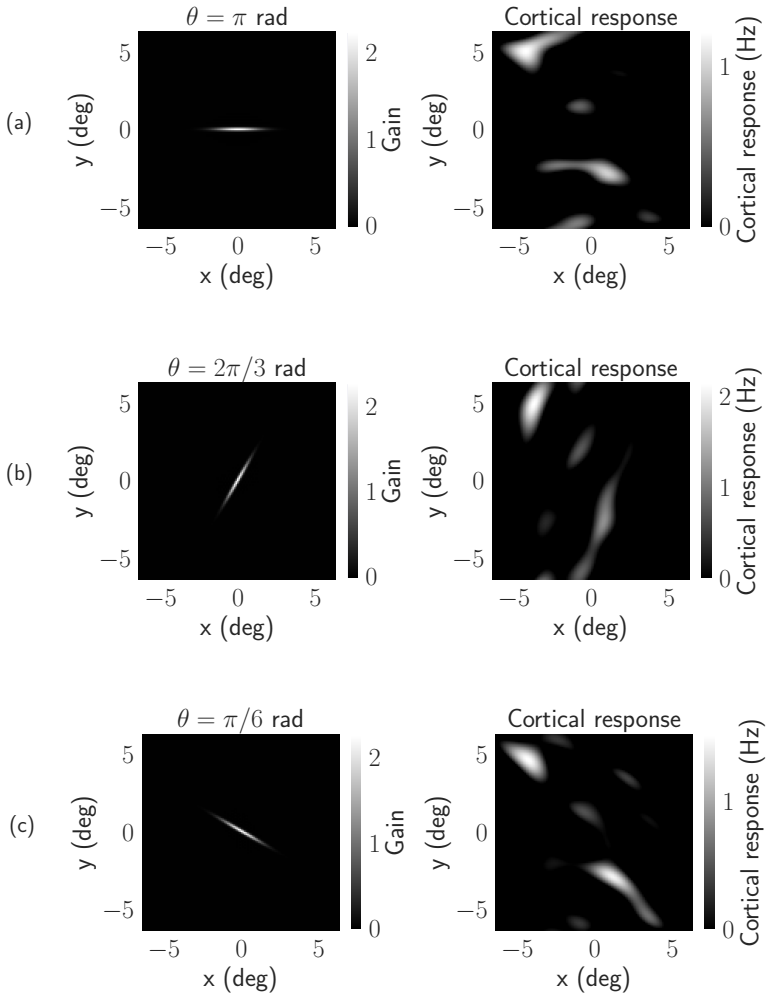

Figure 11: Each of the panels shows the orientation of the elliptic Gaussian kernel and the corresponding cortical response. The network used in this simulation is the network with the kernel parameters as listed in table 1. The orientation θ of the elliptic Gaussian is the only adjusted parameter. Panel (a) shows the cortical response and the ellipse with an orientation of $\theta = \pi$, panel (b) for $\theta = 2\pi/3$ rad, and panel (c) for $\theta = \pi/6$ rad.

The cortical cells show a clear preference for which orientations give the highest response values, as the response pattern of the cortical cells is "smoothed out" in the same orientation as the ellipse. The edges from the natural image aligned with the long axis of the ellipse dominate the cortical response pattern.

4.4 Widening the elliptic Gaussian kernel

The elliptic Gaussian kernel is determined by $C_{\mathrm{rc_nr}}$, the sizes of the long and narrow axes, σ_l and σ_n, θ from the definition in equation 15. Elongation of the receptive field is expected to affect the selectivity of specific orientations (Hubel & Wiesel, 1962). Furthermore, diameter preference, suppression and spatial frequency are other characteristics which may be affected as well.

By changing the dimension of the narrow axis σ_n, while keeping the long axis σ_l fixed, the matter of elongation of the ellipse can be tested. Four different values of σ_n were used for computing four different tuning curves in each simulation. The real space image plots of the ellipse shapes are shown in figure 12.

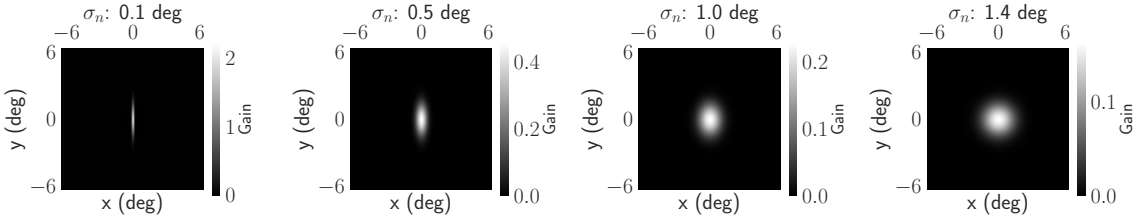

Figure 12: The different ellipse shapes are achieved by changing the narrow axis σ_n from equation 15 of the elliptic Gaussian. The long axis σ_l is held fixed at 1.4 deg. The rest of the elliptic Gaussian kernel parameters are kept as listed for the ellipse in table 1. This means that both $C_{\mathrm{rc_nr}}$ and θ are the same for the four ellipses shown. As the shape changes from elliptic to circular, the strength of the amplitude decreases. This is a result of the factor in front of the exponential in equation 14. Panel (a) shows the ellipse with $\sigma_\mathrm{n} = 0.1$ deg, (b) with $\sigma_\mathrm{n} = 0.5$ deg, (c) with $\sigma_\mathrm{n} = 1.0$ deg and (d) with $\sigma_\mathrm{n} = 1.4$ deg

4.4.1 Orientation tuning for different values of σ_n

The ellipse orientation was changed in a drifting full-field grating, and this was done for each shape of the ellipse shown in figure 12. The full-field grating was positioned with the parameter θ_{fg} on 90 deg, which means that the grating is vertically oriented. The spatial frequencies are determined by a wavenumber k_{fg} on 1.96 /deg, and the temporal angular frequency $\omega_{\mathrm{fg}} = 0.055$ rad/ms. This means that the stimulus is drifting full-field grating.

The frequencies of the simulations in general are kept to the same values as far as it is reasonable. The spatial frequency value 1.96 /deg gives responses of an order of high, and somewhat similar magnitudes for both full-field and patch gratings. The optimal wavenumber for full-field gratings lies on a higher value, but to avoid too much variation of stimuli parameters, 1.96 /deg was chosen for both stimuli types. The temporal angular frequency on 0.055 rad/ms is chosen because it is the optimal value for all cases of the network structure used. The selectivity for temporal frequency is discussed more closely in section 4.5.

The tuning curves for this simulation are shown combined in panel (a) in figure 13. The orientation index, shown in panel (b), was also computed for each curve. This index is computed by the definition from equation 35. This was done to demonstrate the orientation selectivity of the cortical

cells dependent on the degree of elongation of the spatial receptive field.

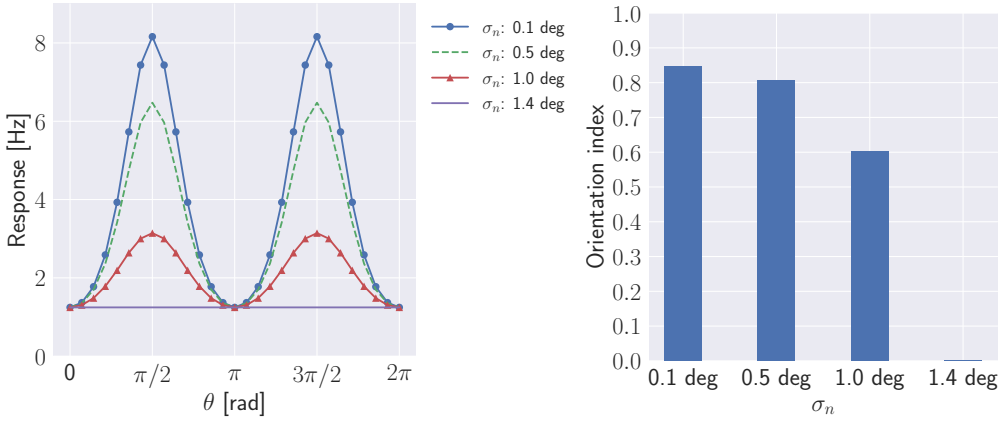

(a) (b)

Figure 13: (a) The orientation of θ for the elliptic Gaussian was rotated 2π rad. Tuning curves were created for the four different values of σ_{n} of the ellipse. All other parameters were fixed on values as listed in table 1. The stimulus used for the simulation is a drifting full-field grating, with parameters as described in table 2. (b) The orientation index computed for each value of σ_{n}. The index is defined by equation 35.

As σ_{n} gradually increases to the same size as σ_{l}, the selectivity for orientation decreases. The orientation index in panel (b) of figure 13 decreases first when σ_{n} is changed from 0.1 deg to 0.5 deg, and further when changed to 1.0 deg. For 1.4 deg, the orientation index is zero. The curves in panel (a) of figure 13 also show that the difference between the peaks and the minima decreases as the shape of the ellipse becomes more circular. The preferred orientation is when the ellipse is aligned with the stimulus grating, which in this case is when θ is $\pi/2$ rad and $3\pi/2$ rad. The ellipse lies orthogonal to the stimulus grating when θ is at 0, π and 2π rad.

However, another effect observed in figure 13 is that the maximum response of the preferred orientation is lower for more circular-shaped ellipses. This is probably a consequence of the amplitude of the ellipse. As the σ_{n} increases while σ_{l} is held fixed, the total area of the receptive field increases. By the definition of the elliptic Gaussian in equation 14, the factor in front of the exponential term depends on σ_{n} and σ_{l}. This factor determine the amplitude of the elliptic Gaussian function in the filtering process. As σ_{n} increase, the value of the factor decrease. Thus, a fraction of the decrease in magnitude may be caused by the amplitude as well as the two-dimensional shape of the ellipse.

4.4.2 Diameter tuning for different values of σ_{n}

The diameter of a drifting grated patch was also changed for the different ellipse shapes. When computing diameter tuning curves, response magnitude, diameter preference, and suppression are features worth considering.

In figure 14, diameter tuning curves for a drifting patch grating are shown in panel (a). The responses belongs to a cortical cell population. The relay cell population is not included, since it

is independent on the ellipse shape. One curve was computed for each of the four shapes of the ellipse.

The wavenumber value was 3.93 /deg, which deviates from the wavenumber of drifting patch gratings in table 2. The reason is that suppression is dependent on wavenumber, as shown in more detail in figure 26 from section 4.8. A wavenumber of 3.93 /deg reveals clearer suppression patterns compared to a drifting patch grating with a wavenumber of 1.96 /deg. At the same time, the magnitude of the response is held on a reasonable high value. If the wavenumber would be larger, the magnitude of the response would drop to lower values. A wavenumber value of 3.93 /deg makes it easier to evaluate the effect ellipse shapes have on suppression in the cortical cell population.

In addition, the temporal angular frequency of the drifting patch grating was set to 0.055 rad/ms. This yields the highest maximum response compared to other choices of the temporal frequency. The orientation of the grating was 90 deg, which means that it is aligned with the long axis of the elliptic Gaussian.

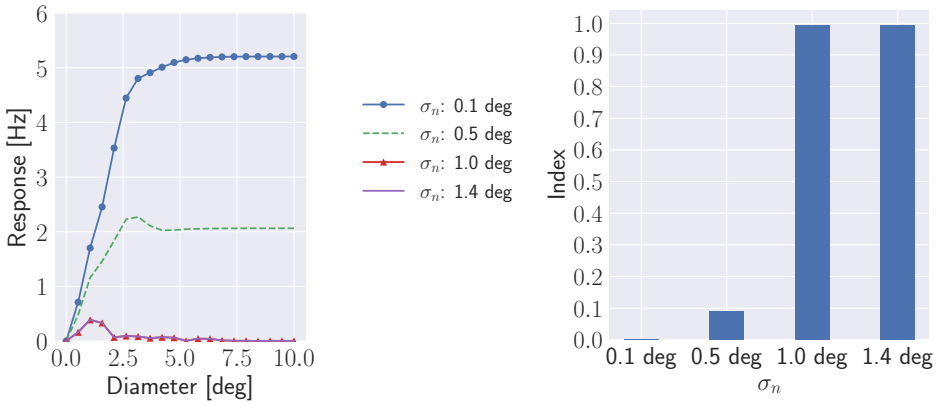

(a) (b)

Figure 14: (a) Diameter tuning curves of a drifting patch grating. The parameter d_{pg} is tuned for the four different values of σ_{n} of the elliptic Gaussian. The temporal angular frequency was set to 0.055 rad/ms, and the orientation of the grating was 90 deg. The wavenumber was 3.93 /deg, rather than the wavenumber for patch gratings listed in table 2. Diameter suppression effects are dependent on the wavenumber, which is described in more detail in section 4.8. The wavenumber on 3.93 /deg was chosen to easier evaluate suppression effects. (b) The suppression index of the four diameter tuning curves from panel (a) was computed by the definition in equation 34.

The change of the elliptic Gaussian kernel shape yields interesting results for the suppression and diameter preference. From panel (b) of figure 14, it can be read out that there is suppression present for $\sigma_{\text{n}} = 0.5$ deg, 1.0 deg and 1.4 deg. As σ_{n} increases, the ellipse is widened, and the suppression increases. The shape of the ellipse thus influences the suppression in cortical cells.

Another observed effect is that the diameter preference is shifted to a smaller diameter as the elliptic Gaussian is widened. The maximum response magnitude does also decrease for a wider

ellipse, just as for the orientation tuning curves in figure 13. However, the cause is probably the same in this case as it was for the orientation. The decrease of magnitude can be related to the amplitude of the elliptic kernel as well as the two-dimensional shape.

4.4.3 Wavenumber tuning for different values of σ_n

If the ellipse is aligned with the stimulus grating, the highest response would be achieved when the ellipse is completely covered in light along its long axis. However, this can change if σ_n is increased. If a wide ellipse should be completely covered in light, the wavelength of the grating need to be just as wide. The shape of the ellipse is thus expected to shift wavelength preference to larger values when the σ_n increases. A larger value for the wavelength means a smaller value for the wavenumber from the relation $k = 2\pi/\lambda$.

In panel (a) in figure 15, the wavenumber is tuned for a drifting full-field grating. The full-field grating is defined with the frequencies $k_{fg} = 1.96$ /deg and $\omega_{fg} = 0.055$ rad/ms. The orientation is on 90 deg, such that the grating aligns with the long axis of the elliptic Gaussian kernel. A shift effect in preferred wavenumber appears in the cortical cell response. As σ_n increases, the preferred wavenumber for the cortical cells in a full-field drifting grating is shifted towards smaller values.

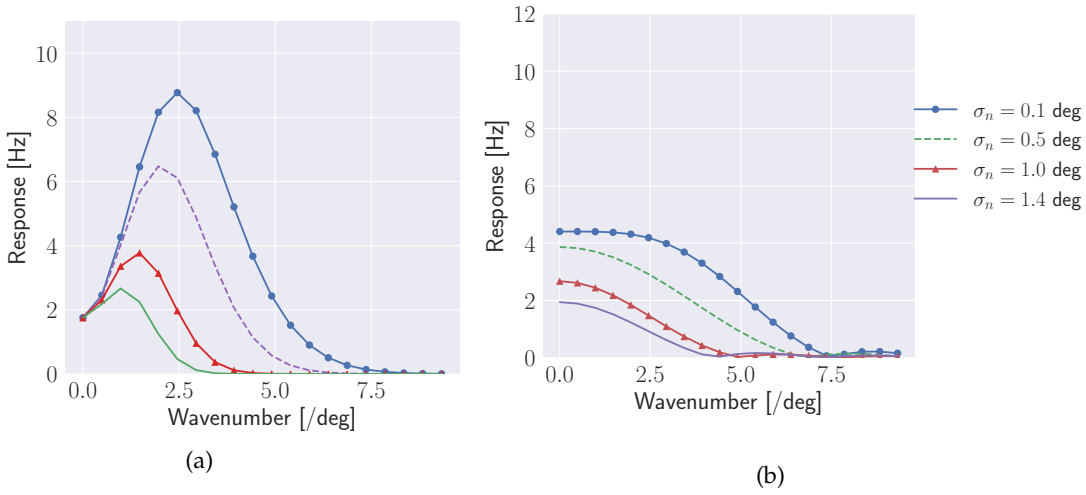

Figure 15: (a) Wavenumber tuning curves plotted for each value of σ_n as responses to a drifting full-field grating. Other than the ellipse orientation θ, all other parameters for the kernels in the network are as listed in table 1. The stimulus parameters follow the values of a drifting full-field from table 2, except the wavenumber. The value of the wavenumber ranged from zero to 9.33 /deg. (b) Wavenumber tuning curves computed by the same process as in (a), but for a drifting patch grating instead. The parameters, except wavenumber, follow the drifting patch grating values from table 2.

The explanation for the effect on the response magnitude seen for the orientation tuning curves in figure 13 applies to the wavenumber tuning curves as well. The amplitude of the elliptic Gaussian, as well as the two-dimensional shape, may play a part in the reduction of magnitude.

The same procedure for wavenumber tuning was done for a drifting patch grating as well. The observed effect was mainly a reduction in the magnitude of the response without any preference shifts. The results from this simulation is shown in panel (b) of figure 15. However, the preferred wavenumber is zero for patches with a diameter of 2.0 deg; see figure 21 from section 4.6. Shifts in wavenumber preference will thus not be observed for patch gratings.

Under section 4.6, it is described how the responses of the cell populations are dependent on stimulus type. There is a difference in response if stimulus is for example a patch or if it is a full-field grating as shown in figure 15. This is the reason of why the tuning curves reveal different preferences, even though the parameters of wavenumber and ellipse shape are the same.

4.5 The role of the temporal kernels

The temporal kernels for the network were chosen inspired by the argumentation based on the papers by M. H. Mobarhan et al. (2018) and Einevoll and Plesser (2012). Parameter choices are based on a balance between staying on a simple level, and still have a reasonable approach for modeling the biological system of the brain.

The standard network setup, which has been described in section 3.2, is the network involved in most simulations of the result section. The spatial kernel used for the retinal ganglion cell population is a DOG function defined by equation 13. The relay cell population and feedback have Gaussian functions as defined in equation 11, whereas the spatial feedforward connection to the cortical cell population is the elliptic Gaussian function as was defined by equation 15.

The standard network described in section 3.2 sums up the temporal kernels chosen for each cell layer as well. The retinal ganglion cell population is chosen to include biphasic temporal kernels as defined in equation 21, whereas the relay cell population and feedback connections include exponential decaying kernels as defined in equation 19. Delta kernels, from equation 17, are involved in the feedforward connection between the relay and the cortical cell populations. This network is consistent with the network used in the paper by M. H. Mobarhan et al. (2018).

The temporal kernels take part in the receptive field along with the spatial kernels. Thus, the signals passed on through the receptive fields are expected to be affected by the temporal kernels as well. These effects will relate to the max response and temporal frequency preferences during the simulation. However, since the spatial and temporal part of the receptive field are separable, the elliptic Gaussian is not expected to impact temporal filtering of signals.

Nevertheless, the temporal kernels do change the magnitude of the maximum response and temporal frequency preferences. According to literature, the temporal features of the feedback are believed to affect several response patterns of the relay cells (Hasse & Briggs, 2017; Sillito & Jones, 2002; Gulyás et al., 1990). However, the new element of this thesis is the connection with the cortical cells, with the elliptic Gaussian function as the spatial component of the receptive field. Thus, the issues of this thesis are not directly related to the effects of the temporal kernels. However, it is still important to show their role in influencing the magnitude of the maximum response and temporal frequency preferences.

The angular temporal frequency is a parameter option for patch gratings and full-field gratings in PyLGN. The temporal kernels will affect the temporal filtering of the stimulus. Thus, temporal

frequency tuning curves are a natural choice for investigating the temporal effect on maximum response.

The biphasic kernel changes the polarities of the center and surround of the receptive field over time (Yousif & Denham, 2007; Cai et al., 1997). However, since the maximum response is computed as the maximum value for all time steps, the effect of this polarity change will not be visible when plotting tuning curves. The highest gain on the top of the positive phase of the biphasic kernel will dominate when computing maximum responses. Biphasic kernels will contribute to band-pass characteristics for temporal frequencies in drifting stimuli. On the other hand, the exponential decay is expected to filter out the highest frequencies. Thus, the temporal kernel will contribute to a shift in temporal preference for lower frequencies. The delta kernels themselves do not alter the frequency coefficients, and pass the signals through without any modification other than a possible delay by the delay parameter Δ_{exp}.

Three networks with different temporal kernels are compared to observe the effect of the temporal kernel choices. For each network temporal frequency tuning curves are computed. The first is the standard network, including the biphasic kernel, exponential decay, and delta kernels as described above. The other network has only delta kernels in the temporal connections. The third has the biphasic kernel for the retinal ganglion cell population, whereas the other temporal connections have delta kernels. The spatial kernels in the network are not changed and have the same parameters as described in table 1.

The parameters of the temporal kernels are also the same for the three networks. The biphasic kernel has $a = 43$ ms, $B = 0.38$ and $\Delta_{\text{biph}} = 0$ ms, the exponenital decay kernels has $\tau = 5$ ms and $\Delta_{\text{exp}} = 0$ ms, and the delta kernel has $\Delta_{\text{delta}} = 0$ ms.

The tuning curves of temporal frequency to a drifting full-field grating are computed for ganglion, relay, and cortical cell populations. The wavenumber of this full-field grating is $k_{\text{fg}} = 1.96$ /deg, whereas the temporal angular frequency ω_{fg} is varied. The grating orientation θ_{fg} is 90 deg, which makes it aligned with the elliptic Gaussian. Results from the simulation are presented in figure 16. One tuning curve was created for each of the three different network structures.

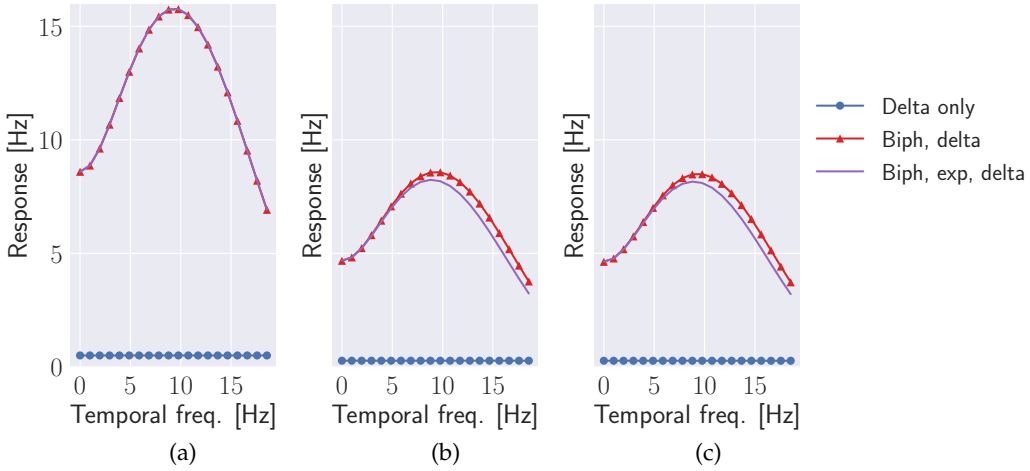

Figure 16: The figures show temporal frequency tuning curves for each of the networks with different temporal connecting kernels. This was done for both (a) retinal ganglion, (b) relay, and (c) cortical cell populations. "Biph, exp, delta" represents the network that has biphasic temporal kernels for retinal ganglion cell populations and exponential decay kernels for relay cell populations and in the feedback connections. Temporal delta kernels are included in the feedforward connection between the relay and cortical cell population. This setup for temporal kernels are used throughout the results section. "Biph, delta" represents for the network where all temporal kernels are delta functions, except from the temporal kernel of the retinal ganglion cell population with its biphasic function. "Delta only" is the network with delta functions in all temporal kernels. The kernel parameters are listed in table 1. The cell populations respond to a drifting full-field grating with ω_{fg} ranging from zero to 0.12 rad/ms. This corresponds to a temporal frequency ranging from zero to 19.1 Hz. The wavenumber k_{fg} is 1.94 /deg and the orientation is aligned with the elliptic Gaussian by letting θ_{fg} be 90 deg.

At first sight, the contribution of the temporal kernels indeed have a large impact on the maximum response, especially the biphasic kernel. When the biphasic kernel is included, the maximum response is high for all cell types. Retinal ganglion cells seem to have the highest response of them all. In fact, the results reveal that the biphasic kernel lacks a scaling factor. The response for the network with only delta functions as temporal kernels is much lower than for the networks with biphasic kernels in the retinal ganglion cell layer. This makes the temporal kernel effects on the maximum response hard to compare between the networks. The standard network used for all other simulations in the results section contain this difference in scale between the biphasic kernel and the other temporal kernels.

The networks including biphasic kernels contribute to a band-pass filtering effect, giving the network preferences of temporal frequencies. The exponential decay kernels contribute to a slight shift to lower preferred temporal frequencies in both relay and cortical cell populations. The network consisting of only delta kernels is harder to interpret since the values are close to zero. By the first look, the network with only delta kernels in the temporal connections has no filtering effects on the temporal frequency of the signal. However, this can be a consequence of the scale difference, and potential effects on the temporal frequency from this network are not visible in the

figure.

4.6 Selectivity of stimulus is dependent on stimulus type

Figure 16 from the previous section showed the effects from three networks with different temporal kernels for a drifting full-field grating. However, the fact that the stimulus was a full-field grating, and not a patch grating, may have affected the results. This section compares tuning curves of responses to different stimuli types, like full-field gratings, patch-gratings and flashing spots. In addition, by plotting tuning curves for static stimuli together with stimuli which change over time, it is possible to evaluate whether moving stimuli give higher responses than static stimuli, which was claimed by Hubel and Wiesel (1962).

4.6.1 Temporal frequency tuning for different stimuli

Temporal frequency tuning curves were computed in both relay and cortical cell populations for a drifting full-field grating and for a drifting patch grating. The results are shown in figure 17. The panels (a) and (b) show the relay response and cortical response respectively. The full-field grating has the parameters $k_{\text{fg}} = 1.96$ /deg and $\theta_{\text{fg}} = 90$ deg, which makes it aligned with the elliptic Gaussian kernel. The patch grating has the same values for both k_{pg} and θ_{pg}, but in addition, the diameter of the patch d_{pg} is 2.0 deg. This diameter is the optimal diameter for both patch gratings and flashing spots in relay cells, as will be shown in more detail later.

By comparing the tuning curves of these two stimuli, it is possible to reveal if there is a difference in response pattern. When the response for both relay and cortical cell populations are included, the effect of the elliptic Gaussian kernel can be revealed as well.

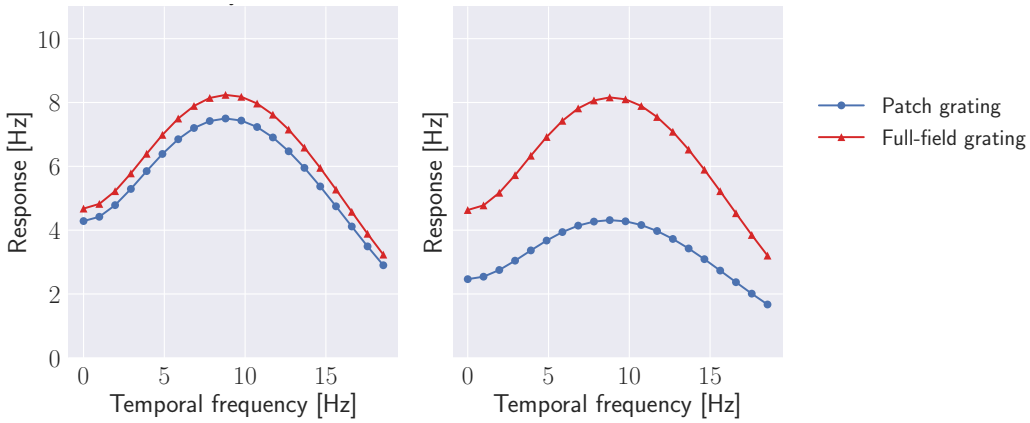

(a) (b)

Figure 17: (a) Temporal frequency tuning curves plotted for the relay cell population. The two curves correspond to the two stimulus types, which are drifting patch grating and full-field grating. Both stimuli have wavenumber 1.96 /deg and orientation 90 deg. The patch grating has a diameter of 2.0 deg. The angular temporal frequency range from zero to 0.12 rad/ms. The network used is built with kernels as described in table 1. (b) The cortical responses to the same stimuli from the same network.

For both relay and cortical cell populations in panel (a) and (b) of figure 17, the full-field grating stimulus yields a higher maximum response than for the patch grating. The response is reduced in the cortical cell population relative to the relay cell population for the patch grating stimulus. The effect from the elliptic Gaussian kernel thus seems to depend on whether the stimulus is a patch grating of diameter 2.0 deg, or a full-field grating with the same frequencies.

4.6.2 Orientation tuning for different stimuli

The curves which were shown in panel (a) of figure 13 are the responses computed for different values of the parameter σ_n as the orientation θ of the ellipse changed. The stimulus was a full-field grating with the parameters $k_{fg} = 1.96$ /deg, $\omega_{fg} = 0.055$ rad/ms and orientation $\theta_{fg} = 90$ deg. The fact that the stimulus was a drifting full-field grating with its parameters as mentioned, may have affected the response.

To verify the effect of the stimulus type, the maximum response curves for rotation of θ were computed for both drifting and static full-field and patch gratings. The results are shown in figure 18. The drifting full-field grating still has the same parameters as in figure 13. The drifting patch grating with $d_{pg} = 2.0$ deg has the same values for the frequency parameters k_{pg} and ω_{pg} as the full-field grating has for k_{fg} and ω_{fg}. What differs the drifting stimuli from their respective static stimuli is that ω_{pg} and ω_{fg} are zero for the latter.

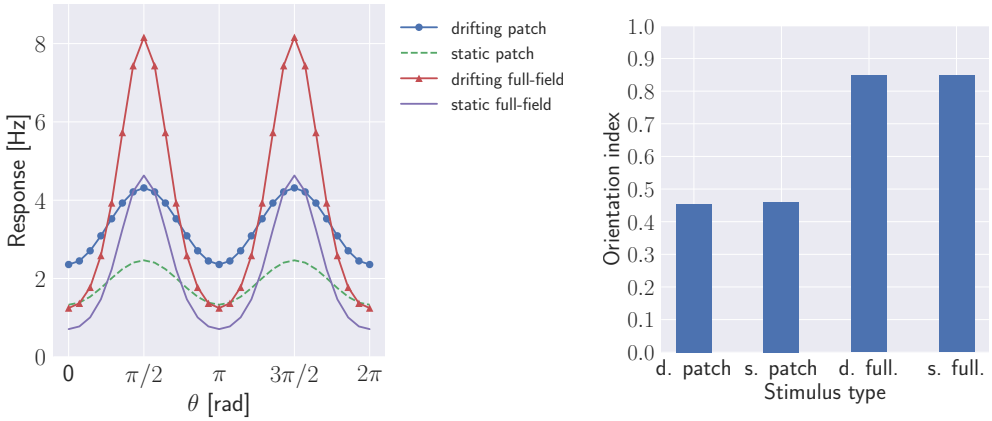

(a) (b)

Figure 18: (a) Orientation tuning for different types of stimuli. Both the stimulus and kernel parameters are described in tables 1 and 2. Only the orientation parameter θ of the elliptic Gaussian kernel was varied in the simulation. θ ranged from 0 to 2π rad, which corresponds to a turn of 360 degrees. (b) The orientation index computed for each stimulus type corresponding to the curves in figure (a). The index was computed from the definition in equation 35. "d." stands for drifting, whereas "s" stands for static. "Full" means that it is a full-field grating.

It is only the cortical cell population which is shown in figure 18. This is because the relay cell population is not affected by the rotation of the elliptic Gaussian kernel. However, as was seen for temporal frequency tuning curves in figure 17, figure 18 shows that full-field gratings yield higher peaks of the maximum responses than for patch gratings. The ellipse is aligned with the grating when θ reaches $\pi/2$ rad and $3\pi/2$ rad. The peaks in the maximum response are at these values for θ for all stimulus types.

In addition, there is an interesting relation between aligned and orthogonal positioned ellipse relative to the grating. When looking at the orientation index in panel (b) in figure 18, the index is higher for full-field gratings than for patch-gratings. Although the response is higher for the drifting gratings than for their respective static gratings in panel (a), the orientation index is independent of whether the stimulus is drifting or not.

4.6.3 Diameter tuning for different stimuli

In this section, diameter tuning curves are plotted for both patch gratings and circular spots. Both panels of figure 19 show tuning curves for drifting patch grating, static patch grating, static spot and flashing spot. The drifting patch grating has the parameters $k_{\text{pg}} = 1.96$ /deg, $\omega_{\text{pg}} = 0.055$ rad/ms and $\theta_{pg} = 90$ deg. The static patch grating differs from the drifting patch grating by having $\omega_{\text{pg}} = 0$. The static spot was computed simply by letting the wavenumber parameter k_{pg} be zero. The diameter was still at 2.0 deg. The diameter d_{fs} of the flashing spot is also at 2.0 deg, and is defined by the parameters for duration $dt = 50$ ms and delay $\Delta_{\text{fs}} = 0$ ms.

The responses were computed for both relay and cortical cell populations, as shown in panel (a) and (b) in figure 19, respectively. The suppression indexes for patch gratings were computed by

the definition from equation 34, and for the spots, the definition from equation 33 was used. The indexes were computed for both relay and cortical cell populations, and are shown in figure 20.

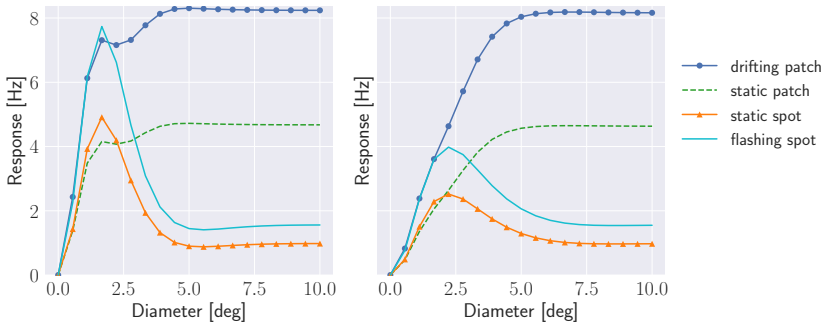

Figure 19: (a) Diameter tuning curves computed for the relay cell population responding to a drifting patch grating, a static patch grating, a static spot and a flashing spot. The kernels used are described in table 1, and the stimuli are in table 2. The diameter ranged from zero to 10.0 deg for all stimuli in the simulation. (b) The corresponding diameter tuning curves for the cortical cell population in the same network.

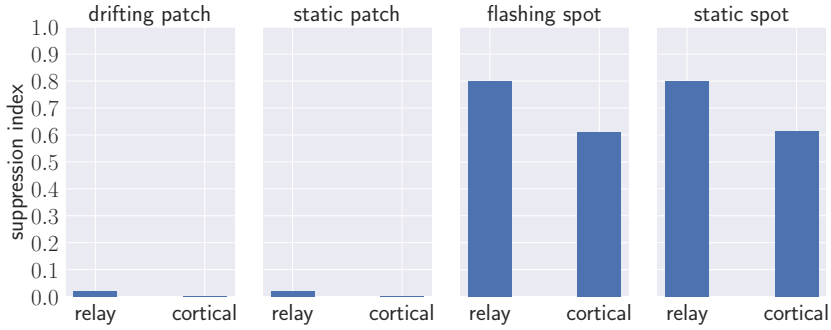

Figure 20: Suppression indexes corresponding to the curves in figure 19. For each stimulus, the suppression index was computed for both the relay and cortical cell population. The indexes for the spots were computed by the definition in equation 33, while for the patch gratings equation 34 was used.

As seen in figure 19, the moving or flashing stimuli give higher maximum responses than their corresponding static stimuli. The same tendencies for the difference between moving and static stimuli were observed for the orientation tuning curves in figure 18. However, the diameter tuning curves reveal a shift in preferred diameter and that suppression behaviour is dependent on whether there is a patch grating or a spot considered. Diameter seems to have the biggest influence on suppression for spots rather than patch gratings with the chosen parameters. However, the suppression indexes in panel (b) show that suppression is not affected by whether the stimulus is static or not.

Another result worth noticing is the difference between responses of relay cells and cortical cells. When it comes to suppression, it is significantly present for both relay and cortical cells for spots. For patch gratings, on the other hand, suppression is small for relay cell populations ($2.10 \cdot 10^{-2}$ for drifting patch grating and $1.96 \cdot 10^{-2}$ for static patch grating), and almost nonexistent for cortical populations ($2.84 \cdot 10^{-3}$ for drifting patch grating and $3.60 \cdot 10^{-3}$ for static patch grating). This can be a consequence of the wavenumber dependence of the preferred diameter. That is discussed in more detail in section 4.8 related to the results in figure 26.

The highest maximum response is different for relay and cortical cells as well, but only for spots. For patch gratings, the response reaches its maximum for both relay and cortical cells when the diameter increases to the largest values. This maximum is not as different between the cell layers as it is for the spots. Furthermore, the preferred diameter for cortical cells responding to spots is shifted towards higher values, compared to relay cells. For the flashing and static spot, the preferred diameter is 1.67 deg in the relay cell population, and 2.22 deg in the cortical cell population.

4.6.4 Wavenumber tuning for different stimuli

Wavenumber was the last stimulus property to plot for different stimuli types. The wavenumber preferences prove to be dependent on stimulus types as well. This was already seen in figure 15. In that case, the drifting full-field in panel (a) yielded different responses than for the drifting patch grating in panel (b).

Reasonable stimuli to compute wavenumber tuning curves are drifting and static patch gratings and full-field gratings. The temporal angular frequency of the drifting stimuli were chosen to be 0.055 rad/ms. This is the optimal temporal angular frequency of drifting stimuli, corresponding to a temporal frequency of 8.75 Hz. The static stimuli have the temporal angular frequency on zero. The wavenumber on 1.96 /deg is the same for all stimuli in the simulation. Even though this is not the preferred wavenumber for either patch gratings or full-field gratings, it yields reasonable high responses around the same value for both stimuli. The diameter pg on 2.0 deg for the patch gratings is not the preferred diameter either. The preferred diameter for patches with wavenumber is 1.96 /deg is actually the biggest diameters, which can be interpreted from figure 26. The results from the simulation are shown in figure 21.

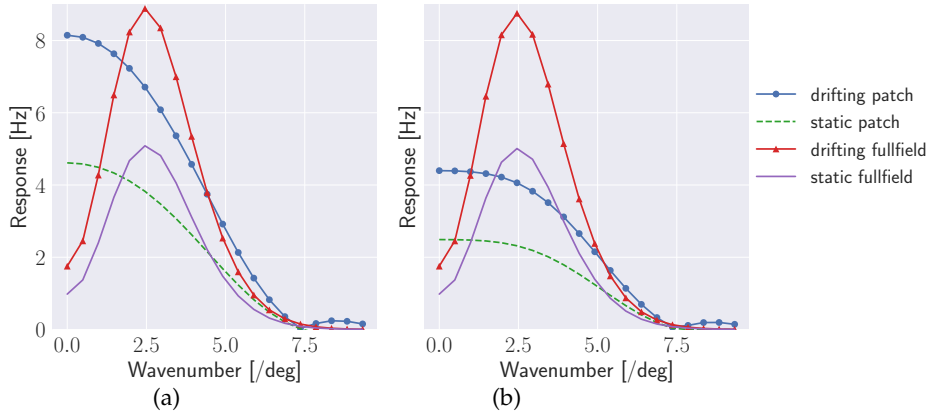

Figure 21: (a) Wavenumber tuning curves computed for a relay cell population responding to different types of stimuli. These stimuli are both drifting and static patch gratings and full-field gratings. Wavenumber values ranged from zero to 9.33 /deg, whereas the other parameters were held fixed as listed in table 2. The network had kernels as described in table 1. (b) The wavenumber tuning curves for a cortical cell population responding to the same stimuli as in panel (a). The same network was used.

The responses are higher, also in this case, for the drifting gratings compared to their corresponding static gratings. As already mentioned for the wavenumber tuning curves related to figure 15, the preferred wavenumber of patch gratings with a diameter on 2.0 deg is zero. A patch grating with the wavenumber equal to zero is equivalent to a spot of constant intensity. Full-field gratings, however, shifts the preferred wavenumber towards the optimal value, as the wavenumber increases. When the wavenumber increases past the optimal value, the maximum response drops.

In addition, there is an effect from the elliptic Gaussian kernel in the connection between the relay and cortical cells. However, this effect appears only for patch gratings, just as observed for the temporal frequency tuning curves from figure 17. The effect seems to be that the maximum response achieved for the preferred wavenumber is lowered. Furthermore, the difference between the maximum response to a drifting and a static patch grating is smaller for cortical cells than for the relay cells.

4.7 Orientation of the elliptic Gaussian kernel may shift stimulus preferences

From the results above, it is possible to have an idea of what to expect from the maximum response when different stimuli are used in the simulations. The choices of the kernels used in the network, temporal and spatial, have proven to have a crucial role in how the response patterns behave. Something is going on in the filtering process between relay and cortical cells, especially for stimuli like patch gratings and spots.

Until now, the orientation of stimulus gratings and the long axis of the elliptic Gaussian have been aligned in tuning curves computed for wavenumber, diameter, and temporal frequency. As seen in figures 13 and 18, the peaks of the maximum responses are achieved when the ellipse orientation

θ reaches $\pi/2$ rad and $3\pi/2$ rad. At these orientations, the long axis of the ellipse and stimulus grating are aligned.

The response of the cortical cell population depends on what spatial properties pass through the elliptic Gaussian kernel. The orientation parameter θ of the ellipse will have an effect on the magnitude of the maximum response, for example will a non-optimal orientation give lower maximum responses. However, shifts of preferences and suppression effects are just as interesting to investigate. If shifts due to ellipse orientation are present, this means that θ has the potential to change how cortical cells react to other stimulus parameters as well as determining the strength of the response.

4.7.1 Diameter preferences for different elliptic Gaussian orientations

The response of a cortical cell population was computed to a drifting patch grating, and the results are shown in figure 22. The curves in panel (a) correspond to the response computed for each value of θ in the elliptic Gaussian kernel. The patch grating was chosen to have the parameters $k_{\text{pg}} = 1.96$ /deg, $\omega_{\text{pg}} = 0.055$ rad/ms and diameter $d_{pg} = 2.0$ deg. It is oriented to 90 deg. For each curve, the suppression index was computed by the definition from equation 34, and the value for each of these computations was plotted against θ as shown in panel (b).

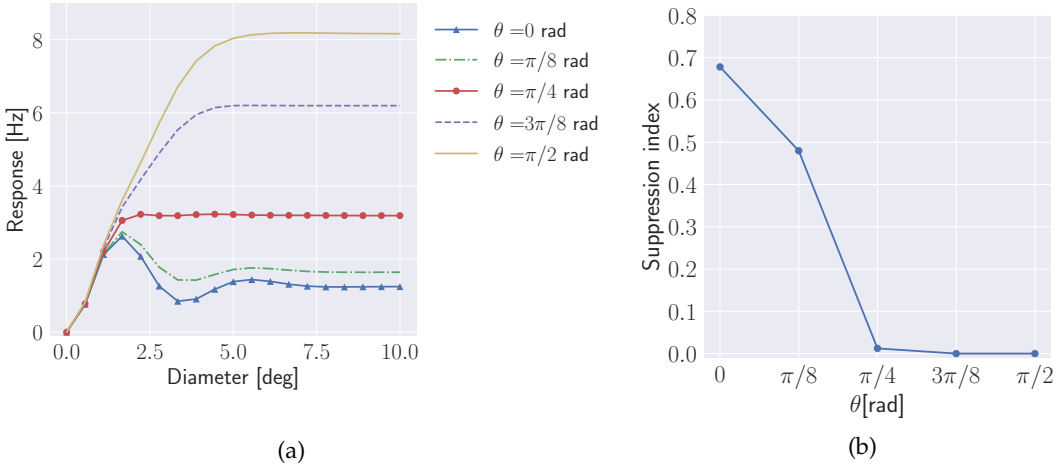

(a) (b)

Figure 22: (a) Diameter tuning curves for each orientation θ of the elliptic Gaussian. The stimulus is a drifting patch grating with its diameter ranging from zero to 10.0 deg. The other parameters are held fixed at the values for a drifting patch grating, as listed in table 2. Whereas θ ranges from zero to $\pi/2$ rad, the other kernel parameters are held fixed on the values as listed in table 1. (b) The suppression index for each curve was computed by the definition in equation 34. The line shows the relation between the suppression index and orientation of the elliptic Gaussian.

The results show that diameter preference of a drifting patch grating with the mentioned parameters is highly dependent on ellipse orientation. Panel (a) in figure 22 shows that the preferred diameter is shifted towards larger values as the orientation of the ellipse closes in to $\pi/2$ rad. When θ is $\pi/2$ rad, its long axis is aligned with the grating. The orientation only goes from zero to

$\pi/2$ rad, because the radial symmetry of ellipse rotation would give the same responses, if the orientation would exceed $\pi/2$ rad. In addition, the preferred diameter produces the largest response when the ellipse is aligned with the stimulus grating.

The suppression index was computed for each of the diameter tuning curves. Each index was plotted against the corresponding value of θ, and together, they form a curve as shown in panel (b) of figure 22. The suppression index decreases as the ellipse closes in to align with the stimulus grating orientations. Thus, the elliptic Gaussian seem to shift the diameter preference and cause suppression effects in the cortical response by its orientation parameter.

4.7.2 Wavenumber preferences for different elliptic Gaussian orientations

Figure 23 shows wavenumber tuning curves for different orientations of the elliptic Gaussian kernel. The responses in panel (a) are due to a drifting full-field grating, and in panel (b), a drifting patch grating. The wavenumber 1.96 /deg is equal for both stimulus types, and so is the temporal angular frequency on 0.055 rad/ms. The orientations of the gratings are both 90 deg. This means that the elliptic kernel is aligned with the grating when $\theta = \pi/2$ rad, for the curves in both panel (a) and (b). The patch grating in panel (b) has a diameter $d_{pg} = 2.00$ deg. It is only the cortical responses that are shown in both panels because the relay cell population is not affected by the rotation of the ellipse.

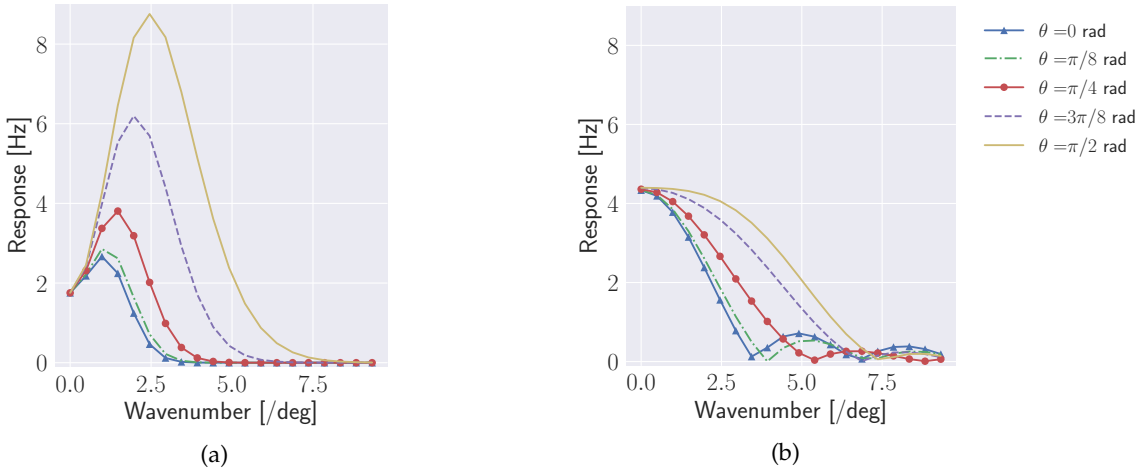

(a) (b)

Figure 23: Wavenumber tuning curves were computed as responses to (a) a drifting full-field grating and (b) a drifting patch grating. Each curve was computed for a new value of θ. θ ranged from zero to $\pi/2$ in the simulations. The other parameters of the kernels were as described in table 1. The drifting patch grating and full-field grating had a wavenumber ranging from zero to 9.33 /deg. The rest of their parameters were held fixed on the values described in table 2.

The cortical preference of the wavenumber to a full-field grating stimulus shown in panel (a) depends on ellipse orientation. As the ellipse aligns with the stimulus grating, the preferred wavenumber of the grating shifts to higher values. A higher value of wavenumber means a

smaller wavelength. The effect on the maximum response magnitude is present as well, with the highest peak for ellipse aligned with stimulus grating.

For the response to a drifting patch grating, represented in panel (b), the effect of orientation is different. When the ellipse is aligned with the stimulus grating, the value of the wavenumber can increase further without causing a response-drop as fast as it does for the other orientations. However, an oscillating effect on the response appear for the highest values of the wavenumber, most vigorously for the orthogonal positioned ellipse (when $\theta = 0$ rad).

For a patch grating, the maximum response is still the highest if the wavenumber equals zero, no matter the ellipse orientation. When the wavenumber is zero, the stimulus is equivalent to a spot of constant intensity. For a spot, orientation has no influence on the response.

4.7.3 Temporal frequency preferences for different elliptic Gaussian orientations

Since the spatiotemporal kernel is separable, the orientation of the elliptic Gaussian kernel should not be expected to shift any preferences in the temporal domain. It can, however, affect the magnitude of the response overall. To check the effects of the ellipse orientation on temporal frequency curves, responses for cortical cell populations were computed for θ ranging from zero to $\pi/2$ rad. The stimuli considered were a drifting full-field grating and a drifting patch grating. The results for each of the stimuli are shown in panel (a) and (b) in figure 24, respectively. Both stimulus types had the same wavenumber on 1.96 /deg and orientation on 90 deg. The gratings were aligned with the ellipse when $\theta = \pi/2$ rad. The patch grating had a diameter $d_{\text{pg}} = 2.0$ deg.

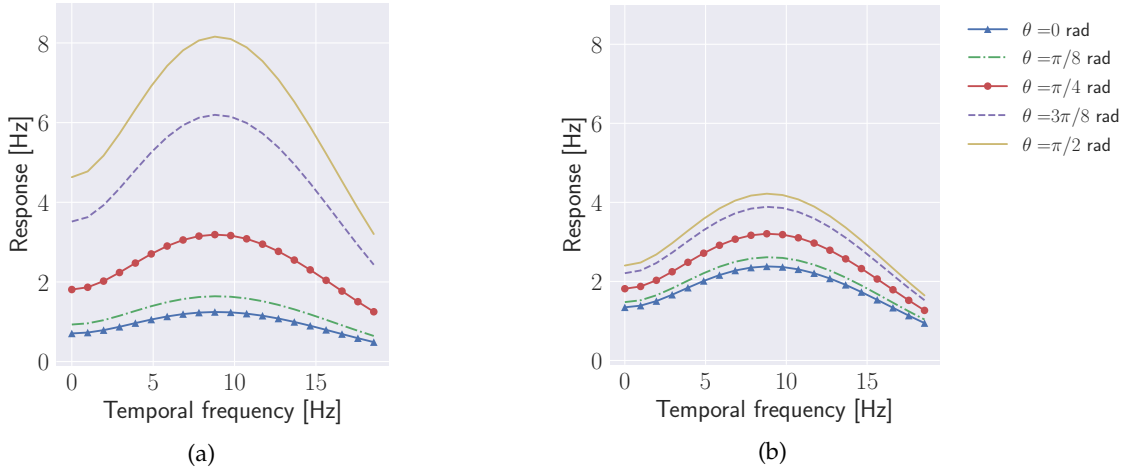

Figure 24: The temporal frequency tuning curves for cortical cell populations responding to different orientations θ of the elliptic kernel. Computation of response was done for (a) a drifting full-field grating and (b) a drifting patch grating. The stimulus parameters for the respective stimuli used are described in table 2. However, the temporal angular frequency ranges from zero to 0.12 rad/ms. θ ranges from zero to $\pi/2$ rad, whereas the other kernel parameters were fixed on the values in table 1.

Preference shift due to ellipse orientation was not observed for temporal frequency, but the maximum response is higher for the ellipse aligned with the stimulus grating. This is the case for both the full-field and patch grating. However, there are bigger differences between the orthogonal ($\theta = 0$ rad) and the aligned ellipse ($\theta = \pi/2$ rad) for full-field gratings than for patch gratings. The stimulus types indeed play an important role for the maximum response.

Moreover, it seems that the selectivity for temporal frequency is the sharpest for full-field gratings when the ellipse is aligned with the stimulus grating. The fact that the curve with $\theta = \pi/2$ rad has a bigger difference between the lowest and highest maximum responses than other values of θ reveal a potential relation between ellipse orientation and temporal frequency.

4.7.4 Ellipse orientation preferences for different wavenumbers

The results above reveal that the orientation of the elliptic Gaussian affects cell responses to other stimulus characteristics. The orientation affects not only the response magnitude, but also suppression and stimulus prefereces. It was even observed a sharpening effect on temporal frequency tuning curves.

However, what about the opposite situation? Is it possible to observe shift effects in orientation preferences due to other stimulus properties? As mentioned in section 2.7, Ayzenshtat et al. (2016) observed a case where spatial frequency shifted the orientation preferences of the stimulus. Even though this is not expected to happen in the network setup in the simulations, this could be verified if orientation tuning curves were computed for different wavenumbers.

The cortical response curves to different wavenumbers of a drifting full-field grating are represented in panel (a) in figure 25. The full-field grating had the fixed parameters $\omega_{\text{fg}} = 0.055$ rad/ms and $\theta_{\text{fg}} = 90$ deg. The wavenumber ranged from 0.49 /deg to 4.91 /deg. The ellipse was aligned with the grating when $\theta = \pi/2$ rad and $3\pi/2$ rad. Panel (b) shows the orientation index computed by the definition from equation 35. Each point corresponds to each of the curves in panel (a). These points are plotted against the wavenumber to show the relation between orientation selectivity and wavenumber.

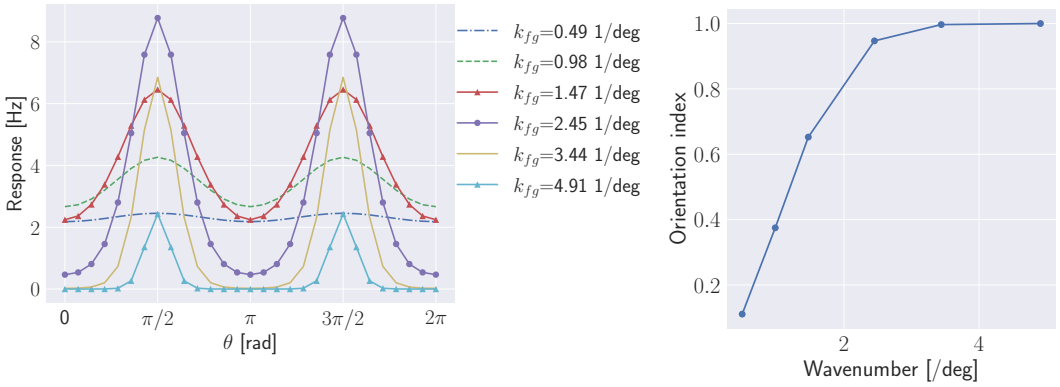

(a) (b)

Figure 25: (a) Orientation tuning curves for the elliptic Gaussian computed for different values of the wavenumber. The wavenumber k_{fg} of a drifting full-field grating varied, whereas the rest of the parameters were held fixed on the values for a drifting full-field grating in table 2. In addition, the orientation θ of the ellipse was changed, whereas the rest of the kernel parameters were fixed as defined in table 1. (b) Orientation indexes corresponding to the curves in panel (a) plotted against wavenumber.

Panel (a) in figure 25 shows that the curves are sharper when close to the optimal wavenumber. The highest peaks of the maximum value are reached when k_{fg} is 2.45 /deg. If the wavenumber increases beyond the optimal value, the maximum values of the curves drop. The relation between the orientation index and wavenumber is shown in panel (b). It seems that orientation selectivity increases for increasing wavenumber. There are no preference shifts observed, only change in orientation selectivity and magnitude of the highest maximum response.

4.8 Response patterns due to wavenumber and diameter

The diameter preferences and suppression of cortical cells depend on stimulus types and properties of the elliptic Gaussian, such as elongation and orientation. However, the wavenumber dependence of the preferred diameter has already been mentioned a couple of times, referring to this section. A suggestion is that the wavenumber of stimulus gratings, as well as ellipse orientation and shape, has the potential to change diameter preferences and suppression patterns. Diameter tuning curves computed for different values of the wavenumber can reveal the relation.

Cortical responses as diameter tuning curves were produced, each for drifting patch gratings of a different wavenumber. The patch gratings had a diameter $d_{\text{pg}} = 2.0$ deg, the temporal angular frequency ω_{fg} was 0.055 rad/ms, and the orientation of the grating θ_{pg} was 90 deg. The grating was thus aligned with the long axis of the elliptic Gaussian. The tuning curves are combined in panel (a) in figure 26. In addition, the suppression index of each curve was computed. The relation between suppression index and wavenumber is plotted in panel (b) in figure 26.

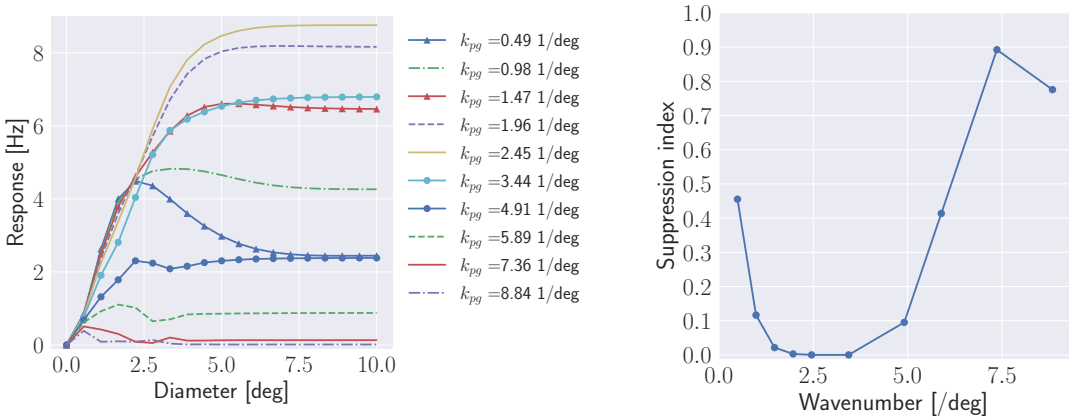

(a) (b)

Figure 26: (a) Diameter tuning curves were computed for a cortical cell population responding to drifting patch gratings of different wavenumbers. The wavenumbers ranged from 0.49 /deg to 8.84 /deg. The patch had a temporal angular frequency of 0.055 rad/ms and its orientation $\theta_{\text{pg}} = 90$ deg. Its diameter ranged from zero to 10.0 deg. Kernel parameters are as described in table 1. (b) The suppression index computed by the definition in equation 34. The indexes are plotted against the wavenumber.

As the wavenumber increases, the curves in panel (a) expose a shift from small to large diameter preferences. The highest maximum value is reached for the biggest patch diameters with a wavenumber of $k_{\text{pg}} = 2.45$ /deg. However, wavenumbers beyond this value lower the maximum value. In addition, the diameter preference shifts back to small diameters.

The suppression index in panel (b) decreases rapidly as wavenumber increase from the lowest values. However, the suppression increases again for wavenumbers higher than 3.44 /deg. The suppression indexes for the curves were computed by the definition in equation 34.

The wavenumber has the power to change diameter preference, the magnitude of the maximum response, and the suppression behaviour of cortical cell populations. However, the effect of preference shifts between diameter and wavenumber goes in both directions.

As diameter changes, so does the amount of light and dark regions from the grating inside the patch. Since the wavenumber decides the wavelength of the grating, there will be different wavenumbers which are the most effective in reproducing the highest response for each diameter. The diameter relative to the size of the elliptic kernel may also affect the response. As the size of the patch increases outside the reach of the ellipse, the ellipse will no longer perceive the edges of the patch.

To investigate the wavenumber dependence of patch diameter, wavenumber tuning curves were computed for diameters ranging from 0.1 deg to 10.0 deg. The wavenumber itself ranged from zero to 9.33 /deg. Figure 27 shows the results for a cortical cell population responding to a drifting patch grating. The parameters of this stimulus were $\omega_{\text{pg}} = 0.055$ rad/ms and $\theta_{\text{pg}} = 90$ deg, thus the grating was aligned with the elliptic Gaussian.

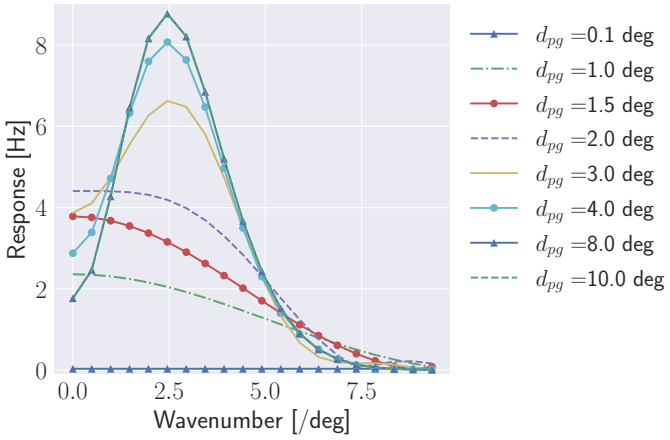

Figure 27: Cortical wavenumber tuning curves for different patch diameters of a drifting patch grating. The wavenumber ranged from zero to 9.33 /deg, whereas the diameter was varied between 0.1 deg and 10.0 deg. The other parameters of the stimulus were held fixed on $\omega_{\text{pg}} = 0.055$ rad/ms and $\theta_{pg} = 90$ deg. Kernel parameters were as described in table 1. Thus, the elliptic kernel was aligned with the grating of the stimulus.

The spatial filter shifts from low pass to band pass of spatial frequency as the diameter increases. The response actually change from being similar to responses of patch gratings, with preferred wavenumber being zero, to a response pattern similar wavenumber tuning curves of full-field gratings as seen in figure 21 from section 4.6. The maximum response is also highest for preferred wavenumbers, if the patch diameter is on its largest.

4.9 The effects of the feedback weights

Now, as the different stimuli and elliptic Gaussian properties have been investigated for the different tuning curves, the remaining question is whether the feedback in the eDOG model affects the cortical response.

The sum of the elliptic kernels in the feedback loop is simplified into a circular Gaussian. Thus, orientation of the elliptic Gaussian does not contribute to the feedback effects on the relay cell population. The feedback effects the cortical cell population is expected to experience are directly inherited by the feedforward connection between the relay and cortical cell layer. The cortical cell population which produces the responses shown in the figures below is not the population which is included in the feedback connection. The cortical population considered does not have any other connections than the direct feedforward from the relay cell population. Thus, similar effects of feedback in relay response should appear in cortical response as well. Any differences between relay and cortical cell responses are a consequence of the ellipse, not the feedback.

The feedback effects observed in studies have been various and have a range of different causes. eDOG is restricted to linear relations, and the cell populations are only dependent on the stimulus and their connections included in the model. Other external factors are not considered. However, similar simulations, like the one done by M. H. Mobarhan et al. (2018) revealed that the eDOG

model with feedback caused changes in the center-surround antagonism of relay cells. In addition, the amount of suppression was increased with strong mixed (both inhibitory and excitatory) feedback present. The feedback in eDOG is expected to cause a modulation effect on the magnitude of the response as well (Einevoll & Plesser, 2005).

Furthermore, observations of preference shifts have been observed for relay cells with the presence of mixed feedback. For example, Andolina et al. (2013) observed a shift to smaller diameters without feedback present. However, studies have achieved various results for diameter preferences. Spatial frequency has also been observed to shift with feedback (M. H. Mobarhan et al., 2018).

Related to the temporal domain, Hasse and Briggs (2017) suggested a sharpening of the temporal precision as a consequence of the presence of feedback.

Feedback was varied by changing the corresponding kernel weights, to evaluate whether some of these effects appear in the simulations. The feedback kernels used are two Gaussian functions corresponding to excitatory and inhibitory signals for the feedback kernel $K_{\mathrm{RC_n}}$. The amplitude of these kernels have opposite signs; positive for the excitatory kernel, and negative for the inhibitory kernel. If the feedback connections were not included in the simulation, the weights for these kernels would both be equal to zero. The responses computed for this situation were compared with responses computed with only excitatory feedback, only inhibitory feedback, and for the mixed feedback.

4.9.1 Response curves for rotation of the elliptic Gaussian for different combinations of feedback weights

Cortical responses were computed for different feedback weight combinations as the elliptic Gaussian kernel was rotated. The stimulus was a drifting full-field grating with $k_{\mathrm{fg}} = 1.96$ /deg, $\omega_{\mathrm{fg}} = 0.055$ rad/ms, and $\theta_{\mathrm{fg}} = 90$ deg. Thus, the long axis of the elliptic Gaussian was aligned with the grating as it reached the value $\theta = \pi/2$ rad and $3\pi/2$ rad. The results for this simulation are shown in panel (a) in figure 28. The orientation indexes were computed for each feedback combination by the definition from equation 35. The indexes are shown in panel (b).

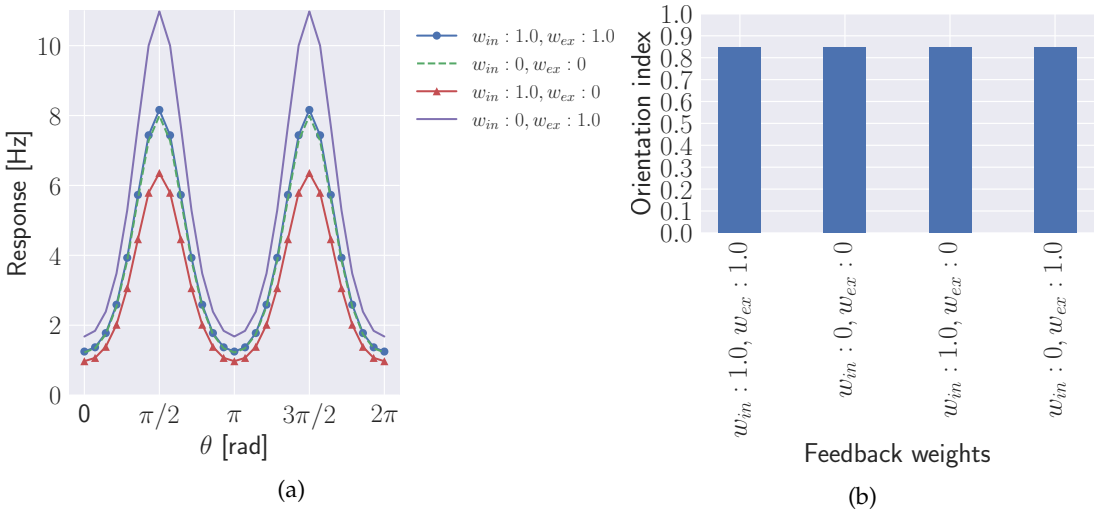

(a) (b)

Figure 28: (a) Orientation tuning curves for the elliptic Gaussian were plotted for different combinations of the weights w_{ex} and w_{in} of the feedback kernels $K^{ex}_{RC_n}$ and $K^{in}_{RC_n}$. The kernel parameters, other than these feedback weights and the value of θ were as listed in table 1. The stimulus was a drifting full-field grating with parameters $\omega_{\text{fg}} = 0.055$ rad/ms, $k_{\text{fg}} = 1.96$ /deg and $\theta_{fg} = 90$ deg. (b) The orientation indexes were computed by the definition from equation 35.

The modulation effect, mentioned by (Einevoll & Plesser, 2005), seem to appear as the feedback combinations are changed. With excitatory feedback only, the cells produce higher response values than for any other of the combinations. The response with only inhibitory feedback is, on the other hand, the lowest. No feedback, and the mixed feedback seem to give somewhat similar response patterns, with only a difference of 0.17 Hz for the peak of the maximum response. The orientation index in panel (b) does not reveal any difference in orientation selectivity. However, the response achieved is the highest for excitatory feedback only.

4.9.2 Diameter tuning for different combinations of the feedback weights

In figure 29, diameter tuning curves of both relay and cortical cell populations were computed for the different weight combinations. The stimulus was a flashing spot with duration $dt = 50$ ms and delay $\Delta_{\text{fs}} = 0$ ms. The corresponding suppression indexes were computed as shown in figure 30.

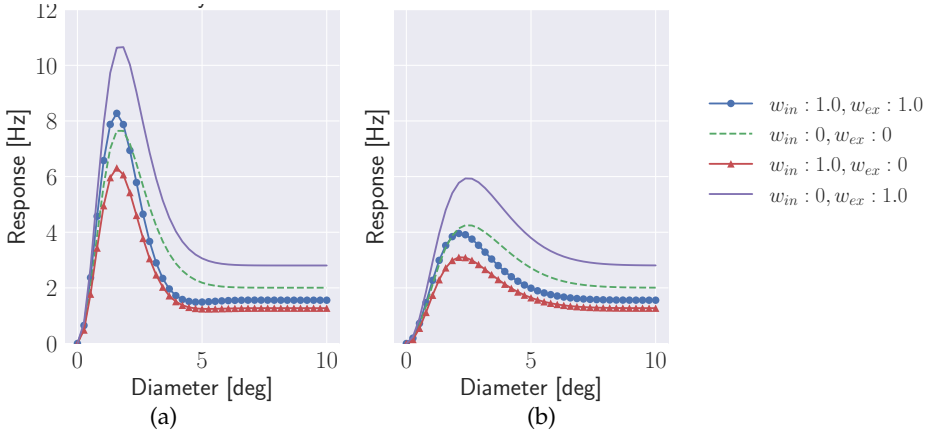

Figure 29: Diameter tuning curves for different combinations of the excitatory w_{ex} and the inhibitory w_{in} feedback weights. The responses were computed for both (a) relay and (b) cortical cell populations. The stimulus was a flashing spot with the diameter ranging from zero to 10.0 deg. Its other parameters were held fixed on the values for flashing spots in table 2. The kernel parameters, other than the feedback weights were as listed in table 1.

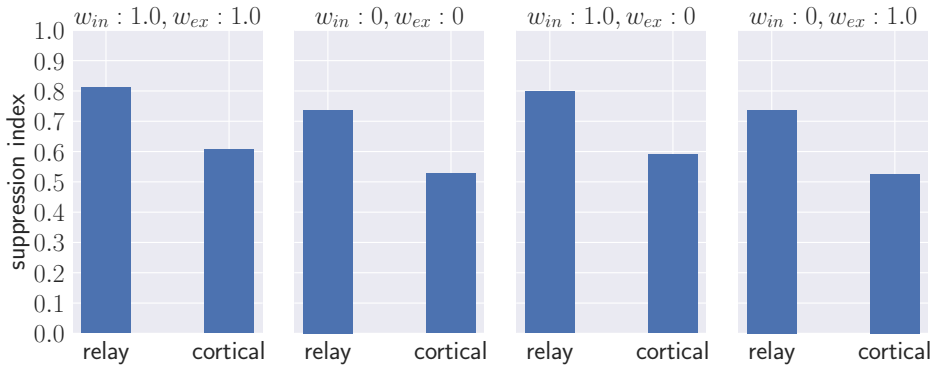

Figure 30: Suppression indexes for diameter tuning curves corresponding to figure 29. The suppression indexes were computed from the definition in equation 33, for both relay and cortical cell populations.

The curves in figure 29 reveal that there is indeed a slight shift i diameter preference, which is most visible for the cortical response. A shift towards smaller diameters is observed for both mixed feedback and inhibitory feedback. They share a preferred diameter of 2.10 deg, in contrast to the purely excitatory feedback and no feedback, which share a preferred diameter of 2.63 deg (the accuracy of these numbers are restricted by the resolution).

The suppression index is slightly affected for both mixed and inhibitory feedback as well. The suppression index is higher for both cases compared to the pure excitatory feedback or no feedback

at all. The biggest difference is 0.071 for the relay cell population and 0.084 for the cortical cell population between mixed feedback and no feedback.

4.9.3 Wavenumber tuning for different combinations of feedback weights

Wavenumber tuning curves are interesting in the context of the shifted preferences observed in the paper by M. H. Mobarhan et al. (2018). If shifts were observed for the relay cell population with feedback present, it should be validated if this would appear in the cortical cell population as well.

The tuning curves of figure 31 show relay and cortical responses to a drifting full-field grating in panel (a) and (b) respectively. The wavenumber of the full-field grating ranged from zero to 9.33 /deg, whereas the the other parameters were $\omega = 0.055$ rad/ms and $\theta_{fg} = 90$ deg. The grating was aligned with the long axis of the elliptic Gaussian.

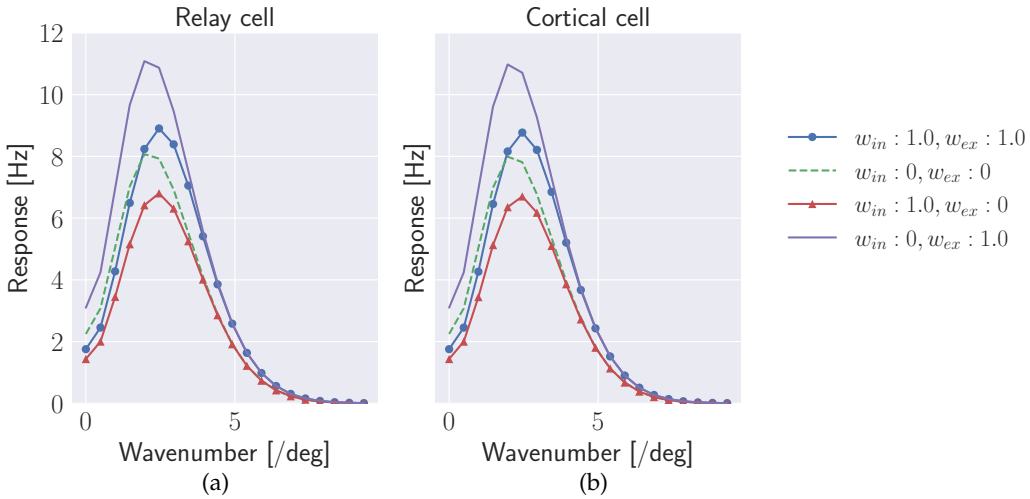

Figure 31: Wavenumber tuning curves for both (a) relay, and (b) cortical cell populations. The curves correspond to responses computed with different combinations feedback weights. The stimulus was a drifting full-field grating with parameters as in table 2, except for the wavenumbers, which ranged from zero to 9.33 /deg. Kernel parameters other than the feedback weights are listed in table 1.

The curves reveal that there is a shift towards higher frequencies for both mixed feedback and inhibitory feedback. The preferred wavenumber for the simulation with no feedback, and the one with the excitatory are both 1.96 /deg. For the mixed feedback, and the feedback which is only inhibitory, the preferred wavenumber is rather 2.45 /deg (the resolution restricts the accuracy of these numbers). Furthermore, excitatory feedback enhances the maximum response, whereas inhibitory response decreases it.

4.9.4 Temporal frequency tuning for different combinations of feedback weights

Temporal frequency tuning curves for relay and cortical cell populations are shown in panel (a) and (b) in figure 32, respectively. The cell populations respond to a drifting full-field grating with wavenumber $k_{\text{pg}} = 1.96$ /deg and orientation $\theta_{\text{fg}} = 90$ deg. Thus, the grating is aligned with the long axis of the elliptic Gaussian, since its orientation is $\theta = \pi/2$. The temporal angular frequency ranged from zero to 0.12 rad/ms, which corresponds to a range in temporal frequency from zero to 19.1 Hz. Each curve in both panels correspond to the responses computed with different feedback weights.

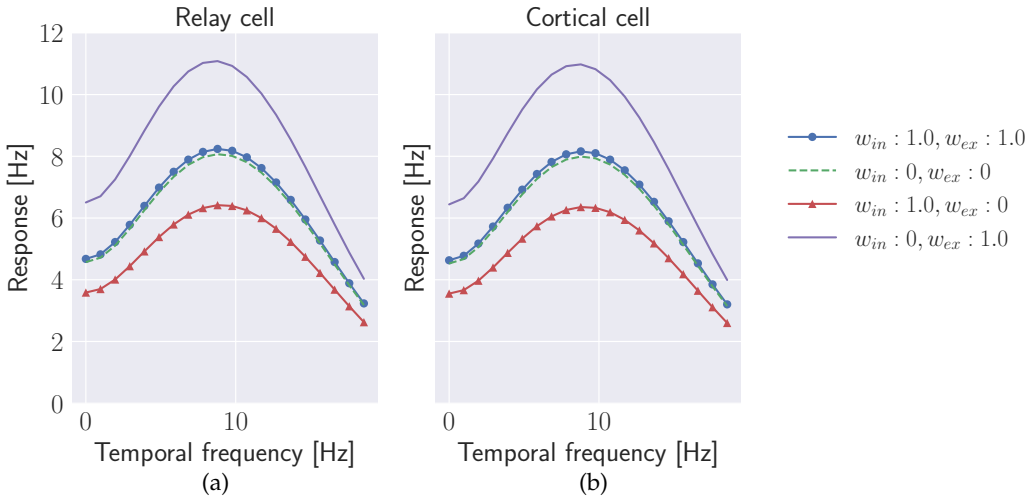

Figure 32: Temporal frequency tuning curves for different combinations of excitatory w_{ex} and inhibitory w_{in} feedback weights for (a) a relay cell population and (b) a cortical cell population. The stimulus was a drifting full-field grating with parameters as listed in table 2. However, the temporal angular frequency ranged from zero to 0.12 rad/ms. Kernel parameters, other than the feedback weights, are listed in table 1.

The curves in both panels of figure 32 show no shifts in frequency preference. Nevertheless, excitatory feedback enhances the maximum response, and inhibitory feedback decreases it. Just as with wavenumber tuning curves in figure 31, the temporal frequency tuning curves are similar for both relay and cortical cell populations. However, this is a consequence of the stimulus type, which is a drifting full-field grating for both cases, and has nothing to do with the feedback.

5 Discussion

By validating the definition of the elliptic Gaussian kernel for the eDOG model, it is possible to interpret results from simulations on more stable ground. The model gives a good representation of the cortical cell layer of the early visual system if the inclusion of the elliptic kernel matches expectations.

The results investigated how stimuli, kernels, and feedback affect the cell population responses. This was done by using the eDOG model including the elliptic Gaussian. The cortical cell population with this spatial kernel was connected to the relay cell population, and gave the responses presented in the results.

Effects changing suppression patterns, response magnitude, and shift preferences have earlier been observed in LGN relay cells for this model (M. H. Mobarhan et al., 2018). However, in this thesis, these effects appear in cortical cell populations as well. This thesis provides answers on whether the eDOG model with the elliptic Gaussian kernel implemented in the software PyLGN can be used to predict cortical cell response.

Since eDOG is a linear model, it considers only linear relations between stimulus and response. However, rectification of the cortical response is included in all simulations. The effects that appear in cortical cells depend on the network kernels, connection weights and stimulus type. The spatiotemporal connection between the relay cell population and the cortical cell population consists of the elliptic Gaussian kernel and a temporal delta kernel. Thus, cortical response may differ from relay response because of the difference in the shape of the receptive fields.

However, to what extent the responses are formed depends on the parameters of the stimuli used in the simulations. This is why the results section contains figures where properties of the stimulus parameters are varied to produce response. By investigating the responses in this way, it is possible to predict how a cortical cell population with particular parameters for the elliptic Gaussian kernel responds to specific stimuli.

Since the cortical cell population is directly connected to the relay cell population, it is expected that effects appearing in the relay cell population are inherited in the cortical cell population. This also includes the effects of the feedback loop. By changing the weights of the feedback loop in the model, response curves can be produced to reveal the effects in both relay and cortical cell populations.

5.1 The validation of the elliptic Gaussian

The validation performed in section 4.2 was meant to secure that the ellipse defined computed responses as would be expected by an elliptic Gaussian kernel. The filter operation is a convolution between the input and the filter kernel. In the Fourier domain, this operation is simplified into a multiplication. The relay response works as the input signal for the cortical cell population, and the elliptic Gaussian is the spatial filter. With this in mind, the ellipse should appear by a simple division of the Fourier domain cortical response by the relay response.

The division does not yield the exact same ellipse as the defined one. However, the difference between the two is of the order 10^{-18}, and is thus negligible. It should be a safe conclusion to say that the ellipse is correctly defined, and is applicable for use in PyLGN.

5.2 Different orientation preferences contribute to build the interpretation of edges in an image

The elliptic Gaussian kernel is crucial for the orientation selective properties of cortical cells. The highest cortical cell responses to the natural image in figure 10 follow the edges that align with the ellipse orientation. The cortical response shown in figure 11 has been through several layers of filtering by the cells upstream in the early visual system, and the image is barely recognizable. However, this means that each cell population, with its preferred orientation, deals with only a few features at the time. The responses are computed for only three different preferred orientations. If there was a sufficiently large number of cell populations, each dealing with their preferred features, they would all contribute to the brain's interpretation of most edges in the image as a whole.

5.3 Spatial effects

The elongation of the receptive fields is believed to be central in orientation and spatial frequency selectivity of cells in the visual system. The elliptic Gaussian is the function used to represent the spatial feedforward connection between the relay and cortical cells in this thesis. Firstly, the elongated shape is consistent with how cells are selective for orientation. However, the fact that the function is a Gaussian function also makes it applicable to include in computations from the eDOG model.

The elongated shape of the ellipse is important for cortical cell response to visual stimuli. The elongation of the kernel not only sharpens the orientation selectivity of the cells, it also has the power of shifting preferences in patch diameter and wavenumber. Furthermore, elongation of the ellipse has the potential to remove surround suppression for a drifting patch grating. A weakness of the ellipse parameter choices for this thesis is that the parameters of the ellipse were taken from the paper by Einevoll and Plesser (2012), whereas the other kernels were inspired by M. H. Mobarhan et al. (2018). This leads to a mismatch between the length of the long axis of the ellipses and the diameter of the Gaussian in the feedback.

Preference shifts due to elongation of the ellipse may be related to the fraction of the spatial receptive field covered in light as the light and dark bars of the grating drift over the field. When the grating and ellipse are aligned, the narrow ellipse is more likely to be fully covered in light than for the more circular shaped fields. This is, however, dependent on grating wavenumber and diameter in the case of patch gratings.

To say something about the effect of ellipse shape on the magnitude of the maximum response, a different approach should be performed. The maximum response was observed to decrease as the kernel between relay and cortical cells became wider. The reason for this is most certainly because the amplitude of the elliptic Gaussian is adjusted dependent on the spatial area of the ellipse. When the narrow axis increases while the long axis is held fixed, the spatial area of the kernel increases. Consequently, the factor in front of equation 14 decreases in magnitude, thus lowering the maximum response. If the area of the field rather was held constant, as it changed shape, this would prevent the amplitude from changing. This approach would eliminate effects caused by change in amplitude.

Orientation of the elliptic Gaussian was changed to produce orientation tuning curves for cortical cells. The highest response were in all cases achieved when the elliptic kernel was aligned with

the stimulus grating. This result follows the argumentation of Hubel and Wiesel (1962). In simple cells, the explanation for this is related to the contributions from the ON-centered receptive fields. These contributions build the the elongated field of the cortical spatial connection kernel. When the elongated field aligns with stimulus grating, more of the ON-center contributions are covered in light. Thus, the response increases.

However, one should be careful claiming that the curve with the highest peak of the maximum response reveals the highest orientation-selectivity. An example is shown in figure 28, where there is a clear difference between the peaks of the maximum responses. When looking at the corresponding orientation index, it discloses that the orientation selectivity is the same for all combinations. The difference between the aligned and the orthogonal position of the ellipse is included in the definition and defines orientation selectivity. Furthermore, this is a simulation without noise in the firing rates. A situation with noisy firing rates would weaken the definition of the orientation index, since noise can disturb the firing rates (Mazurek et al., 2014).

As pointed out by Dayan and Abbot (2001), direction selectivity would require that the space-time receptive fields are non-separable. This is not yet been implemented in the software of PyLGN. If there was direction selectivity, curves like the ones produced by Usrey et al. (2009) should appear. The maximum response would be different when the ellipse would have turned $\pi/2$ rad from its original position for drifting gratings. In the results of this thesis, the maximum response is the same for both directions.

The observed effect from Ayzenshtat et al. (2016), where spatial frequency adjusts orientation preference, deviates from results achieved in figure 25. This figure does not show that the wavenumber shifts preferred orientation. The only effect observed from this is a change in the magnitude of the maximum response for the orientation tuning curves. Orientation preferences for the ellipse will in the eDOG model mainly be based on the orientation relative to the stimulus grating. A shift in orientation preference due to spatial frequency would require a more complex model. However, lower wavenumbers give broader grating patterns. A receptive field would, for example, for the lowest wavenumbers of drifting patch gratings, perceive the grating passing by more like a flashing spot than a grated patch. In such cases, selectivity of orientation would not be as vigorous as for higher wavenumbers. Nevertheless, spatial frequency has a significant impact on orientation selectivity.

On the contrary, the ellipse orientation itself has the potential to shift preferences of other stimulus properties. Both the wavenumber of full-fields and the diameter of patch gratings shift preferences, not only depending on ellipse shape, but also depending on ellipse orientation. Suppression effects for diameter tuning curves seem to appear as well.

Suppression effects commonly appear for circular shaped Gaussian functions because circular Gaussian functions respond by surround-suppression, inherited by the response of the DOG kernel from the retinal ganglion cells. In the case of ellipse orientation, with the elongated shape intact, suppression appears as well. This happens in diameter tuning curves as the ellipse is positioned orthogonally on the grating. A reason can be that when the ellipse is orthogonal to the grating, both the central ON and flanking OFF-fields inherited by DOG from retinal ganglion cells are covered by the same stimulus intensity at the same time. This can be the cause why a suppression effect is observed on the surround for increasing diameters of patch gratings. However, as mentioned, suppression effects, related to diameter tuning, are also dependent on wavenumber. Small wavenumbers, corresponding to big wavelengths, cause suppression. This can also be a

consequence of the stimulus covering the ellipse with its flanks by the same intensity values at a time it drifts over the receptive field.

For wavenumber, the observed preference shift as the ellipse rotates, possibly has something to do with how much of the ellipse is covered in light as it responds to a grated stimulus. If the ellipse lies orthogonally to the stimulus grating, the wavelengths have to be wider to cover the whole ellipse. Thus, the preferred wavenumber shifts to lower values. Moreover, the maximum value is at its lowest for an orthogonally positioned ellipse. This is the orientation which is the least optimal for a cell responding to a grated stimulus.

The tendency of lower cortical response than relay response seems to be a common effect for patch gratings. As the signals change through the feedforward connection from relay to cortical cell populations, the differences should be caused by the elliptic Gaussian kernel. The question is then, why does this happen for patch gratings and not for full-field gratings? One possible cause could be related to that the patches have a diameter limit. If the diameter of the patch is within the range of the ellipse, the edges of the patch can restrict the amount of light covering the ellipse, and thus restrict the maximum response achieved.

The relationship between preferred diameter and wavenumber is important for patch gratings. As the diameter of a patch grating increases, the wavenumber tuning curves get more similar with as if the cell population had responded to a full-field grating. This is consistent with what has been discussed for stimuli in the paper by Einevoll and Plesser (2005). A full-field grating can be achieved by letting the patch diameter go to infinity. The reason can be that the edges of the patch are no longer within the reach of the ellipse. Thus, at this point, the receptive field perceives the stimulus as a full-field grating rather than a patch grating. If the diameter is much smaller than the wavelength, the response becomes similar to responses for iso-luminar spots (Einevoll & Plesser, 2005). However, they observed a larger response for full-field gratings in the range of the wavenumber from 3.5 to 8 /deg than a patch grating covering the receptive-field center. In this thesis, a higher maximum response was also observed for full-field gratings, but this was within the range of roughly 2 to 4.5 /deg for relay responses to drifting gratings. For cortical responses the range was roughly from 1 to 5 /deg. Differences can be due to kernel and stimulus parameters.

Preferences of diameter are dependent on wavenumber, and opposite. The results reveal that for small diameters, there is a low-pass effect on spatial frequency. The smallest values of the wavenumber are the preferred ones for the small diameter patches. This was also seen in the simulations from the paper by M. H. Mobarhan et al. (2018). Furthermore, large patch diameters shift the wavenumber preferences to higher frequencies, which is also confirmed by M. H. Mobarhan et al. (2018).

The cells are sensitive to spatial resolution, and at a point, the wavenumber is too big for the cell populations to perceive the stimulus. This is why the response eventually drops to zero for the biggest wavenumbers. This happes both in relay and cortical cell populations for all tuning curves related to wavenumber.

Furthermore, this behaviour is common for temporal frequencies as well. The temporal parameters set limits for which frequencies the cells are able to perceive. The highest temporal frequencies will eventually cause the response to drop to zero.

5.4 Temporal effects

The temporal effects observed are not expected to be caused by the elliptic kernel itself, because there are only used spatiotemporally separable kernels in all simulations. However, the temporal kernels do have an important role when responses are produced. The response magnitude, the phase shift, and preferred temporal frequency are all influenced by the temporal kernels.

The biphasic phase shift is a common observation for relay cells (Yousif & Denham, 2007; Cai et al., 1997; Reid et al., 1997). Eventually, since only the maximum response over time has been computed in all cases in this thesis, the effect of the phase shift is not visible when plotting the tuning curves. To evaluate response over time, it is possible to create movies by setting responses computed on each time step together. Snapshots from different time steps can give an idea of what happens during the simulation. In this thesis, the temporal effects were not the main focus, but it is possible to do such simulations to explore temporal effects.

When plotting figure 16, it was revealed that there is a scale difference between the biphasic kernel and the other temporal kernels. It is the biphasic kernel that contributes to the high magnitudes of the maximum response, whereas the temporal delta kernels do not seem to influence the maximum response at all. However, this comparison is not necessarily representative for the kernels. The big scale difference minimizes the visibility of possible effects from other than the biphasic kernel. For a better comparison, the biphasic kernel could be scaled down to the level of the exponential decay and delta kernel, or the effects of the curves could be plotted in separate figures.

The exponential decay kernels contribute to the simulation as a more realistic approach over time than delta kernels, because of the closer relation with how signals generally propagate through axons. For simplicity, delta kernels were used in the feedforward connection between the relay and cortical cell layer, and the delay parameter for all temporal delta kernels was set to zero. This is a feature that could be further investigated for cortical cell populations. For example, M. H. Mobarhan et al. (2018) found that delay in the temporal kernels had different effects on relay response regarding feedback.

Parameters used in simulations have shown to have a great influence on how responses are produced. The resolution of the temporal grid sets limits for which inputs are allowed in computing stimuli and the value of each sampling point in the temporal space. The temporal resolution was chosen to be 1024 time points, with a magnitude of 1 ms between each point. This means that each simulation corresponds to a time duration of 1024 ms $\approx$ 1 s. This is an important feature to keep in mind when producing biologically realistic cell responses.

The resolution is also important for choosing which other temporal parameters to be included in the simulation. For example, if the temporal resolution is on 1 ms, the time constant τ of the exponential decay kernel cannot be smaller than that.

In this thesis, the temporal resolution has limited the number of points that could be chosen for other simulations, for example when tuning for gradually changing spatial parameters of a stimulus. Since the results produced are simulations, small changes are still worth mentioning. The resolution of the plots catches the effects from the simulations. On the contrary, if this thesis was an experimental study, statistical approaches would be needed to say that a change is significant or not.

The simulations support that moving stimuli give higher maximum responses than static stimuli.

Hubel and Wiesel (1962) suggested that a reason could be the effect of the stimulus leaving an inhibitory area, simultaneously with entering an excitatory area.

Otherwise, the results for temporal frequency tuning curves reveal only changes in magnitude of the maximum response based on ellipse orientation and feedback. The differences are probably a consequence of the ellipse orientation in general giving lower maximum responses, if the ellipse is not aligned with stimulus grating. However, the result for a drifting full-field grating in figure 24 is worth further investigation. The elliptic orientation seemed to have a sharpening effect on temporal frequency selectivity. Furthermore, excitatory and inhibitory feedback excites and inhibits the response regardless of the temporal frequency. Nevertheless, selectivity of the temporal frequency contributes to the highest maximum response.

5.5 The role of the feedback loop

The suggestion from Hasse and Briggs (2017), where feedback sharpens the temporal precision of LGN responses, is not shown in the results. However, in the paper by (M. H. Mobarhan et al., 2018), it was observed that the feedback could sharpen the temporal frequency selectivity in LGN. This applied to feedbacks with nonzero delays. In this thesis, all delay parameters are zero. Further investigation of temporal effects should include different feedback delays instead of keeping it on zero for all simulations.

The modulation change of the response as a consequence of feedback is expected to happen for the spatial features as well. For orientation of the elliptic Gaussian kernel, there is expected to be effects only regarding the response magnitude. The reason is that the feedback spatial kernel is a circular Gaussian function in the simulations. Thus, ellipse orientation is not relevant for the feedback effects. Any shifts in preferred orientation as a consequence of feedback would indicate a bias in orientations of the ellipses that are summed. This requires another setup for the feedback kernels.

As expected, the feedback effects on orientation tuning curves are only by change of response magnitude. The difference between no feedback and mixed feedback is not very different. The observations are that excitatory feedback excites, and inhibitory feedback inhibits the response magnitude. A mix of the two, equally weighted, work both ways. Thus, the difference observed is probably caused by the different magnitudes of their amplitudes.

In the case of feedback for diameter tuning curves, shifts in preferred diameter were observed in the paper by Andolina et al. (2013). In their case, with feedback present, there was a preferred diameter of 0.7 deg. Without, it was rather 1.5 deg. In figure 29, there was a shift to smaller diameters as well, but only for mixed and inhibitory feedback.

Another result from the same study by Andolina et al. (2013) was that with feedback present, the suppression was larger than for the case without, for a flashing spot. They experienced a reduction of 74.6 % on the response with feedback present compared to 34.1 % without. This means that the difference they observed for the suppression index with feedback present, and the index with feedback absent, was 40.5 %. This corresponds to a difference of 0.405 of the suppression index. The parameters used for the flashing spot in this study were not the same as what was used for the flashing spot in figure 29. In this figure, the biggest difference between feedback and no feedback was 0.071 for relay and 0.083 for cortical cells. Even though the magnitude of the

difference is far off the result from the paper of Andolina et al. (2013), it supports that feedback increases suppression, at least for mixed and inhibitory feedback.

In the paper by M. H. Mobarhan et al. (2018), there was a shift in preferred spatial frequency as a result of feedback as well. The preference of spatial frequency was shifted towards higher values when mixed feedback was present. This is supported by the results from figure 31, where mixed feedback and inhibitory feedback shifted to a 0.49 /deg higher wavenumber, relative to no feedback. Excitatory feedback does not seem to shift the preference of spatial frequency relative to no feedback. However, M. H. Mobarhan et al. (2018) had a simulation where excitatory feedback shifted the preferred frequency to lower values than the case of no feedback.

Similar for all feedback results is that the feedback can affect the magnitude of the response, and that the cortical cell populations indeed inherit the effects seen in relay cell populations. Shifts for preferences of diameters and wavenumbers are present, and suppression increase in both relay and cortical cell populations as a result of mixed and inhibiting feedback.

5.6 Suggestions for further research

PyLGN is very much adaptive to use for different situations. One suggestion for further research could be to investigate whether retinotopic firing patterns could be modeled by using PyLGN. This could be implemented by introducing several cortical populations positioned relative to each other. The matter of retinotopy is well mapped out, and is known to be important for visual processing (Kremkow & Alonso, 2018). Furthermore, recurrent connections between cortical cells could also be a topic for future research. This is a topic much discussed related to orientation selectivity. However, the complexity of the network may expand outside the bounds for the linear eDOG model. Nevertheless, the potential for such a simple model to be a basis for of more complex models remains to be investigated. In the first go, simpler biological phenomena, which are applicable to a linear model could be included in the simulations. Secondly, the non-separable spatiotemporal kernels could be added to the software. This would open for simulations including phenomena dependent on these types of kernels, for example direction selectivity.

The elliptic Gaussian is assumed to be the spatial receptive field of cortical cells in this thesis. Thus, the results must be interpreted in the light of the fact that the elliptic Gaussian is just a function independent on the script of PyLGN.

The ellipse is a beneficial choice of the spatial kernel of cortical cells because it is a Gaussian function, just as the rest of the spatial kernels in the model. The convolutions are easy to implement, and analytical solutions are computed by simple multiplication operations in the Fourier domain. The elongated shape contributes to orientation selectivity following the logic of elongated receptive fields in the paper by Hubel and Wiesel (1962).

The flexibility of the elliptic Gaussian function allows building of spatial receptive fields in other shapes as well. For example, a biased sum of elliptic Gaussian functions can be used to model asymmetry. Assymmetry is a response pattern which is commonly observed for cortical cells in the visual cortex (Ayzenshtat et al., 2016). A weighted sum of several ellipses with offsets or bias in stimulus preference can contribute to build spatial receptive fields with asymmetric properties.

The elliptic Gaussian function, as defined in the paper by Einevoll and Plesser (2012) was used for this thesis. However, this does not mean that it is the only function which can be used for the

spatial receptive fields of cortical cells.

Another example of asymmetry is different shapes of the flanking regions of the cortical spatial receptive field. The flanking regions are inherited by the surround field of DOG kernels earlier in the system. A common modeling strategy for the cortical receptive fields is the use of Gabor filters. Usrey et al. (2009) compared recorded cortical responses with the Gabor function. The Gabor function is a product of a Gaussian and a sinusoid, and models the receptive fields as elongated shapes with separate ON and OFF regions (Dayan & Abbot, 2001). These functions could possibly be an alternative to the elliptic Gaussian function in the eDOG model.

6 Conclusion

The elliptic Gaussian function is very much involved in how cortical response behaves, which can be seen by the difference between relay and cortical responses.

The elongation of the elliptic Gaussian is important for orientation selectivity, diameter and wavenumber preferences, and suppression effects in cortical cell populations. The same applies for the ellipse orientation. In addition, and magnitude of the maximum response value is dependent on the ellipse. Even though the spatiotemporal receptive fields are separable, the ellipse orientation caused a sharpening effect on the temporal frequency selectivity for a relay cell population responding to a drifting full-field grating.

The feedback loop effects on the relay response are inherited by the cortical cell population. Feedback of mixed inhibitory and excitatory weights, along with pure inhibitory feedback, cause shifts of preferred diameter and wavenumber. In addition, these feedback weight combinations enhance suppression in diameter tuning, however, not as vigorous as have been observed earlier. Excitatory and inhibitroy feedback contribute to increase or decrease the magnitude of the maximum response in both relay and cortical cell populations.

Together with the elliptic Gaussian kernel, eDOG has shown to support many of the expected cortical responses, based on linear relations. The network connections can be adjusted to fit into several situations. Any stimulus can be used in the simulations, as long as the dimensions fit into the software. Further adjustments of the parameters and connections in the model could produce response patterns not observed in the results of this thesis. Furthermore, topics like retinotopy, temporal patterns and recurrent connections could be explored by using the software PyLGN with eDOG and the elliptic Gaussian function. The model and software open new doors for modeling cortical responses including the thalamocortical loop.

References

Adesnik, H., Bruns, W., Taniguchi, H., Huang, Z. J., & Scanziani, M. (2012). A neural circuit for spatial summation in visual cortex. *Nature*, *490*, 226-231. doi: https://doi.org/10.1038/nature11526

Alitto, H. J., & Usrey, W. M. (2003). Corticothalamic feedback and sensory processing. *Current Opinion in Neurobiology*, *13*(4), 440-445. doi: https://doi.org/10.1016/S0959-4388(03)00096-5

Alitto, H. J., & Usrey, W. M. (2015). Surround suppression and temporal processing of visual signals. *Journal of Neurophysiology*, *113*(7), 2605–2617. doi: https://doi.org/10.1152/jn.00480.2014

Allen, E., & Freeman, R. D. (2006). Dynamic spatial processing originates in early visual pathways. *Journal of Neuroscience*, *26*(45), 11763-11774. doi: https://doi.org/10.1523/JNEUROSCI.3297-06.2006

Andolina, I. M., Jones, H. E., & Sillito, A. M. (2013). Effects of cortical feedback on the spatial properties of relay cells in the lateral geniculate nucleus. *Journal of Neurophysiology*, *109*(3), 889-899. doi: https://doi.org/10.1152/jn.00194.2012

Andolina, I. M., Jones, W., Helen E. Wang, & Sillito, A. M. (2007). Corticothalamic feedback enhances stimulus response precision in the visual system. *PNAS*, *104*(5), 1685-1690. doi: https://doi.org/10.1073/pnas.0609318104

Angelucci, A., & Bressloff, P. C. (2006). Contribution of feedforward, lateral and feedback connections to the classical receptive field center and extra-classical receptive field surround of primate v1 neurons. *Progress in Brain Research*, *154*(Part A), 93-120. doi: https://doi.org/10.1016/S0079-6123(06)54005-1

Ayzenshtat, I., Jackson, J., & Yuste, R. (2016). Orientation tuning depends on spatial frequency in mouse visual cortex. *eNeuro*, *3*(5). (ENEURO.0217-16.2016) doi: https://doi.org/10.1523/ENEURO.0217-16.2016

Billeh, Y. N., Cai, B., Gratiy, S. L., Dai, K., Iyer, R., Gouwens, N. W., ... Koch, C. (2020). Systematic integration of structural and functional data into multi-scale models of mouse primary visual cortex. *Neuron*, *106*(3), 388-403. doi: https://doi.org/10.1016/j.neuron.2020.01.040

Born, G., Schneider, F. A., Erisken, S., Klein, A., Lao, C. L., Mobarhan, M. H., ... Busse, L. (2021). *Corticothalamic feedback sculpts visual spatial integration in mouse thalamus.* (**Unpublished**) doi: https://doi.org/10.1101/2020.05.19.104000

Briggs, F., & Usery, W. M. (2007). A fast, reciprocal pathway between the lateral geniculate nucleus and visual cortex in the macaque monkey. *The Journal of Neuroscience*. doi: https://doi.org/10.1523/JNEUROSCI.1035-07.2007

Briggs, F., & Usery, W. M. (2011). Corticogenucleate feedback and visual processing in the primate. *The Journal of Neuroscience*. doi: https://doi.org/10.1113/jphysiol.2010.193599

Bruno, M., Randy, & Sakmann, B. (2006). Cortex is driven by weak but synchronously active thalamocortical synapses. *Science*, *312*(5780), 1622-1627. doi: https://doi.org/10.1126/science.1124593

Cai, D., Deangelis, G. C., & Freeman, R. D. (1997). Spatiotemporal receptive field organization in the lateral geniculate nucleus of cats and kittens. *Journal of Neurophysiology*, *78*(2), 1045–1061. doi: https://doi.org/10.1152/jn.1997.78.2.1045

Carandini, M., Heeger, D. J., & Senn, W. (2002). A synaptic explanation of suppression in visual cortex. *Journal of Neuroscience*, *22*(22), 10053-10065. doi: https://doi.org/10.1523/

JNEUROSCI.22-22-10053.2002
Chung, S., & Ferster, D. (1998). Strength and orientation tuning of the thalamic input to simple cells revealed by electrically evoked cortical suppression. *Neuron*, *20*(6), 1177-1189. doi: https://doi.org/10.1016/S0896-6273(00)80498-5
Citri, A., & Malenka, R. C. (2008). Synaptic plasticity: multiple forms, function and mechanisms. *Neuropsykopharmacology*, *33*, 18-41. doi: https://doi.org/10.1038/sj.npp.1301559
Cruikshank, S. J., Urabe, H., Nurmikko, A. V., & Connors, B. W. (2010). Pathway-specific feedforward circuits between thalamus and neocortex revealed by selective optical stimulation of axons. *Neuron*, *65*(2), 230-245. doi: https://doi.org/10.1016/j.neuron.2009.12.025
Cudeiro, J., & Sillito, A. M. (1996). Spatial frequency tuning of orientation-discontinuity-sensitive corticofugal feedback to the cat lateral geniculate nucleus. *Journal of Physiology*, *490*(2), 481-492. doi: https://doi.org/10.1113/jphysiol.1996.sp021159
Dagnelie, G. (2011). *Visual prosthetics physiology, bioengineering, rehabilitation*. Springer US. doi: 10.1007/978-1-4419-0754-7
Dayan, P., & Abbot, L. F. (2001). *Computational neuroscience, computational and mathematical modeling of neural systems* (Vol. 2). Cambridge: Massachussetts Institute of Technology.
DeAngelis, G. C., Ohzawa, I., & Freeman, R. D. (1993). Spatiotemporal organization of simple-cell receptive fields in the cat's striate cortex. i. general characteristics and postnatal development. *Journal of Neurophysiology*, *69*(4), 1091-1117. doi: https://doi.org/10.1152/jn.1993.69.4.1118
Denman, D. J., & Contreras, D. (2015). Complex effects on in vivo visual responses by specific projections from mouse cortical layer 6 to dorsal lateral geniculate nucleus. , *35*(25), 9265-9280. doi: https://doi.org/10.1523/JNEUROSCI.0027-15.2015
DeWeerdt, S. (2019). How to map the brain. *Nature*, *571*, S6-S8. doi: https://doi.org/10.1038/d41586-019-02208-0
Einevoll, G. T., & Plesser, H. E. (2002). Linear mechanistic models for the dorsal lateral geniculate nucleus of cat probed using drifting-grating stimuli. *Network: Computation in Neural Systems.*, *13*, 503-530. doi: https://doi.org/10.1088/0954-898x/13/4/305
Einevoll, G. T., & Plesser, H. E. (2005). Response to the difference-of-gaussians model to circular drifting-grating patches. *Visual Neuroscience*, *22*(4), 437-446. doi: https://doi.org/10.1017/S0952523805224057
Einevoll, G. T., & Plesser, H. E. (2012). Extended difference-of-gaussians model incorporating cortical feedback for relay cells in the lateral geniculate nucleus of cat. *Cognitive Neurodynamics*, *6*, 307-324. doi: https://doi.org/10.1007/s11571-011-9183-8
Enroth-Cugell, C., & Robson, J. G. (1966). The contrast sensitivity of retinal ganglion cells of the cat. *Journal of Physiology*, *187*, 517-552. doi: https://doi.org/10.1113/jphysiol.1966.sp008107
Ferster, D., & Miller, K. D. (2000). Neural mechanisms of orientation selectivity in the visual cortex. *Annual review of neuroscience*, *23*(1), 441-471. doi: https://doi.org/10.1146/annurev.neuro.23.1.441
Funke, K., Nelle, E., Li, B., & Wörgötter, F. (1996). Corticofugal feedback improves the timing of retino-geniculate signal transmission. *Neuroreport*, *7*(13), 2130—2134. doi: 10.1097/00001756-199609020-00013
Gabbiani, F., & Cox, S. J. (2017). *Mathematics for neuroscientists* (second ed.). doi: https://doi.org/10.1016/B978-0-12-801895-8.00022-1
Geisert, E. E., Langsetmo, A., & Spear, P. D. (1981). Influence of the cortico-geniculate pathway on response properties of cat lateral geniculate neurons. *Brain Research*, *208*(2), 409-415. doi:

https://doi.org/10.1016/0006-8993(81)90568-0
Godwin, D. W., Vaughan, J. W., & Sherman, S. M. (1996). Metabotropic glutamate receptors switch visual response mode of lateral geniculate nucleus cells from burst to tonic. *Journal of Neuroscience*, *76*(3), 1800-1816. doi: https://doi.org/10.1152/jn.1996.76.3.1800
Gulyás, B., Lagae, L., Eysel, U., & Orban, G. A. (1990). Corticofugal feedback influences the responses of geniculate neurons to moving stimuli. *Experimental Brain Research*, *79*, 441-446. doi: https://doi.org/10.1007/BF00608257
Hasse, J. M., & Briggs, F. (2017). Corticogeniculate feedback sharpens the temporal precision and spatial resolution of visual signals in the ferret. *PNAS*, *114*(20). doi: https://doi.org/10.1073/pnas.1704524114
Heeger, D. (1991). Nonlinear model of neural responses in cat visual cortex. In M. Landy & J. Movshon (Eds.), *Computational models of visual processing* (p. 119-134). Cambidge: MIT Press.
Hubel, D. H., & Wiesel, T. N. (1959). Receptive fields of single neurones in the cat's striate cortex. *The Journal of Physiology*, *148*(3), 574–591. doi: https://doi.org/10.1113/jphysiol.1959.sp006308
Hubel, D. H., & Wiesel, T. N. (1962). Receptive fields, binocular interaction and functional architecture of the cat's visual cortex. *The Journal of Physiology*, *160*, 106-154. doi: https://doi.org/10.1113/jphysiol.1962.sp006837
Jones, H. E., Andolina, I. M., Ahmed, B., Shipp, S. D., Clements, J. T. C., Grieve, K. L., … Sillito, M., Adam (2012). Brief communications differential feedback modulation of center and surround mechanisms in parvocellular cells in the visual thalamus. *Journal of Neuroscience*, *32*(45), 15946-15951. doi: https://doi.org/10.1523/JNEUROSCI.0831-12.2012
Kremkow, J., & Alonso, J.-M. (2018). Thalamocortical circuits and functional architecture. *Annual Review of Vision Science*, *4*(1), 263-285. doi: https://doi.org/10.1146/annurev-vision-091517-034122
Lam, Y.-W., & Sherman, S. M. (2010). Functional organization of the somatosensory cortical layer 6 feedback to the thalamus. , *20*(1), 13-24. doi: https://doi.org/10.1093/cercor/bhp077
Landisman, C. E., & Connors, B. W. (2007). Vpm and pom nuclei of the rat somatosensory thalamus: intrinsic neuronal properties and corticothalamic feedback. *Cerebral Cortex*, *17*(12), 2853–2865. doi: https://doi.org/10.1093/cercor/bhm025
Mallot, H. A. (2013). *Computational neuroscience, a first course* (Vol. 2). Springer. Retrieved from `https://link.springer.com/content/pdf/10.1007/978-3-319-00861-5.pdf`
Marrocco, R. T., McClurikin, J. W., & Young, R. A. (1981). Modulation of lateral geniculate nucleus cell responsiveness by visual activation of the corticogeniculate pathway. *Journal of Neuroscience*, *2*(2), 256-263. doi: https://doi.org/10.1523/JNEUROSCI.02-02-00256.1982
Mazurek, M., Kager, M., & Van Hooser, S. D. (2014). Robust quantification of orientation selectivity and direction selectivity. *Frontiers in Neural Circuits*, *8*, 92. doi: https://doi.org/10.3389/fncir.2014.00092
McCormick, D. A., & Krosigk, M. v. (1992). Corticothalamic activation modulates thalamic firing through glutamate "metabotropic" receptors. *PNAS*, *89*(7), 2774-2778. doi: https://doi.org/10.1073/pnas.89.7.2774
Mobarhan, M. (2018). *Computational tools for modeling, data storage, and education in neuroscience* (Unpublished doctoral dissertation). University of Oslo, Oslo.
Mobarhan, M., Halnes, G., Martínez-Cañada, P., Hafting, T., Fyhn, M., & Einevoll, G. (2018). *Pylgn* [software]. Retrieved 17.05.2021, from `https://github.com/miladh/pylgn` (version 0.92)

doi: https://doi.org/10.1371/journal.pcbi.1006156
Mobarhan, M. H., Halnes, G., Martìnez-Cañada, P., Hafting, T., Fyhn, M., & Einevoll, G. (2018). Firing-rate based network modeling of the dlgn circuit: Effects of cortical feedback on spatiotemporal response properties of relay cells. *PLOS Computational Biology*. doi: https://doi.org/10.1371/journal.pcbi.1006156
Molotchnikoff, S., Tremblay, F., & Lepore, F. (1984). The role of visual cortex in response properties of lateral geniculate cells in rats. *Experimental Brain Research*, *53*(2), 223-232. doi: https://doi.org/10.1007/BF00238152
Movshon, J. A., Thompson, I. D., & Tolhurst, D. J. (1978a). Receptive field organization of complex cells in the cat's striate cortex. *The Journal of Physiology*, *283*, 79-99. doi: https://doi.org/10.1113/jphysiol.1978.sp012489
Movshon, J. A., Thompson, I. D., & Tolhurst, D. J. (1978b). Spatial summation in the receptive fields of simple cells in the cat's striate cortex. *The Journal of Physiology*, *283*(1), 53-77. doi: https://doi.org/10.1113/jphysiol.1978.sp012488
Murphy, P. C., & Sillito, A. M. (1987). Corticofugal feedback influences the generation of length tuning in the visual pathway. *Nature*, *329*(6141), 727-9. doi: https://doi.org/10.1038/329727a0
Myklebust, L. (2020). *Exploring a network model of the mouse primary visual cortex* (Master's thesis, University of Oslo, Oslo). Retrieved from `http://urn.nb.no/URN:NBN:no-81791`
Nassi, J. J., Lomber, S. G., & Born, R. T. (2013). Corticocortical feedback contributes to surround suppression in v1 of the alert primate. *Journal of Neuroscience*, *33*(19), 8504-8517. doi: https://doi.org/10.1523/JNEUROSCI.5124-12.2013
Norheim, E. S., Wyller, J., Nordlie, E., & Einevoll, G. T. (2012). A minimal mechanistic model for temporal signal processing in the lateral geniculate nucleus. *Cognitive Neurodynamics*, *6*, 259–281. doi: https://doi.org/10.1007/s11571-012-9198-9
Ozeki, H., Finn, I. M., Schaffer, E. S., Miller, K. D., & Ferster, D. (2009). Inhibitory stabilization of the cortical network underlies visual surround suppression. *Neuron*, *62*(4), 578-592. doi: https://doi.org/10.1016/j.neuron.2009.03.028
Przybyszewski, A. W., Gaska, J. P., Foote, W., & Pollen, D. A. (2000). Striate cortex increases contrast gain of macaque lgn neurons. *Visual Neuroscience*, *17*(4), 485-494. doi: https://doi.org/10.1017/S0952523800174012
Rao, P. N., Rajesh, & Ballard, D. H. (1999). Predictive coding in the visual cortex: a functional interpretation of some extra-classical receptive-field effects. *Nature Neuroscience*, *2*, 79-87. doi: https://doi.org/10.1038/4580
Reid, R. C., Victor, J. D., & Shapley, R. M. (1997). The use of m-sequences in the analysis of visual neurons: Linear receptive field properties. *Visual Neuroscience*, *14*, 1015-1027. Retrieved from `https://citeseerx.ist.psu.edu/viewdoc/download?doi=10.1.1.452.7602&rep=rep1&type=pdf`
Rodieck, R. W. (1965). Quantitative analysis of cat retinal ganglion cell response to visual stimuli. *Vision Research*, *5*, 583-601. doi: https://doi.org/10.1016/0042-6989(65)90033-7
Self, M. W., Lorteije, J. A. M., Vangeneugden, J., Beest, E. H. v., Grigore, M. E., Levelt, C. N., ... Roelfsema, P. R. (2014). Orientation-tuned surround suppression in mouse visual cortex. *Journal of Neuroscience*, *34*, 9290-9304. doi: https://doi.org/10.1523/JNEUROSCI.5051-13.2014
Shapley, R., & Lennie, P. (1985). Spatial frequency analysis in the visual system. *Annual Review of Neuroscience*, *8*, 547-83. doi: 10.1146/annurev.ne.08.030185.002555

Sherman, S. M. (1996). Dual response modes in lateral geniculate neurons: mechanisms and functions. *Visual Neuroscience*, *13*, 205-13. doi: 10.1017/s0952523800007446

Sherman, S. M. (2016). Thalamus plays a central role in ongoing cortical functioning. *Nature Neuroscience*, *19*, 533–541. Retrieved from `https://doi.org/10.1038/nn.4269`

Sherman, S. M., & Guillery, R. W. (2002). The role of the thalamus in the flow of information to the cortex. , *357*, 1695–1708. Retrieved from `https://doi.org/10.1098/rstb.2002.1161`

Sillito, A. M., & Jones, H. E. (2002). Corticothalamic interactions in the transfer of visual information. *Phil. Trans. R. Soc. Lond. B*, *357*, 1739–1752. doi: https://doi.org/10.1098/rstb.2002.1170

Sillito, A. M., Jones, H. E., Gerstein, G. L., & West, D. C. (1994). Feature-linked synchronization of thalamic relay cell firing induced by feedback from the visual cortex. *Nature*, *369*, 479-482. doi: https://doi.org/10.1038/369479a0

Sterratt, D., Graham, B., Gillies, A., & Willshaw, D. (2011). *Principles of computational modelling in neuroscience*. Cambridge University Press.

Stettler, D. D., Das, A., Bennet, J., & Gilbert, C. D. (2002). Lateral connectivity and contextual interactions in macaque primary visual cortex. *Neuron*, *36*, 739-50. doi: 10.1016/s0896-6273(02)01029-2

Suematsu, N., Naito, T., Miyoshi, T., Sawai, J., & Sato, H. (2013). Spatiotemporal receptive field structures in retinogeniculate connections of cat. *Frontiers in Systems Neuroscience*, *7*, 103. doi: 10.3389/fnsys.2013.00103

Usrey, W. M., Sceniak, M. P., & Chapman, B. (2009). Receptive fields and response properties of neurons in layer 4 of ferret visual cortex. *Journal of Neurophysiology*, *89*, 1003-1015. doi: 10.1152/jn.00749.2002

Vaiceliunaite, A., Erisken, S., Franzen, F., Katzner, S., & Busse, L. (2013). Spatial integration in mouse primary visual cortex. *Journal of Neurophysiology*, *110*, 964-972. doi: https://doi.org/10.1152/jn.00138.2013

Wang, W., Jones, H. E., Andolina, I. M., Salt, T. E., & Sillito, A. M. (2006). Functional alignment of feedback effects from visual cortex to thalamus. *Nature Neuroscience*, *9*, 1330–1336. doi: https://doi.org/10.1038/nn1768

Webb, B. S., Tinsley, C. J., Barraclough, N. E., Easton, A., Parker, A., & Derrington, A. M. (2002). Feedback from v1 and inhibition from beyond the classical receptive field modulates the responses of neurons in the primate lateral geniculate nucleus. *Visual Neuroscience*, *19*, 583-592. doi: 10.1017/S0952523802195046

Weisstein, E. W. (n.d.). *"fourier transform" from mathworld - a wolfram web resource.* Retrieved 04.03.2021, from `https://mathworld.wolfram.com/FourierTransform.html` (last updated: 10.05.2021)

Wilent, W. B., & Contreras, D. (2005). Dynamics of excitation and inhibition underlying stimulus selectivity in rat somatosensory cortex. *Nature Neuroscience*, *8*, 1364-1370. doi: https://doi.org/10.1038/nn1545

Yousif, N., & Denham, M. (2007). The role of cortical feedback in the generation of the temporal receptive field responses of lateral geniculate nucleus neurons: a computational modelling study. *Biological cybernetics*, *97*, 269–277. doi: https://doi.org/10.1007/s00422-007-0171-3

Zaltsman, J. B., Heimel, J. A., & Van Hooser, S. D. (2015). Weak orientation and direction selectivity in lateral geniculate nucleus representing central vision in the gray squirrel sciurus carolinensis. *Journal of Neurophysiology*, *113*, 2987-2997. doi: 10.1152/jn.00516.2014

A Elliptic Gaussian syntax

```
[ ]: def create_elliptic_gauss_ft(A=1, al=1.4*pq.deg, an = 0.1*pq.deg,
                                  dx=0.*pq.deg, dy=0.*pq.deg, theta=0.*pq.rad):
         """
         Create Fourier transformed
         elliptic Gaussian function closure.

         Parameters
         ----------
         A : float
             peak value (loop coupling strength)
         al : spatial width of the loop kernel along its long axis in degrees
         an : spatial width of the loop kernel along its narrow axis in degrees
         dx: float/quantity scalar
             shift in x-direction
         dy: float/quantity scalar
             shift in y-direction
         theta: angle the longest axis makes with the x-axis in rads
         (from Einevoll and Plesser, 2012)

         Returns
         -------
         out : function
             Evaluate function
         """
         def evaluate(kx, ky):
             """
             Evaluates the Fourier transform of elliptic Gaussian function

             Parameters
             ----------
             kx : float/quantity scalar
             ky : float/quantity scalar

             Returns
             -------
             out : ndarray
                 Calculated values
             """

             return A * np.exp(-(al**2)/4 * (kx*np.cos(theta)+ky*np.sin(theta))**2
                       - ((an**2)/4 * (ky*np.cos(theta)-kx*np.sin(theta))**2))

         return evaluate
```

Norges miljø- og biovitenskapelige universitet
Noregs miljø- og biovitskapelege universitet
Norwegian University of Life Sciences

Postboks 5003
NO-1432 Ås
Norway